Exploring the Interactions between Mesenchymal Stem Cells and Endothelial Cells in Engineered Perivascular Niches

by

Bita Carrion

A dissertation submitted in partial fulfillment
of the requirements for the degree of
Doctor of Philosophy
(Biomedical Engineering)
in the University of Michigan
2013

Doctoral Committee:

Associate Professor Andrew J. Putnam
Assistant Professor Darnell Kaigler
Associate Professor Michael Mayer
Associate Professor Jan P. Stegemann

DEDICATION

to

my parents for years of unwavering love and support.

ACKNOWLEGMENTS

I would like to express my deepest gratitude to my advisor, Dr. Andrew Putnam for his guidance, support, and kindness. It was my greatest luck that I had a chance to work with him. I would also like to thank my thesis committee, Dr. Jan Stegemann, Dr. Michael Mayer, and Dr. Darnell Kaigler for their valuable input on my dissertation.

I extend my gratitude to my past and current colleagues, including Dr. Suraj Kachgal, Dr. Ekaterina Kniazeva, Dr. Carlos Huang, Peter Kim, Isaac Janson, and Dr. Yen Kong.

Mom and Dad, thanks for your constant love and encouragement! I would not have gotten here without you.

TABLE OF CONTENTS

LIST OF FIGURES

ABSTRACT

The long term survival of engineered tissue constructs is strongly dependent on oxygen delivery and nutrient exchange provided by the vasculature. Therapeutic approaches to induce neovascularization comprise cell-based therapies using endothelial cells (ECs) co-cultured with stromal cells to form long lasting functional blood vessels. This dissertation investigates the role of cross-talk between ECs and stromal cells in governing the processes of neovascularization in fibrin matrices, representative of the wound healing environment *in vivo*. Special attention was paid to a specific molecular interaction between the α6β1 integrin adhesion receptor on bone marrow derived stromal cells (BMSCs) and EC-deposited laminin.

Prior studies have shown that co-delivery of ECs and stromal cells supports the formation of robust blood vessel networks. To validate this phenomenon *in vitro*, we utilized an established three dimensional (3D) microfluidic device as a model system. ECs suspended within 2.5 mg/mL fibrin gels patterned in the device adjacent to stromal cells (either fibroblasts or BMSCs) executed a morphogenetic process akin to vasculogenesis, forming a primitive vascular plexus and maturing into a robust capillary network with hollow well-defined lumens. Both BMSCs and fibroblasts associated with the ECs like pericytes, but promoted capillary morphogenesis with distinct kinetics. Furthermore, biochemical assays revealed that the perivascular association of BMSCs required their α6β1 integrin receptor, presumably to mediate an interaction with EC-deposited laminin.

To further investigate the α6β1 integrin-laminin interactions, we used a 3D *in vitro* model of angiogenesis in which ECs coated on microcarrier beads were co-cultured with BMSCs within a fibrin matrix. Using RNA interference, we demonstrated that α6 integrin inhibition in BMSCs reduced capillary sprouting, and blocked their ability to associate with nascent blood vessels. Furthermore, we demonstrated that the BMSCs with attenuated α6 integrin expression levels proliferate at a significantly lower rate relative to either control cells expressing non-targeting shRNA or wild type BMSCs. Despite the addition of cells to compensate for this deficit in proliferation, deficient sprouting persists.

These data collectively underscore the importance of understanding integrin-mediated interactions between EC-deposited basement membranes and supporting stromal cells during the complex process of vessel formation. The results presented in this dissertation could have significant implications for both physiological and pathological neovascularization.

CHAPTER 1

INTRODUCTION

1.1 MOTIVATION AND BACKGROUND

The need for donated organs and tissues is growing at a much greater rate than their availability. More than 114,000 people are waiting for organ transplants in the United States. In 2011, a total of 6,669 patients died while waiting for organ transplants. On average, 18 people died each day because of the shortage of donated organs. A new name is added to the national organ transplant waiting list every 10 minutes. Additionally, there is a staggering annual cost of $35 billion associated with treating patients awaiting transplants in the United States [1].

Tissue engineering potentially offers dramatic improvements in medical care for hundreds of thousands of patients annually, and equally dramatic reductions in medical costs providing patient-specific tissue substitutes for the replacement or reconstruction of organs damaged by disease, trauma, or congenital defects. There are three basic strategies pursued in tissue engineering in order to retrieve loss of normal tissue structure and function [2]: (1) delivery of healthy cells directly to a tissue site to replenish a loss of cells, (2) delivery of tissue-inducing molecules to stimulate host cells to function normally, and (3) development of a three dimensional (3D) matrix or scaffolding material within which cells grow to create living 3D transplantable tissues. In almost all cell-based strategies, transplanted cells within tissue constructs compete for oxygen and nutrients between themselves and with the native cells recruited to an implant site for inflammatory response. Because oxygen diffusion is slower than

oxygen consumption for many tissues in the human body, oxygen is the limiting factor in cell survival. As a result, few cells tolerate distances of more than 100-200 μm from a blood vessel [3].

While progress has been made in some clinical applications, long term viability of thick, 3D engineered tissue constructs remains an ongoing challenge due to the inability to provide sufficient blood supply in the initial phase after implantation. The need for vasculature to deliver nutrients and oxygen and to remove waste materials is particularly crucial for engineering metabolically demanding organs such as the heart, brain and liver. Addressing this challenge requires enhancement of blood vessel growth into these tissues to permit survival of constructs and promote their integration with the host vasculature after implantation.

Therapeutic angiogenesis is an active area of research that provides strategies to enhance blood vessel growth. One strategy to promote vascularization is to deliver combinations of pro-angiogenic molecules in order to recruit the host vasculature. However, this approach can be hindered by the relatively short half-lives of these factors, and the fact that even multiple combinations may not fully recapitulate the complex milieu of pro-angiogenic factors presented to cells *in vivo*. On the other hand, ECs alone have a limited capacity to form vasculature *in vitro*, even in the presence of multiple proangiogenic factors. An alternative approach is to form a primitive vascular network *in vitro* by co-culturing endothelial cells (ECs) with mural cells within 3D engineered tissue constructs, which can then be implanted to create long-lasting and stable microvessels *in vivo*. Similar co-culture systems can be used *in vitro* to gain molecular and functional insight into the mechanisms of vessel maturation [4, 5], which should help to promote angiogenesis in these cell-based strategies. In this context, the purpose of this dissertation is to explore the role of bone marrow derived stromal cells (BMSCs) as stabilizing pericytes in EC-

derived vessel formation and maturation. In particular, this study assessed the requirement of the molecular interactions between α6β1 integrin adhesion receptor on BMSCs and EC-deposited laminin for pericyte association of the BMSCs with the nascent capillary blood vessels, and explored the role of this integrin-mediated interaction in capillary morphogenesis.

1.2 NEOVASCULARIZATION

The formation of new endothelial cell (EC)-lined vascular tubes in three dimensional (3D) extracellular matrix (ECM) environments is of critical importance during both embryonic development and in postnatal life [6, 7]. These vascular tubes arise via the physiological occurrence of two processes, vasculogenesis and angiogenesis, that are strictly regulated in the healthy adult. Vasculogenesis, the formation of new blood vessels from ECs and their progenitors (angioblasts) [8], takes place mainly during embryogenesis. However, some studies have reported it can occur in adults as well [9, 10]. Vasculogenesis and angiogenesis, sprouting of capillaries from preexisting parental vessels, share a common set of mechanisms which are regulated by the same genetic machinery [11]. Therefore, it is reasonable to assume that molecules involved in vessel formation and maturation during embryonic development are also involved in the postnatal period. ECs originate from hemangioblasts present in various organs (prenatal vasculogenesis), from bone marrow-derived cells (postnatal vasculogenesis), or by the migration and proliferation of ECs of existing vessels (angiogenesis) [12-15]. Despite being a broadly accepted mechanism of vessel growth, there are few studies that touch upon post-developmental sprouting in detail. For example, it is not known how sprouts connect to each other, how sprouts succeed in finding their counterparts (sprouting efficiency), and how and

when newly formed capillaries and parent vessels differentiate into functional capillaries, veins, and arteries.

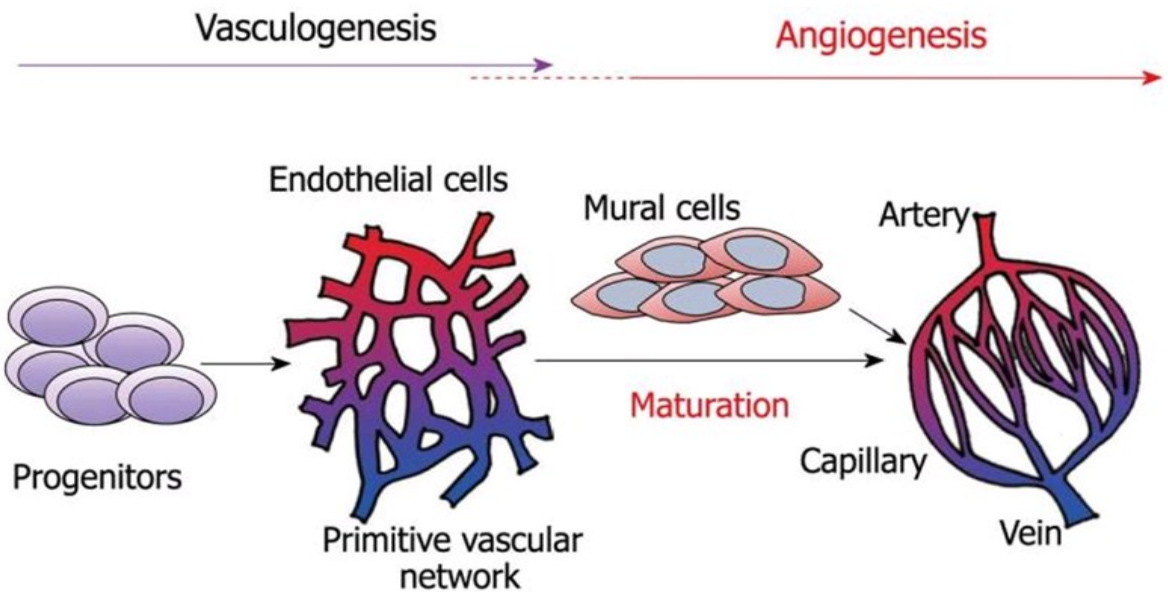

Figure 1-1: Schematic representation of vascular formation. The process includes vasculogenesis and angiogenesis. During vasculogenesis and angiogenesis, various growth factors and their receptors play spatiotemporally specific roles. Newly formed vessels are stabilized by the recruitment of mural cells, smooth muscle cells and pericytes. Images reproduced from: Takuwa, Y. *WJBC*. 2010; 1(10): 298-306.

Angiogenesis and the maturation of vessels contribute to a number of physiological processes, including wound healing. After wound or tissue injury, activated platelets stimulate vessel formation by releasing a number of proteins, including transforming growth factor-β (TGF-β) and platelet-derived growth factor (PDGF) [16]. Then, formation of the granulation tissue is facilitated by chemotactic recruitment of neutrophils, monocytes, fibroblasts, myofibrobalsts, and ECs [17]. In the early stages of wound healing, a large number of immature vessels form. Later, some of the vessels are pruned and the remainder branch out and form anastomoses with other vessels while maturing into fully functional perfused blood vessels [18].

Despite significant effort to dissect the molecular basis of neovascularization, the mechanisms underlying vessel maturation involving mural cells remain to be fully elucidated.

1.3 ROLE OF MURAL CELLS IN NEOVASCULARIZATION

After EC vascular networks are formed, recruitment of supporting mural cells occurs along the tube abluminal surfaces [19-21]. This latter step represents a crucial event regulating further vascular remodeling, maturation and stabilization [22-27]. Maturation of a nascent vessel is attained through EC-pericyte interactions and concomitant ECM remodeling, including deposition and cross-linking of ECM components (i.e., basement membranes (BMs) and interstitial matrices) at distinct places surrounding nascent vasculature. These processes are dependent on the vessel type [27-30]. Both ECs and pericytes produce matrix molecules and facilitate assembly of the matrix from its constituents. A number of studies suggest that alteration of endothelial-derived integrin expression *in vivo* may be specific to the vascular bed undergoing neovascularization [31-33]. Mural cells are closely involved in the processes that ultimately lead to maturation and stabilization of nascent vasculature. Prenatally, mural cells originate from multiple sources during embryonic development, including the local and distal mesenchyme [34, 35]. In the adult, the mural cells can be derived from the bone marrow or its stroma [11], and then they become pericytes or vascular smooth muscle cells (SMCs). Pericytes can differentiate into SMCs [36] concomitant with vessel growth and remodeling. Pericytes establish direct cell-cell contact with ECs and cover capillaries and immature blood vessels, whereas SMCs cover mature and larger diameter vessels, such as arteries and veins [37].

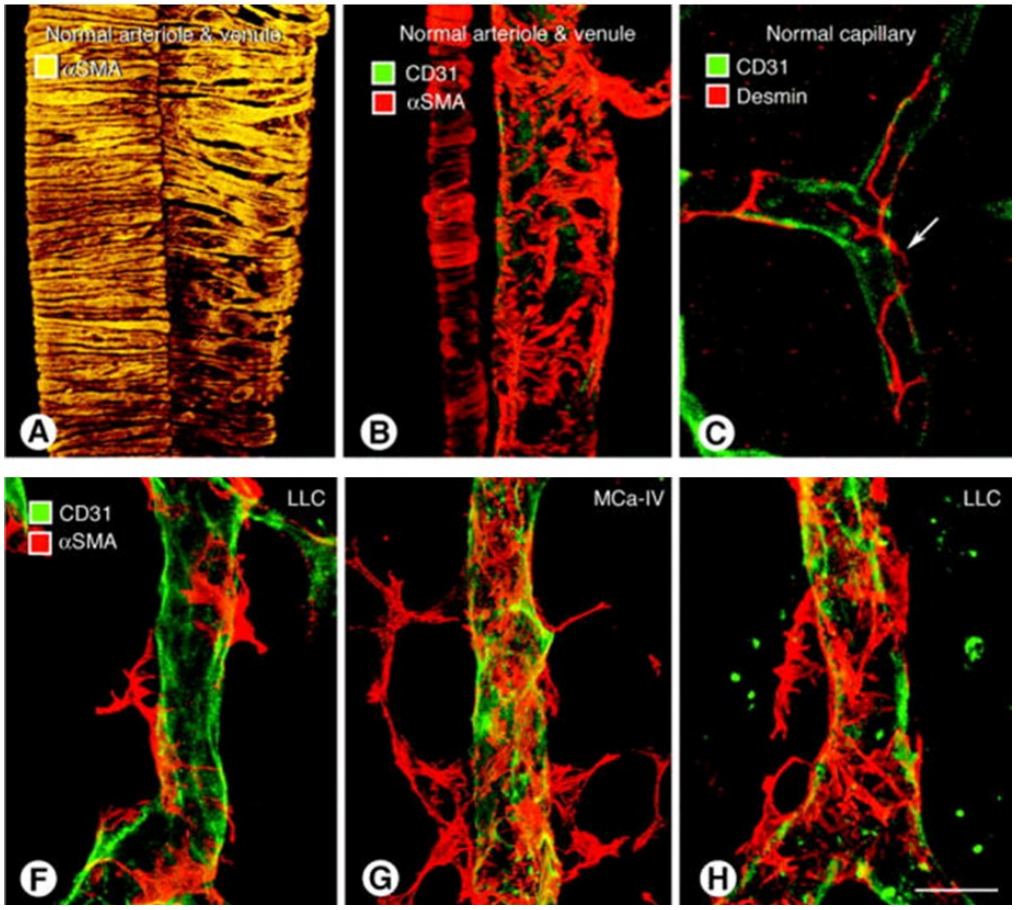

Figure 1-2: Tumor vasculature exhibits sparse pericytic coverage. (A, B) Arterioles, venules, and (C) capillaries from normal pancreas were stained for an antibody against CD31, a surface marker of endothelial cells, and α-smooth muscle actin; displaying significant mural coverage. (F-H) Images are representative of vessels from carcinomas demonstrating loose association with mural cells and overall decrease in the amount of pericytic coverage. Images reproduced from: Morikawa, S, *Am J Pathol,* 2002; 160(3): 985-1000

In addition to their ability to modulate their phenotype to SMCs, pericytes may also give rise to other mesenchymal cells, including fibroblasts, osteoblasts, chondrocytes, and adipocytes [38, 39]. EC-derived release of platelet derived growth factor β (PDGFβ) helps attract mural cells to immature vasculature [37]. Subsequent endothelial binding of mural cell-secreted Ang-1 stimulates recurrence of VE-cadherin expression [40] and prevents VEGF-induced phosphorylation of a gene, Sex comb reduced (Scr), and thereby obstructs vessel leakage. Recent analyses of tumor-associated vasculature have demonstrated evidence of

hyperpermeability owing to increased VEGF concentrations [41, 42]. Not surprisingly, pericytic coverage of tumor vessels is sparse (Fig. 1-2) [43]. Mural cells also contribute to the maintenance of vascular tone and prevent vessel hyperdilation [37, 44-46]. With their sparse pericytic coverage, tumor vessels are highly distended [37, 43, 47].

Recent evidence also implicates EC-MSC crosstalk to promote tumor angiogenesis *in vivo* [48]. ECs have been shown to attract undifferentiated MSCs through paracrine mechanisms [49]. While, the exact mechanisms for how MSCs would enhance angiogenesis is unclear, there is compelling evidence that implies maturation of a nascent vessel is attained through EC-MSC interactions and concomitant ECM remodeling, including deposition and cross-linking of ECM components [50]. However, despite being perivascular, not all MSCs can be referred to as pericytes. Functionally heterogeneous cell subsets, including but not limited to MSCs are loosely termed pericytes for displaying pericytic functions, including vessel stabilization, phagocytosis, and regulation of vascular tune [51]. Not all pericytes exhibit MSC-specific properties either [52]. A better understanding of the molecular mechanisms by which MSCs facilitate neovascularization is crucial to enhance or suppress blood vessel growth and maturation under physiological or pathological conditions, respectively.

Studying neovascularization in the absence of stromal cells is not physiologically relevant. Our group has in fact performed vasculogenesis-type assays with ECs only, and has found that although ECs in 3D gels are capable of forming a primitive vascular plexus, but this plexus is unstable and eventually deteriorates over time in culture. In a different model system that mimics angiogenesis, our group has shown that capillary-like networks do not form in the absence of stromal cells, and that replacing the stromal cells with conditioned medium is not sufficient [53]. These observations are consistent with the published results of many other investigators.

Moreover, it has been recently demonstrated that stromal cells are required for the formation of capillaries with basement membranes [27].

1.4 INTEGRINS AND THEIR ROLE IN VASCULARIZATION

Integrins are heterodimeric cell surface receptors composed of an α and a β subunit, forming more than 20 combinations [54] that have diverse functions, including regulation of EC-adhesion to the vascular basement membrane. Integrins not only mediate cell adhesion, but they also transduce signals via activation of kinases such as focal adhesion kinase (FAK) and mitogen-activated protein (MAP) kinase [55]. In various steps of neo-vessel formation, cross talk between integrins and their receptors is important. Integrins not only directly bind to ECM proteins and thus regulate adhesion and migration [56], but also facilitate cross-talk with pro- and anti-angiogenic growth factors. Different integrin combinations may recognize a single ECM ligand, while others bind several different ECM proteins. Integrin-mediated adhesion leads to intracellular signaling events that regulate cell survival, proliferation, and migration [57].

ECs and pericytes both express a subset of integrins, including the collagen receptors, α1β1, α2β1; and the laminin receptors, α3β1, α6β1, and α6β4. During neovascularization, it appears that a number of integrins expressed on the surface of activated ECs regulate critical adhesive interactions with a variety of ECM proteins, including fibronectin, vitronectin, laminin, collagen types I and IV, von Willebrand factor, fibrinogen, and denatured collagen. Each of these adhesive interactions may regulate distinct biological events such as cell migration, proliferation, and differentiation. In particular, the angiogenic process requires changes in cell adhesion, which are mediated by specific integrins whose expression appears to be upregulated during this process. Recent studies suggest that the EC integrin α4β1 is necessary for an interaction with

vascular cell adhesion molecule 1 (VCAM1) on pericytes, resulting in EC-pericyte interaction and vessel stabilization [58]. A deletion of integrin subunit genes in ECs or pericyte in knockout mice has allowed a better understanding of these molecules in both developmental and pathological angiogenesis [59]. More relevant to this thesis work, the ability of the laminin receptor, the α6β1 integrin heterodimer to promote tube formation in *ex vivo* models of angiogenesis has been highlighted [60, 61]. Furthermore, blocking α6 integrin with a specific antibody, GoH3, inhibits VEGF-induced adhesion and migration of brain microvascular endothelial cells as well as *in vivo* angiogenesis [62]. Taken together, evidence for a role of α6 integrin in angiogenesis is conflicting. As for α6β1, no studies on the function of α6 integrin in pericytes have been reported.

1.5 FIBRIN IN TISSUE ENGINEERING

The relevance of fibrin as a substrate in which to recreate vascularization lies in its appropriate biochemical and mechanical properties as a 3D matrix for angiogenesis *in vitro* , and its unique characteristic of rapid assembly, which is desirable for the generation of co-cultures. Fibrin is a natural biocompatible biopolymer [63], suitable as a model for wound healing and angiogenesis [64], utilizing the body's natural healing capacity. Fibrin supports population expansion, migration and myofibrobalsts [65] and mesenchymal stem cells [66]. Moreover, fibrin itself has been shown to promote angiogenesis and perfusion in animal models of hind limb ischemia [67]; it has also been used as a cell delivery vehicle to reduce ischemic myocardium [68-71]. It has been recently demonstrated that a fibrin composite scaffold provides local and controlled spatial–temporal release of vascular endothelial growth factor (VEGF) and basic fibroblast growth factor (bFGF) [72, 73]. More relevant to this thesis work, the efficacy of

treatment with MSCs in fibrin for promoting neovascularization in the chronically infarcted myocardium has been assessed [74].

Fibrinogen is a soluble protein that is converted by thrombin into fibrin during blood clot formation. During normal blood coagulation, a coagulation cascade activates the zymogen pro-thrombin by converting it into the serine protease thrombin. Thrombin then converts the soluble fibrinogen into insoluble fibrin strands. These strands are then cross-linked by factor XIII to form a blood clot. The aim of this study has been to combine cell studies with advantages of fibrin as a biocompatible matrix. In addition to the results obtained for completing the specific aims of this dissertation, this study also collectively demonstrates that fibrin provides a suitable matrix for cell growth and differentiation.

1.6 SPECIFIC AIMS

A large body of work suggests that many adult stem cells, including neural stem cells (NSCs) (3, 4), mesenchymal stem cells (MSCs) from bone marrow and adipose tissue [76, 77], and hematopoietic stem cells [78], reside in a vascular niche, where they associate with blood vessels [79]. BMSCs, in particular, can act as angiogenic facilitators (Fig. 1-1), in part due to their physiological capability to differentiate into pericytes and line blood vessels *in vivo* [80, 81], and in part due to their immunomodulatory capacity which makes these cells even more attractive for therapeutic angiogenesis. Previously, our group has shown that ECs form robust capillary networks in the presence of BMSCs *in vitro* (Fig. 1-2) [50]. It was demonstrated that BMSCs not only stimulate capillary formation from ECs, but also occupy perivascular locations in these capillary networks and express the pericytic marker α-smooth muscle actin (α-SMA). The

overall goals of this dissertation were to better understand the importance of this close association of MSCs with the vasculature and their role in promoting angiogenesis, focusing closely on the interaction between the α6β1 integrin receptor on BMSCs and EC-deposited laminin within the BM of the capillary networks.

Various molecules and their receptors play important roles in neovascularization. There is compelling evidence in the literature suggesting that, the α6β1 integrin receptor on neural stem cells (NSCs) mediates their interaction with laminin deposited as part of the BM surrounding blood vessels in the subventricular zone of the brain [75]. Given the common perivascular location of NSCs and MSCs *in vivo*, we hypothesize that the interaction between EC-deposited laminin and the α6β1integrin adhesion receptor is critical for proper perivascular localization of BMSCs and their role in promoting neovascularization.

Three specific aims were proposed to achieve the aforementioned goals and test my hypothesis.

1. *Fabricate and utilize a microfluidic platform to demonstrate that ECs recapture their in vivo vasculogenic capacity in the presence of stromal cells, including BMSCs and normal human lung fibroblasts (NHLFs).* The goal of this aim is to demonstrate that our microfluidic devices (MFDs) sustain capillary morphogenesis, and support the formation of pericyte-invested capillary blood vessels in the presence of stromal cells. Our existing 3D fibrin-based model system [50] was transferred into an established MFD [82], and used to support the formation of capillary blood vessels.

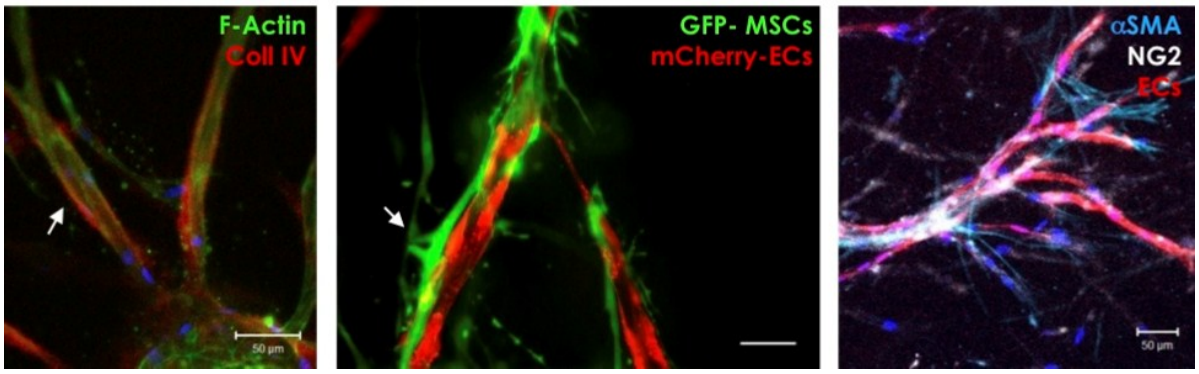

Figure 1-3: 3D co-cultures of ECs and stromal cells generate stable, pericyte-invested capillary networks *in vitro*. BMSCs were distributed throughout fibrin-based 3D matrices in the presence of microcarrier beads coated with ECs. Physical association of the ECs and MSCs were observed (white arrows). Pericyte differentiation of MSCs was also confirmed, as revealed by the expression of pericyte markers, including α-smooth muscle actin (α-SMA) and NG2. Image reproduced from: Ghajar, C.M. *Exp Cell Res.* 2010; 316(5): 813-25.

2. *Investigate the requirement of α6β1 integrin-laminin interactions for pericyte association of BMSCs with capillary blood vessels in the MFDs.* Our hypothesis is that BMSCs, in the presence of EC-derived capillary networks, recapitulate their endogenous perivascular location in the MFDs, and require the α6β1 integrin-laminin interactions in order to properly associate with the capillary networks.

3. *Investigate the role of the interaction between α6β1 integrin on BMSCs and EC-derived laminin-rich BM in sprouting angiogenesis in an established 3D fibrin-based in vitro model.* Our hypothesis is that BMSCs promote angiogenesis in ECs, partly via the interactions between their α6β1 integrin adhesion receptor with EC-deposited laminin. To do the more rigorous analyses in the scope of this aim required retrieving cells from 3D fibrin matrices. In most cases, commonly used proteolytic enzymes, including trypsin and collagenase, have been used for primary cell isolation from a variety of tissue types. However, when used to dissolve fibrin for *in vitro* models, these enzymes do not yield a single cell suspension effectively. Furthermore, longer incubation times with these enzymes required for dissolving the gels may damage the cells

harvested from these gels. Therefore, as part of Aim 3, I developed and applied an efficient and safe method to recover cells encapsulated within 3D fibrin hydrogels.

1.7 PREVIEW OF THE THESIS

An overview of the importance of functional vasculature within engineered viable tissues was given in this chapter. Blood vessel formation is a complex morphogenetic process that comprises several elements of the cellular microenvironment, including ECs, mural cells, cytokines, and the ECM. The maturation of blood vessels involves an intricate interplay with the mural cells during neovascularization. Continuous, reciprocal crosstalk between ECs and mural cells is important in the development and stability of blood vessels. Chapter 2 presents the design and exploitation of a 3D microfluidic platform as a model system to probe the molecular interactions between ECs and stromal cells (either fibroblasts or BMSCs), and the completion of the first specific aim. Following is Chapter 3, where the microfluidic platform is exploited to look more closely at the interaction between the α6β1 integrin receptor on BMSCs and EC-deposited laminin using integrin blocking assays, and the completion of the second specific aim. The ability of our microscale system to meet some essential design constraints was demonstrated. First and foremost, the device was capable of supporting vasculogenesis in a 3D gel. Second, MSCs cultured within the device were capable of occupying a perivascular location. Data demonstrating that these two constraints were satisfied in our devices are provided in Chapter 3. In Chapter 4, a fibrin-based *in vitro* angiogenesis assay was used to address the third specific aim, which uses RNA interference to knockdown the gene responsible for the expression of α6 integrin subunit in BMSCs and investigate the influence of this integrin on angiogenic sprouting. The requirement of α6 integrin subunit expression in BMSCs for their

perivascular association with EC-derived vessel networks was also explored here. Chapter 5 introduces a safe and efficient method to retrieve cells from 3D fibrin matrices. The use of nattokinase, a powerful fibrinolytic enzyme is introduced in this chapter. Finally, results from all three aims are summarized in Chapter 6, along with a discussion of the implications of this study for regulation of physiological and pathological angiogenesis.

1.8 REFERENCES

1. United Network for Organ Sharing website. 2012. p. Available from: http://www.unos.org/index.php.

2. Rustad, K.C., et al., Strategies for organ level tissue engineering. Organogenesis, 2010. 6(3): p. 151-7.

3. Jain, R.K., et al., Engineering vascularized tissue. Nat Biotechnol, 2005. 23(7): p. 821-3.

4. Hirschi, K.K., et al., Endothelial cells modulate the proliferation of mural cell precursors via platelet-derived growth factor-BB and heterotypic cell contact. Circ Res, 1999. 84(3): p. 298-305.

5. Darland, D.C. and P.A. D'Amore, TGF beta is required for the formation of capillary-like structures in three-dimensional cocultures of 10T1/2 and endothelial cells. Angiogenesis, 2001. 4(1): p. 11-20.

6. Hynes, R.O., Cell-matrix adhesion in vascular development. J Thromb Haemost, 2007. 5 Suppl 1: p. 32-40.

7. Iruela-Arispe, M.L. and G.E. Davis, Cellular and molecular mechanisms of vascular lumen formation. Dev Cell, 2009. 16(2): p. 222-31.

8. Risau, W. and I. Flamme, Vasculogenesis. Annu Rev Cell Dev Biol, 1995. 11: p. 73-91.

9. Asahara, T., et al., Bone marrow origin of endothelial progenitor cells responsible for postnatal vasculogenesis in physiological and pathological neovascularization. Circ Res, 1999. 85(3): p. 221-8.

10. Urbich, C. and S. Dimmeler, Endothelial progenitor cells: characterization and role in vascular biology. Circ Res, 2004. 95(4): p. 343-53.

11. Carmeliet, P., Mechanisms of angiogenesis and arteriogenesis. Nat Med, 2000. 6(4): p. 389-95.

12. Carmeliet, P. and R.K. Jain, Angiogenesis in cancer and other diseases. Nature, 2000. 407(6801): p. 249-57.

13. Jiang, Y., et al., Multipotent progenitor cells can be isolated from postnatal murine bone marrow, muscle, and brain. Exp Hematol, 2002. 30(8): p. 896-904.

14. Rafii, S., et al., Contribution of marrow-derived progenitors to vascular and cardiac regeneration. Semin Cell Dev Biol, 2002. 13(1): p. 61-7.

15. Reyes, M., et al., Origin of endothelial progenitors in human postnatal bone marrow. J Clin Invest, 2002. 109(3): p. 337-46.

16. Coussens, L.M. and Z. Werb, Inflammation and cancer. Nature, 2002. 420(6917): p. 860-7.

17. Tomasek, J.J., et al., Myofibroblasts and mechano-regulation of connective tissue remodelling. Nat Rev Mol Cell Biol, 2002. 3(5): p. 349-63.

18. Zawicki, D.F., et al., Dynamics of neovascularization in normal tissue. Microvasc Res, 1981. 21(1): p. 27-47.

19. Bergers, G. and S. Song, The role of pericytes in blood-vessel formation and maintenance. Neuro Oncol, 2005. 7(4): p. 452-64.

20. Betsholtz, C., P. Lindblom, and H. Gerhardt, Role of pericytes in vascular morphogenesis. EXS, 2005(94): p. 115-25.

21. Davis, G.E., et al., Molecular basis for endothelial lumen formation and tubulogenesis during vasculogenesis and angiogenic sprouting. Int Rev Cell Mol Biol, 2011. 288: p. 101-65.

22. Hanahan, D., Signaling vascular morphogenesis and maintenance. Science, 1997. 277(5322): p. 48-50.

23. Benjamin, L.E., I. Hemo, and E. Keshet, A plasticity window for blood vessel remodelling is defined by pericyte coverage of the preformed endothelial network and is regulated by PDGF-B and VEGF. Development, 1998. 125(9): p. 1591-8.

24. Bergers, G., et al., Benefits of targeting both pericytes and endothelial cells in the tumor vasculature with kinase inhibitors. J Clin Invest, 2003. 111(9): p. 1287-95.

25. Davis, G.E. and D.R. Senger, Extracellular matrix mediates a molecular balance between vascular morphogenesis and regression. Curr Opin Hematol, 2008. 15(3): p. 197-203.

26. Hughes, C.C., Endothelial-stromal interactions in angiogenesis. Curr Opin Hematol, 2008. 15(3): p. 204-9.

27. Stratman, A.N., et al., Pericyte recruitment during vasculogenic tube assembly stimulates endothelial basement membrane matrix formation. Blood, 2009. 114(24): p. 5091-101.

28. Davis, G.E. and D.R. Senger, Endothelial extracellular matrix: biosynthesis, remodeling, and functions during vascular morphogenesis and neovessel stabilization. Circ Res, 2005. 97(11): p. 1093-107.

29. Wagenseil, J.E. and R.P. Mecham, Vascular extracellular matrix and arterial mechanics. Physiol Rev, 2009. 89(3): p. 957-89.

30. Senger, D.R. and G.E. Davis, Angiogenesis. Cold Spring Harb Perspect Biol, 2011. 3(8): p. a005090.

31. Nikkari, L., et al., Expression of integrin family of cell adhesion receptors in rheumatoid synovium. Alpha 6 integrin subunit in normal and hyperplastic synovial lining cell layer. Am J Pathol, 1993. 142(4): p. 1019-27.

32. Kagami, S., et al., Coordinated expression of beta 1 integrins and transforming growth factor-beta-induced matrix proteins in glomerulonephritis. Lab Invest, 1993. 69(1): p. 68-76.

33. Johnson, B.A., et al., Recurrence of sarcoidosis in pulmonary allograft recipients. Am Rev Respir Dis, 1993. 148(5): p. 1373-7.

34. Hungerford, J.E. and C.D. Little, Developmental biology of the vascular smooth muscle cell: building a multilayered vessel wall. J Vasc Res, 1999. 36(1): p. 2-27.

35. Sartore, S., et al., Contribution of adventitial fibroblasts to neointima formation and vascular remodeling: from innocent bystander to active participant. Circ Res, 2001. 89(12): p. 1111-21.

36. Nehls, V. and D. Drenckhahn, The versatility of microvascular pericytes: from mesenchyme to smooth muscle? Histochemistry, 1993. 99(1): p. 1-12.

37. Jain, R.K., Molecular regulation of vessel maturation. Nat Med, 2003. 9(6): p. 685-93.

38. Collett, G.D. and A.E. Canfield, Angiogenesis and pericytes in the initiation of ectopic calcification. Circ Res, 2005. 96(9): p. 930-8.

39. Doherty, M.J., et al., Vascular pericytes express osteogenic potential in vitro and in vivo. J Bone Miner Res, 1998. 13(5): p. 828-38.

40. Gavard, J., V. Patel, and J.S. Gutkind, Angiopoietin-1 prevents VEGF-induced endothelial permeability by sequestering Src through mDia. Dev Cell, 2008. 14(1): p. 25-36.

41. Nagy, J.A., et al., Pathogenesis of ascites tumor growth: fibrinogen influx and fibrin accumulation in tissues lining the peritoneal cavity. Cancer Res, 1995. 55(2): p. 369-75.

42. Yeo, K.T., et al., Vascular permeability factor (vascular endothelial growth factor) in guinea pig and human tumor and inflammatory effusions. Cancer Res, 1993. 53(12): p. 2912-8.

43. Morikawa, S., et al., Abnormalities in pericytes on blood vessels and endothelial sprouts in tumors. Am J Pathol, 2002. 160(3): p. 985-1000.

44. Peppiatt, C.M., et al., Bidirectional control of CNS capillary diameter by pericytes. Nature, 2006. 443(7112): p. 700-4.

45. Armulik, A., A. Abramsson, and C. Betsholtz, Endothelial/pericyte interactions. Circ Res, 2005. 97(6): p. 512-23.

46. Hellstrom, M., et al., Lack of pericytes leads to endothelial hyperplasia and abnormal vascular morphogenesis. J Cell Biol, 2001. 153(3): p. 543-53.

47. Song, C.W., et al., Implication of blood flow in hyperthermic treatment of tumors. IEEE Trans Biomed Eng, 1984. 31(1): p. 9-16.

48. Huang, W.H., et al., Mesenchymal stem cells promote growth and angiogenesis of tumors in mice. Oncogene, 2012.

49. Hirschi, K.K., S.A. Rohovsky, and P.A. D'Amore, PDGF, TGF-beta, and heterotypic cell-cell interactions mediate endothelial cell-induced recruitment of 10T1/2 cells and their differentiation to a smooth muscle fate. J Cell Biol, 1998. 141(3): p. 805-14.

50. Ghajar, C.M., et al., Mesenchymal cells stimulate capillary morphogenesis via distinct proteolytic mechanisms. Exp Cell Res, 2010. 316(5): p. 813-25.

51. Hirschi, K.K. and P.A. D'Amore, Pericytes in the microvasculature. Cardiovasc Res, 1996. 32(4): p. 687-98.

52. Caplan, A.I., All MSCs are pericytes? Cell Stem Cell, 2008. 3(3): p. 229-30.

53. Kniazeva, E. and A.J. Putnam, Endothelial cell traction and ECM density influence both capillary morphogenesis and maintenance in 3-D. Am J Physiol Cell Physiol, 2009. 297(1): p. C179-87.

54. Hynes, R.O., Integrins: bidirectional, allosteric signaling machines. Cell, 2002. 110(6): p. 673-87.

55. Oktay, M., et al., Integrin-mediated activation of focal adhesion kinase is required for signaling to Jun NH2-terminal kinase and progression through the G1 phase of the cell cycle. J Cell Biol, 1999. 145(7): p. 1461-9.

56. Serini, G., et al., Besides adhesion: new perspectives of integrin functions in angiogenesis. Cardiovasc Res, 2008. 78(2): p. 213-22.

57. Aplin, A.E., et al., Signal transduction and signal modulation by cell adhesion receptors: the role of integrins, cadherins, immunoglobulin-cell adhesion molecules, and selectins. Pharmacol Rev, 1998. 50(2): p. 197-263.

58. Garmy-Susini, B., et al., Integrin alpha4beta1-VCAM-1-mediated adhesion between endothelial and mural cells is required for blood vessel maturation. J Clin Invest, 2005. 115(6): p. 1542-51.

59. Gustafsson, E. and R. Fassler, Insights into extracellular matrix functions from mutant mouse models. Exp Cell Res, 2000. 261(1): p. 52-68.

60. Leu, S.J., S.C. Lam, and L.F. Lau, Pro-angiogenic activities of CYR61 (CCN1) mediated through integrins alphavbeta3 and alpha6beta1 in human umbilical vein endothelial cells. J Biol Chem, 2002. 277(48): p. 46248-55.

61. Leu, S.J., et al., Identification of a novel integrin alpha 6 beta 1 binding site in the angiogenic inducer CCN1 (CYR61). J Biol Chem, 2003. 278(36): p. 33801-8.

62. Lee, T.H., et al., Integrin regulation by vascular endothelial growth factor in human brain microvascular endothelial cells: role of alpha6beta1 integrin in angiogenesis. J Biol Chem, 2006. 281(52): p. 40450-60.

63. Shaikh, F.M., et al., Fibrin: a natural biodegradable scaffold in vascular tissue engineering. Cells Tissues Organs, 2008. 188(4): p. 333-46.

64. Janmey, P.A., J.P. Winer, and J.W. Weisel, Fibrin gels and their clinical and bioengineering applications. J R Soc Interface, 2009. 6(30): p. 1-10.

65. Ye, Q., et al., Fibrin gel as a three dimensional matrix in cardiovascular tissue engineering. Eur J Cardiothorac Surg, 2000. 17(5): p. 587-91.

66. Bensaid, W., et al., A biodegradable fibrin scaffold for mesenchymal stem cell transplantation. Biomaterials, 2003. 24(14): p. 2497-502.

67. Fan, C.L., et al., Therapeutic angiogenesis by intramuscular injection of fibrin particles into ischaemic hindlimbs. Clin Exp Pharmacol Physiol, 2006. 33(7): p. 617-22.

68. Christman, K.L., et al., Injectable fibrin scaffold improves cell transplant survival, reduces infarct expansion, and induces neovasculature formation in ischemic myocardium. J Am Coll Cardiol, 2004. 44(3): p. 654-60.

69. Wong, C., et al., Fibrin-based biomaterials to deliver human growth factors. Thromb Haemost, 2003. 89(3): p. 573-82.

70. Sahni, A. and C.W. Francis, Vascular endothelial growth factor binds to fibrinogen and fibrin and stimulates endothelial cell proliferation. Blood, 2000. 96(12): p. 3772-8.

71. Mittermayr, R., et al., Sustained (rh)VEGF(165) release from a sprayed fibrin biomatrix induces angiogenesis, up-regulation of endogenous VEGF-R2, and reduces ischemic flap necrosis. Wound Repair Regen, 2008. 16(4): p. 542-50.

72. Briganti, E., et al., A composite fibrin-based scaffold for controlled delivery of bioactive pro-angiogenetic growth factors. J Control Release, 2010. 142(1): p. 14-21.

73. Losi, P., et al., Tissue response to poly(ether)urethane-polydimethylsiloxane-fibrin composite scaffolds for controlled delivery of pro-angiogenic growth factors. Biomaterials, 2010. 31(20): p. 5336-44.

74. Huang, N.F., et al., Bone marrow-derived mesenchymal stem cells in fibrin augment angiogenesis in the chronically infarcted myocardium. Regen Med, 2009. 4(4): p. 527-38.

75. Kokovay, E., et al., Adult SVZ lineage cells home to and leave the vascular niche via differential responses to SDF1/CXCR4 signaling. Cell Stem Cell, 2010. 7(2): p. 163-73.

76. Crisan, M., et al., A perivascular origin for mesenchymal stem cells in multiple human organs. Cell Stem Cell, 2008. 3(3): p. 301-13.

77. Traktuev, D.O., et al., A population of multipotent CD34-positive adipose stromal cells share pericyte and mesenchymal surface markers, reside in a periendothelial location, and stabilize endothelial networks. Circ Res, 2008. 102(1): p. 77-85.

78. Kiel, M.J. and S.J. Morrison, Uncertainty in the niches that maintain haematopoietic stem cells. Nat Rev Immunol, 2008. 8(4): p. 290-301.

79. Corselli, M., et al., Perivascular ancestors of adult multipotent stem cells. Arterioscler Thromb Vasc Biol, 2010. 30(6): p. 1104-9.

80. Gronthos, S. and P.J. Simmons, The growth factor requirements of STRO-1-positive human bone marrow stromal precursors under serum-deprived conditions in vitro. Blood, 1995. 85(4): p. 929-40.

81. Satomura, K., et al., Receptor tyrosine kinase expression in human bone marrow stromal cells. J Cell Physiol, 1998. 177(3): p. 426-38.

82. Huang, C.P., et al., Engineering microscale cellular niches for three-dimensional multicellular co-cultures. Lab Chip, 2009. 9(12): p. 1740-8.

CHAPTER 2

RECREATING THE PERIVASCULAR NICHE *EX VIVO* USING A MICROFLUIDIC APPROACH

2.1.INTRODUCTION

Post-natal adult stem cell niches are composed of numerous components, including soluble growth factors, cell-cell interactions, cell-ECM (extracellular matrix) adhesion, and physical forces, which coordinately regulate cell fate decisions with precise spatiotemporal control [1, 2]. However, the complexity and integration of these various elements remains poorly understood. Creation of artificial stem cell niches *ex vivo* may augment efforts to identify the specific cues that define stem cell niches, and thereby pave the way for the successful use of stem cells in regenerative medicine [3-5]. To date no suitable method has been developed to fully recapitulate stem cell microenvironments, partly due to a poor understanding of *in vivo* niches.

A combination of appropriate soluble factors and ECM molecules that govern stem cell niches is thought to hold the key to *ex vivo* manipulation [2, 4, 6]. The physical properties of stem cell microenvironments may be equally important for determining stem cell fate [7]. However, recent studies suggest another feature common to many adult stem cell niches may be critically important in the regulation of cell fates: their physical proximity to the vasculature. This anatomic location, the so-called perivascular niche, has been suggested as the *in vivo* location of adult neural stem cells (NSCs) [8-10], MSCs from bone marrow and multiple other adult tissues [11], and hematopoietic stem cells [12]. It has even recently been proposed that all

MSCs are pericytes, and that this anatomic location may enable MSCs to mobilize for repair following injury, and thereby facilitate tissue homeostasis [13]. In prior studies, we have used a 3D fibrin-based cell culture model to explore the mechanisms by which mesenchymal cells (either fibroblasts or MSCs) stimulate capillary formation from human umbilical vein endothelial cells (HUVECs) [14, 15]. While such a system yields pericyte-invested capillaries with hollow lumens that are capable of perfusing tissues *in vivo* [16], the ability to simultaneously control the spatial and temporal presentation of other niche-specific cues (e.g., soluble growth factors, cell-cell interactions) limited the potential for our existing system to carefully study perivascular niches *ex vivo.*

To better understand the importance of the perivascular location of many adult stem cell niches, we developed a simple three dimensional (3D) microfluidic device (MFD) that sustains capillary morphogenesis. This versatile platform contains discrete microchannels into which cells suspended in gel precursor solutions can be injected. Multiple channels can be patterned with distinct cell populations, and even in distinct ECM gels, and then subjected to diffusible gradients of soluble morphogens. In addition to the ability to support a 3D matrix environment that closely mimics the physiological conditions in which capillary morphogenesis occurs, the optical clarity and relatively thin profile of the MFD allow for higher resolution images, while the small volumes allow valuable reagents to be conserved. HUVECs, initially segregated from stromal cells (either fibroblasts or MSCs) in discrete channels, executed a morphogenetic process akin to vasculogenesis, beginning with the formation of a primitive vascular plexus and maturing into a robust, pericyte-invested capillary network with hollow well-defined lumens. Both fibroblasts and MSCs adopted pericytic locations within this system but promoted capillary morphogenesis with distinct kinetics. Because the perivascular localization of MSCs is

effectively recapitulated in this simple MFD, in the next chapter its utility as an artificial perivascular niches will be demonstrated, revealing the novel discovery that the interaction between endothelial cell (EC)-deposited laminin and the α6β1 integrin receptor on the MSCs is required for the proper perivascular localization of MSCs.

2.2.METHODS

Cell isolation and culture: HUVECs, freshly harvested umbilical cords as previously described [14], were grown in endothelial growth medium (EGM-2; Lonza, Walkersville, MD). Primary normal human lung fibroblasts (NHLFs; Lonza) were cultured in Medium 199 (Invitrogen, Carlsbad, CA) with 10% fetal bovine serum (FBS; Media Tech, Manassas, VA), 1% penicillin/streptomycin (P/S; Media Tech), and 0.5% gentamicin (GM; Invitrogen). Human mesenchymal stem cells (MSCs; Lonza) were grown in Dulbecco's modified Eagle's medium (DMEM; Invitrogen) supplemented with 10% FBS, 1% P/S, and 0.5% GM. NHLFs and MSCs were used prior to passage 10, and HUVECs at passage 3.

Microfluidic device design and fabrication: MFDs were fabricated using polydimethylsiloxane (PDMS; Sylgard 184) and soft lithography as previously described [17]. The device consists of two parallel main channels that are 1.5mm wide and 50 mm tall (Fig. 2-1a). These are separated by three smaller chambers that are 400mm wide, 50mm tall, into which gel precursor solutions can be injected (Fig. 2-1b). All the channels are interconnected to allow media, nutrients, and cell-secreted proteins to be transported throughout the system. The main channels provide media and nutrients to support cell culture, while the gel chambers are designed to support 3D microscale tissues. The gel chambers are separated by micropillars, or posts,

which influence surface tension between the gel precursor solutions and the PDMS walls and thereby control where gel formation occurs, as previously described [17]. The chambers easily accommodate gels of virtually any identity [17], but here we utilized fibrin based in part on our prior studies showing the ability of fibrin gels to sustain capillary morphogenesis in 3D [14, 15].

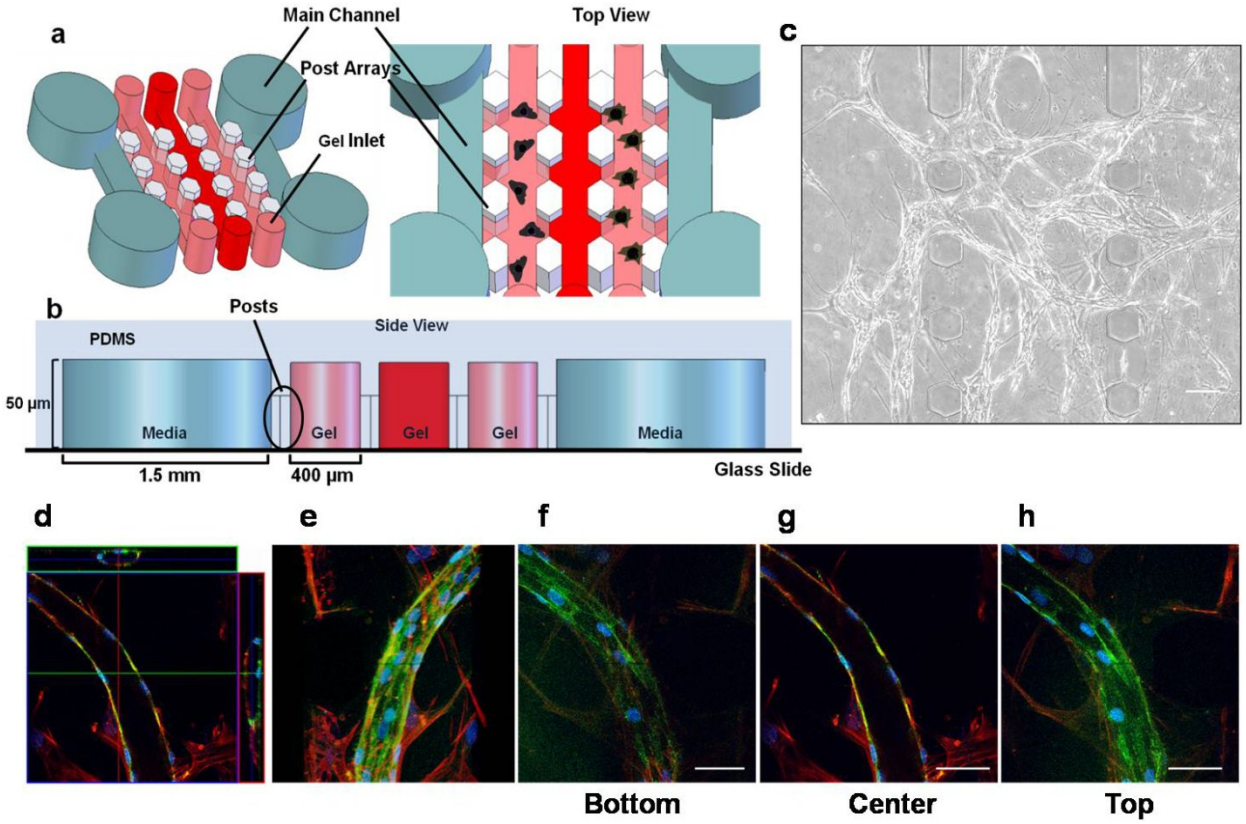

Figure 2-1: Formation of capillary-like networks in 3D fibrin gels within MFDs. (a) a schematic representation of MFD showing two parallel main channels, which provide media and nutrients to the gel channels to support cell culture. Gel channels (400 µm wide each) are injected with hydrogels through the gel inlets, and are separated by periodic hexagonal posts (100 µm in diameter) designed to contain hydrogels during the injection process. (b) side view of the PDMS device shows the location of polymerized hydrogels relative to the media channels (1.5 µm wide) and the hexagonal posts. Each microchannel (c) Phase-contrast image (day 14) of a primitive capillary plexus formed by ECs in the presence of stromal fibroblasts within fibrin gels in the MFDs. Scale bar = 100 µm. (d-h) High magnification (63×) confocal images from day 14 co-cultures stained for F-actin (with tetramethylrhodamine (TRITC)-conjugated phalloidin, red) and CD31 (with a FITC-conjugated donkey anti-mouse secondary, green). The nuclei were stained with DAPI in blue. (d) Confocal images shown in an orthogonal display mode highlight the XZ and the YZ views of the image stack (top and side of image), confirming the presence of hollow lumens. (e) Confocal images were stacked to obtain a 3D projection image. (f-h) A series of confocal slices was taken at 800 nm intervals in the z-direction from the bottom, center, and top sections of the sample being imaged, respectively. The entire thickness of the section of sample being imaged is 26 µm. Scale bar = 50 µm.

Fabrication of 3D cellular gel constructs in MFDs: To embed cells in 3D gel constructs within the MFD, cells were suspended in 100 mL prepolymer solutions containing 2.5 mg/mL bovine fibrinogen (Sigma, St. Louis, MO) and 2 mL of thrombin (50 U/mL; Sigma). From this 100 mL cell suspension, 20 mL was immediately withdrawn and pipetted into the inlet reservoirs of the gel chamber sections (Fig. 2-1). HUVECs (1×10^6 cells/mL) and stromal cells (NHLFs or MSCs, 5×10^6 cells/mL) were embedded separately in discrete gel channels at a constant 1:5 ratio. The cell-seeded gel constructs were allowed to polymerize for 20 min at 37°C and 5% CO2. Following polymerization, the inlet reservoirs of the main channels were filled with 200 mL of EGM-2 medium, which was suctioned through the main flow channels to wet them with media. All four inlet/outlet main channel reservoirs were then filled with EGM-2 culture medium, and the entire system incubated at 37°C and 5% CO2 in a standard cell culture incubator. The existing medium from the main channel reservoirs was removed and replaced with fresh medium daily. Experiments were performed for up to 14 days in MFDs.

Fluorescent labeling of HUVECs for both live-cell and fixed-cell imaging: In some experiments, HUVECs were fluorescently tagged using either red fluorescent protein (RFP) or cell tracker dyes in order to facilitate visualization of the capillary networks. RFP labeling was achieved via retroviral transduction using the Phoenix Retrovirus Expression Kit (Orbigen, San Diego, CA) as previously described [15]. For experiments involving the cell tracker dyes, SP-DiIC18 (3) (D7777) and SP-DiIC18 (3) (D7778) (Invitrogen), cells were labeled according to the manufacturer's protocol. In other experiments, cells within 3D fibrin gels in MFDs were fixed and stained for fluorescent imaging at defined end points. The various staining buffers were added and removed via the inlet/outlet reservoirs of the MFDs. The incubation times for different

stages of a typical staining procedure were extended to allow for diffusion across the 3D gel constructs.

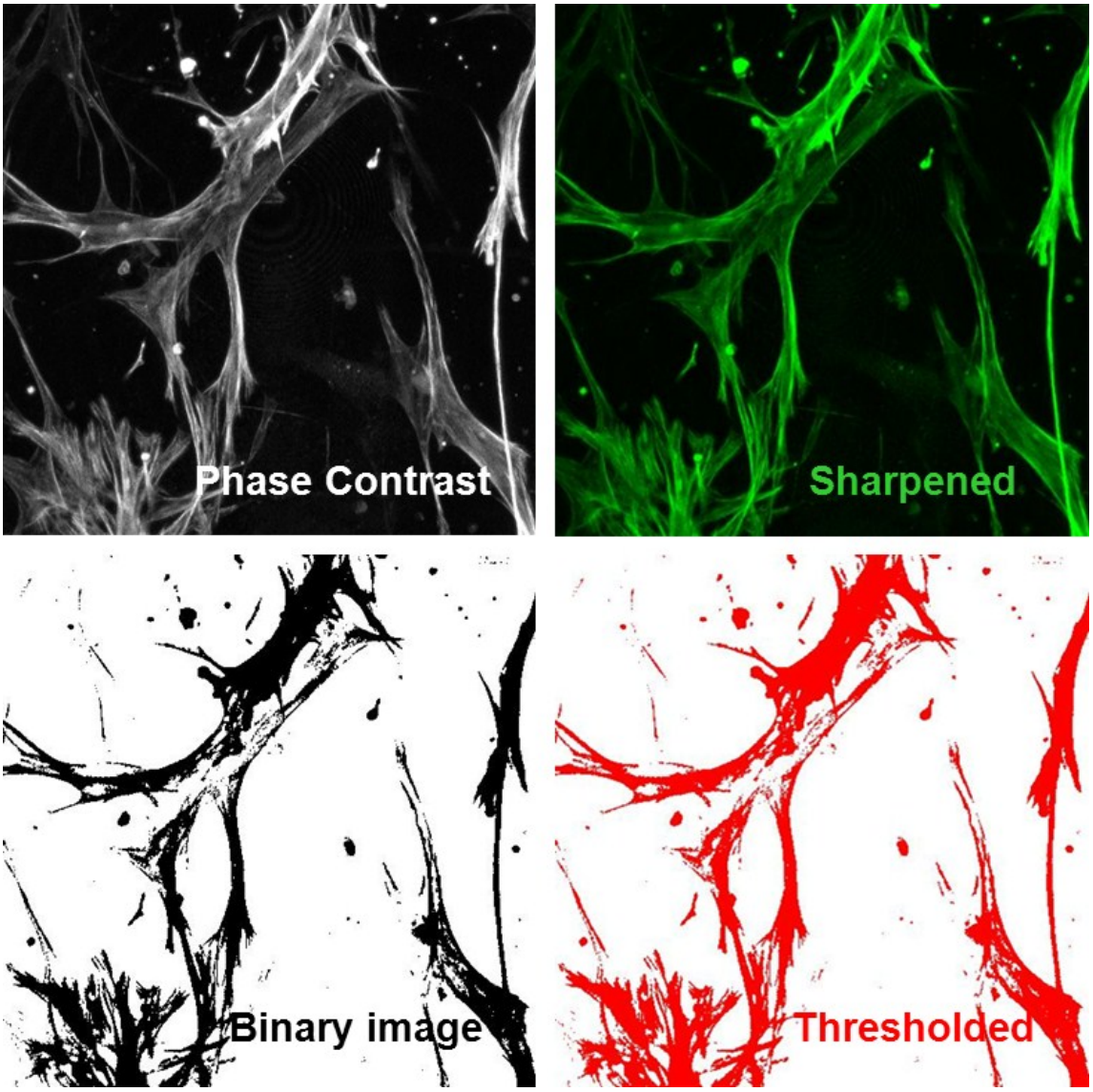

Figure 2-2: A metric to characterize the extent of capillary formation. We developed a quantitative image processing method. The way it works is that first Phase contrast images of the capillaries are sharpened, and then rendered binary and finally thresholded using Image J. The percent area occupied by these thresholded areas is then calculated by the software and reported as the percent of total image area occupied by the capillaries.

Fixed and permeabilized cells within the MFDs were incubated with primary antibodies overnight at 48C, while appropriate secondary antibodies for incubated for 3 h at 48C. Cell

nuclei were stained with DAPI, 1 mg/mL (Sigma) in PBS for 10 min. The following antibodies were used in this study: monoclonal mouse anti-human CD31, endothelial cell antibody, 1:100 (Dako, Glostrup, Denmark); monoclonal mouse a-smooth muscle actin (a-SMA), 1:200 (Abcam, Cambridge, MA); GoH3 rat monoclonal anti-a6 integrin, rat IgG (Millipore, Temecula, CA); monoclonal mouse laminin, 1:100 (Abcam); fluorescein (FITC)-conjugated donkey anti-mouse IgG secondary antibody, 1:100 (Jackson ImmunoResearch, West Grove, PA); Alexa Fluor 488 goat anti-mouse IgG secondary antibody, 1:400 (Invitrogen).

Confocal imaging: Capillary networks were visualized in 3D within MFDs using a Zeiss LSM 510 Meta multiphoton microscope (Carl Zeiss, Jena, Germany). Lasers with 488 and 564 nm wavelengths were used to illuminate samples. Using 63× oil immersion and 40× water immersion Plan-Apochromat objectives, Z-stack images were generated by scanning every 1.2 μm through samples 20-50 μm in thickness. Individual images of a Z stack were then merged using LSM Image Browser Software (Carl Zeiss) to generate 3D projections. These methods were used to qualitatively demonstrate the presence of hollow lumens within the capillary networks, and to visualize interactions between the stromal cells and the HUVECs.

Quantitative analysis of capillary-like structures: The rate of capillary network formation within MFDs was quantified by determining the area occupied by multicellular endothelial cord-like structures at discrete time points. Cord segments comprising RFP-labeled HUVECs were imaged at multiple time points within randomly chosen sections of the gels via an Olympus IX51 microscope equipped with a 100-W high pressure mercury lamp (Olympus America, Center Valley, PA) and QImaging camera. The fluorescent images acquired using QCapture Pro Software were then processed using open-source image processing software (NIH ImageJ, National Institute of Health, Bethesda, MD) as previously described [18]. Briefly, fluorescent

images of cord segments with defined edges were sharpened and thresholded. Next, these thresholded regions were traced, and the area occupied by these thresholded regions was finally calculated and summed to yield a percentage of the total image area occupied by the cord segments (Fig. 2-2). These cord-like segments were confirmed to ultimately develop into capillary networks with hollow lumens after 7 days in culture.

Statistical analysis: Statistical analysis was carried out using GraphPad Prism software. Data are reported as means standard deviations. All statistical comparisons were made by performing a one-way analysis of variance (ANOVA), followed by Bonferroni's multiple comparison tests to judge significance between two data sets at a time. P-values <0.05 are considered statistically significant.

2.3.RESULTS

HUVEC-stromal cell co-cultures form robust capillary networks within MFDs. To validate the use of our MFD as a model system capable of recreating and studying the perivascular niche in 3D, one of two minimal design constraints that must be satisfied is the MFD's capacity to support vasculogenesis in a 3D gel. To satisfy this criterion, endothelial cells (ECs) and stromal cells were embedded separately within 2.5 mg/mL fibrin gels in two discrete microchannels on either side of the MFDs. The microchannels were separated by an acellular microchannel in the middle, which contained only fibrin. Within 1-3 days following cell seeding, both the ECs and fibroblasts invaded the interstitial matrix to occupy the middle channel. We initially used NHLFs as our population of stromal cells based on their known ability to stimulate capillary formation in a similar *in vitro* model of angiogenesis [19]. In this vasculogenesis model, ECs aligned into

small multicellular aggregates, or cords, and within 3-5 days appeared to form complex network structures similar to the primitive capillary plexus observed in vasculogenesis (Fig. 2-3a) [20]. Association between the ECs and fibroblasts occurred by day 7 and increased through day 14. To facilitate visualization of the capillary structures, cultures in MFDs were stained for CD31/PECAM (green), F-actin (red), and nuclei (blue). Fluorescent imaging confirmed that the ECs differentiated into multicellular capillary-like structures in the presence of the fibroblasts (Fig. 2-3b, c, d, and e). The presence of hollow lumens, an important distinction of bona fide capillaries, was confirmed by confocal microscopy. A series of cross-sectional images across the cord-like structures in the Z direction confirmed the presence of hollow lumens, a hallmark of capillary networks observed in other 3D culture systems [14].

MSCs occupy a perivascular location within the MFDs and encourage EC-mediated deposition of basement membrane. A second minimal design constraint that our device needed to satisfy was the capacity to support the perivascular association of MSCs with the EC-derived vessel networks. We also hypothesized that the perivascular location of MSCs depends on the establishment of EC basolateral polarity and the deposition of a basement membrane, a thin network of ECM rich in laminin and collagen-IV that is a hallmark of a stable capillary network [21]. Thus, it was also crucial to demonstrate the presence of a basement membrane in EC-MSC co-cultures within the MFDs. To do so, capillary networks formed by co-culture of ECs and MSCs structures formed in the MFDs were stained for laminin at day 14, and then a series of Z-stack confocal images were captured (Fig. 2-3). These images confirmed that laminin (green) was deposited primarily around the periphery of the vessel structures, wrapping the capillary and more clearly marking the lumens (Fig 2-3a). Furthermore, MSCs were also found to act as vessel pericytes in EC-MSC co-cultures within the MFDs. After 14 days of culture within the MFDs,

microscale tissues were fixed and stained for α-SMA (green), a pericyte marker, and laminin (red). Confocal images showed the perivascular association of MSCs expressing α-SMA with capillary structures composed of ECs (Fig. 2-3b and c).

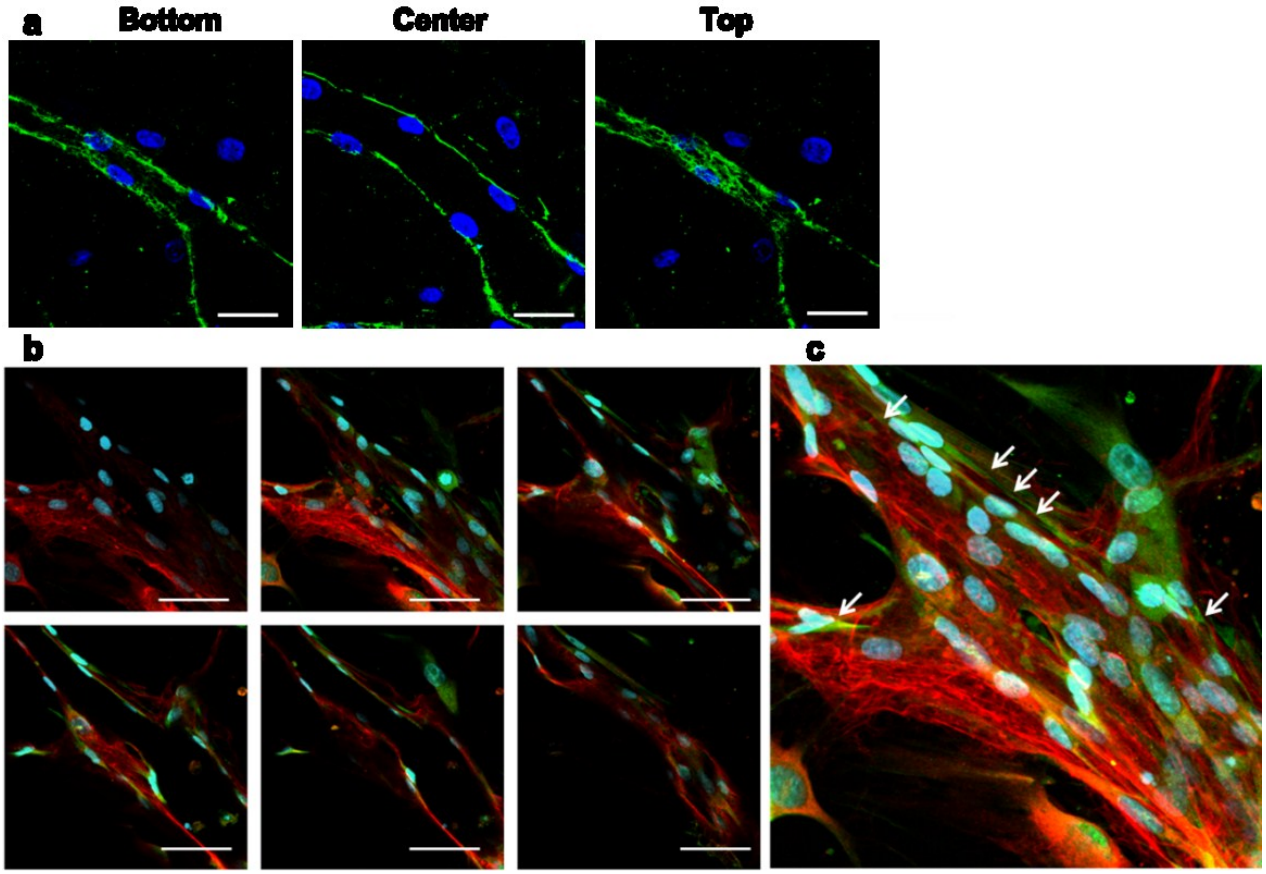

Figure 2-3: Basement membrane deposition and pericyte association in EC-MSC co-cultures. (a) Z-stack confocal slices demonstrate the presence of laminin (green) deposited around the basal surface of a capillary formed in an EC-MSC co-culture. Scale bar = 50 μm. (b) Confocal images from day 14 co-cultures also demonstrate an intimate perivascular association between MSCs and ECs in the nascent capillary network. MSCs stained for α-SMA (green) lie in close proximity to the newly deposited basement membrane (laminin, red). The top-left and bottom-right images represent the top and bottom sections of the sample, respectively. The rest of the confocal images represent a stack of four consecutive slices between the top and the bottom of the sample. Scale bar = 50 μm. (c) High magnification (40×) confocal images were stacked to obtain the 3D projection image. In all panels, nuclei are stained with DAPI (blue).

Confocal slices taken of different XY planes at multiple depths in the Z direction confirmed that the EC-MSC capillaries form hollow lumens (Fig. 2-3b), just as in EC-fibroblast co-cultures (Fig. 2-1). The MSCs retained their close proximity with the nascent capillaries over time, and eventually wrapped themselves around the forming vessels.

Stromal cells co-cultured with ECs in fibrin gels differentially affect the kinetics of capillary morphogenesis within MFDs. Having demonstrated that our MFD satisfies the two minimal design criteria to serve as an artificial perivascular niche, we next utilized it to assess if there were any differences in the rates of vessel formation induced by MSCs versus fibroblasts. Fibroblasts, MSCs and a variety of other stromal cell types (i.e., adipose-derived stem cells) can also stimulate capillary morphogenesis, but whether or not these distinct stromal populations stimulate the ECs via the same or distinct mechanisms remain unknown. Qualitatively, fibroblasts appeared more effective than MSCs in terms of their ability to induce ECs to organize into multicellular cord-like structures (Fig. 2-4a), despite the fact that both stromal cells eventually give rise to bona fide capillaries with hollow lumens. To measure these differences, we adapted a previously described image processing approach [18] to quantify the area occupied by RFP-expressing ECs in a set of randomly selected images within the MFDs. Quantitative analysis of the presence of the RFP signal within the images confirmed that the EC-fibroblast co-cultures generated multicellular cord-like networks at a significantly faster rate than did the EC-MSC co-cultures at both days 1 and 3 following cell seeding (Fig. 2-4a). Snapshots of movies of day 7 cultures show that capillaries driven by fibroblasts possessed well-defined cell-cells junctions, completely enclosed lumens, and a branched morphology, whereas MSC-driven networks were less organized and less mature at the same time point (Fig. 2-5).

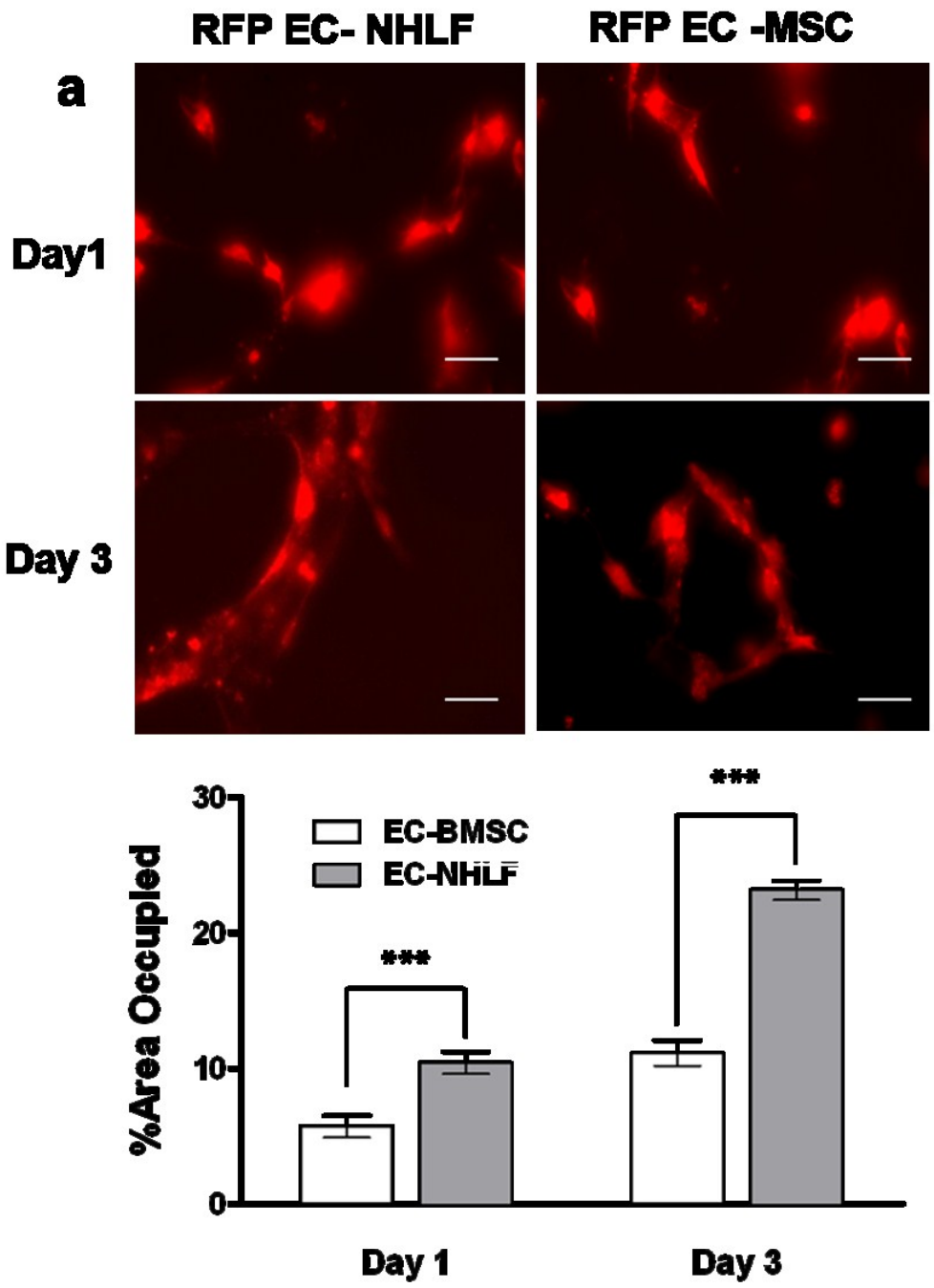

Figure 2-4: Differential effects of stromal cell populations on the rate of capillary morphogenesis within 3D fibrin gels in MFDs. (a) at days 1 and 3, fluorescent images of RFP-expressing ECs co-cultured with either unlabeled MSCs or fibroblasts (NHLFs) were obtained from triplicate MFDs for each condition. Scale bar = 20 μm. (b) The fluorescent areas in randomly selected images (n = 7) were then quantified as a metric of the extent of capillary network formation, revealing that NHLF-mediated network formation was significantly faster than MSC-mediated capillary morphogenesis

2.4.DISCUSSION

In this study, we have demonstrated that a relatively simple microfluidic platform supports the formation of a stable and mature vascular network in 3D, and effectively recapitulates the perivascular localization of MSCs *ex vivo*. ECs co-cultured with either stromal fibroblasts (NHLFs) or bone marrow derived MSCs in this microfluidic platform undergo a vasculogenic program to yield stable, pericyte-invested capillary networks with hollow, well-defined lumens confirmed via confocal microscopy. These results recapitulate the formation of capillary structures observed in larger 3D gel cultures [14, 19], demonstrating that this complex morphogenetic process can easily be scaled down to study within a MFD.

Microfluidic systems have long been touted as ideal tools with which to multifactor regulation of cell biological phenomena, especially given their ability to deliver multiple soluble factors with precise spatial and temporal control [22] and to conserve reagents based on their small size. However, the promise of such approaches has not yet been fully realized in part because most microfluidic systems involve rather cumbersome methodologies, and because their ability to support 3D cell cultures has only recently been demonstrated [23]. A promising recent study similarly utilized MFDs to develop vascular networks within 3D epithelial tissues *in vitro* [24], but the quality, stability, and physiological relevance of these vessel networks lacking mature pericytes was not clear. In our study, confocal images of EC-MSC and EC-NHLF co-cultures seeded within 3D fibrin gels in MFDs unambiguously confirm the presence of hollow lumens. Moreover, both MSCs and fibroblasts occupy perivascular locations and expressed pericyte markers when cultured with ECs within our MFD model.

We have previously shown that both fibroblasts and MSCs are capable of supporting capillary morphogenesis in 3D fibrin gels and in vivo, and that both are capable of acting as

pericytes that express α-SMA [25]. The capillary networks formed in the presence of these two different stromal populations within our MFD also possess similar morphological characteristics. However, the vessels generated from NHLF-EC co-cultures formed at a significantly faster rate than in the MSC-EC co-cultures.

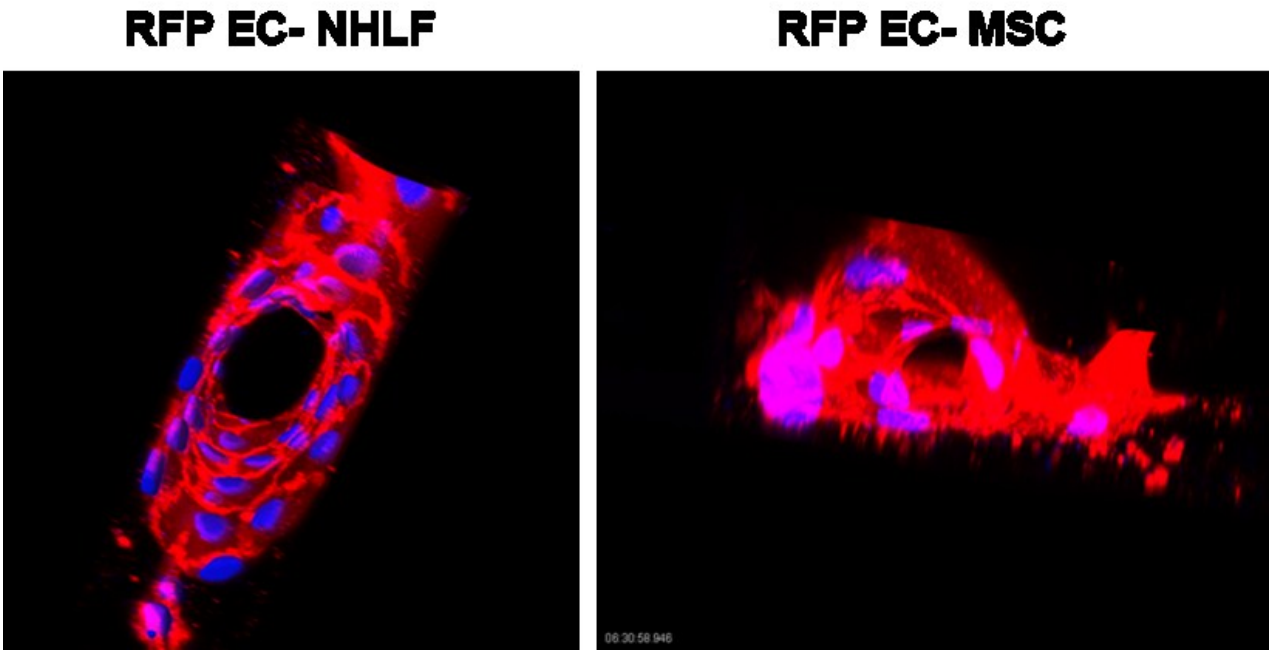

Figure 2-5: Differential effects of stromal cell populations on capillary morphogenesis within 3D fibrin gels within MFDs. Snapshots from the movies generated at day 7 show the presence of hollow lumens in capillary networks formed by EC-NHLF co-cultures and EC-MSC co-cultures.

Some distinctions in the mechanisms by which these two cell types promote capillary morphogenesis have recently been identified [25], and these differences may also account for the differential rates observed here as well. Although these experiments do not directly validate the utility of this platform as a tool for studying perivascular niches per se, it may be possible to utilize the small reagent volumes and amenability to high resolution imaging offered by the MFD to identify additional mechanistic distinctions between MSCs and fibroblasts in future studies.

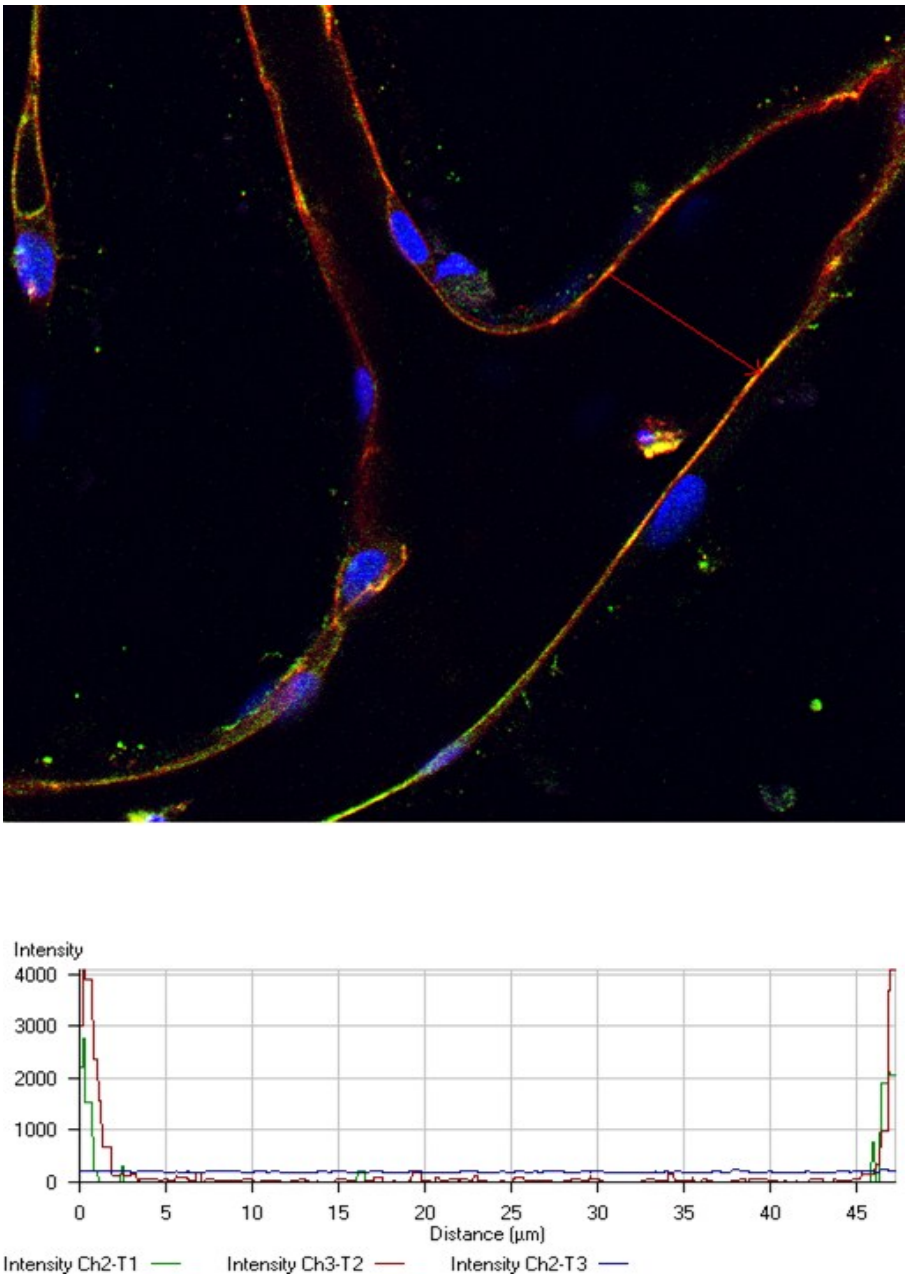

Figure 2-6: A metric for Quantification of lumen diameters. Lumen diameter can be quantified from confocal z-plane images of capillary structures using LSM510 software and fluorescent intensity to mark the edges of the vessel wall. In this case, the acellular lumenal structure bordered by areas of high fluorescence intensity (from tagged ECs with anti-CD31 antibody) is approximately 40 µm in diameter at its widest point.

When embedded within 3D fibrin gel constructs, ECs were surrounded by a fibrillar architecture, with pore sizes on the order of ~0.5 µm and undergo a very profound

morphogenetic program. This program resulted in the formation of capillary networks with well-defined hollow lumens on the order of 30-40 μm. Despite reports in the literature that ECs can form cord-like networks in some 2D cultures [26, 27], there is little evidence that these cord-like networks even remotely resemble capillaries, as they lack hollow lumens, appropriate polarity, and basement membranes. On the contrary, all of these hallmarks are present in the vessels created in our system.

Furthermore, it is noteworthy to mention that methods to quantify lumen diameters (size) of the capillary structures that form in this microscale system were readily available (Fig. 6-2). However, other objective metrics with respect to number and connectivity were not identified. Such metrics are more accurately and reproducibly measured in our previously published model of angiogenesis [14, 19, 25], in which ECs sprout from microcarrier beads that serve as a zero reference to facilitate quantification. In part because of these differences, our microfluidic system described here is more ideally suited for studying the perivascular regulation of MSCs, rather than as a quantitative assay of vasculogenesis.

2.5.CONCLUSION

To facilitate our efforts to understand the significance of the perivascular association of most adult stem cells, the goal of this study was to transfer our existing 3D fibrin-based model system into a novel microfluidic device, and demonstrate the ability of this device to support the formation of capillary blood vessels. Our findings to date validate the use of this novel 3D engineered niche as a model system in which to study capillary morphogenesis.

Microfluidic devices were generated using standard PDMS-based soft lithography and rapid prototyping methods. Resulting PDMS devices were permanently bonded to a glass slide following treatment with an air-plasma, forming enclosed microfluidic channels. ECs suspended within 3D fibrin gels patterned in the device adjacent to stromal cells (either fibroblasts or bone marrow-derived MSCs) executed a morphogenetic process akin to vasculogenesis, forming a primitive vascular plexus and maturing into a robust capillary network with hollow well-defined lumens. Both MSCs and fibroblasts formed pericytic associations with the ECs but promoted capillary morphogenesis with distinct kinetics. Phase contrast microscopy revealed that HUVECs cultured in the presence of stromal cells within these devices form a network structure similar to a primitive capillary plexus. Confocal microscopy confirmed that the ECs formed capillary-like structures with well-defined lumens in the presence of stromal cells in fibrin gels constructed within the microfluidic device. Immunofluorescent staining of α-SMA confirmed an intimate perivascular association of these stromal cells (either fibroblasts or MSCs) with the endothelial cells involved in capillary like structures.

This versatile multichannel device was explicitly designed to allow multiple discrete constructs of three-dimensional cell-laden hydrogels to be easily patterned, and to permit the study of EC-pericyte interactions. These studies demonstrate the potential of this engineered stem cell niche as a multipurpose model system in which to study capillary morphogenesis. This system will allow for studying the interactions between distinct cell types embedded in 3D fibrin gels. In addition, the optical clarity and relatively thin profile of the MFD allow for higher resolution images, while the small volumes allow valuable reagents to be conserved. Having shown that adult stem cells introduced into this system recapitulate their endogenous perivacular niches, the focus of the next chapter is utilize this model to assess whether the interaction

between the α6β1 integrin receptor on MSCs and EC-deposited laminin is required for pericyte association of MSCs with the capillary networks. The system described in this chapter can also be suitable for studying the perivascular regulation of MSCs.

2.6.REFERENCES

1. Discher, D.E., D.J. Mooney, and P.W. Zandstra, Growth factors, matrices, and forces combine and control stem cells. Science, 2009. 324(5935): p. 1673-7.

2. Moore, K.A. and I.R. Lemischka, Stem cells and their niches. Science, 2006. 311(5769): p. 1880-5.

3. Bordignon, C., Stem-cell therapies for blood diseases. Nature, 2006. 441(7097): p. 1100-2.

4. Fuchs, E., T. Tumbar, and G. Guasch, Socializing with the neighbors: stem cells and their niche. Cell, 2004. 116(6): p. 769-78.

5. Scadden, D.T., The stem-cell niche as an entity of action. Nature, 2006. 441(7097): p. 1075-9.

6. Srivastava, D. and K.N. Ivey, Potential of stem-cell-based therapies for heart disease. Nature, 2006. 441(7097): p. 1097-9.

7. Engler, A.J., et al., Matrix elasticity directs stem cell lineage specification. Cell, 2006. 126(4): p. 677-89.

8. Shen, Q., et al., Endothelial cells stimulate self-renewal and expand neurogenesis of neural stem cells. Science, 2004. 304(5675): p. 1338-40.

9. Shen, Q., et al., Adult SVZ stem cells lie in a vascular niche: a quantitative analysis of niche cell-cell interactions. Cell Stem Cell, 2008. 3(3): p. 289-300.

10. Tavazoie, M., et al., A specialized vascular niche for adult neural stem cells. Cell Stem Cell, 2008. 3(3): p. 279-88.

11. Crisan, M., et al., A perivascular origin for mesenchymal stem cells in multiple human organs. Cell Stem Cell, 2008. 3(3): p. 301-13.

12. Kiel, M.J. and S.J. Morrison, Uncertainty in the niches that maintain haematopoietic stem cells. Nat Rev Immunol, 2008. 8(4): p. 290-301.

13. Caplan, A.I., All MSCs are pericytes? Cell Stem Cell, 2008. 3(3): p. 229-30.

14. Ghajar, C.M., et al., Mesenchymal stem cells enhance angiogenesis in mechanically viable prevascularized tissues via early matrix metalloproteinase upregulation. Tissue Eng, 2006. 12(10): p. 2875-88.

15. Ghajar, C.M., et al., The effect of matrix density on the regulation of 3-D capillary morphogenesis. Biophys J, 2008. 94(5): p. 1930-41.

16. Chen, X., et al., Prevascularization of a fibrin-based tissue construct accelerates the formation of functional anastomosis with host vasculature. Tissue Eng Part A, 2009. 15(6): p. 1363-71.

17. Huang, C.P., et al., Engineering microscale cellular niches for three-dimensional multicellular co-cultures. Lab Chip, 2009. 9(12): p. 1740-8.

18. Ghajar, C.M., et al., A novel three-dimensional model to quantify metastatic melanoma invasion. Mol Cancer Ther, 2007. 6(2): p. 552-61.

19. Ghajar, C.M., S.C. George, and A.J. Putnam, Matrix metalloproteinase control of capillary morphogenesis. Crit Rev Eukaryot Gene Expr, 2008. 18(3): p. 251-78.

20. ten Dijke, P. and H.M. Arthur, Extracellular control of TGFbeta signalling in vascular development and disease. Nat Rev Mol Cell Biol, 2007. 8(11): p. 857-69.

21. Jain, R.K., Molecular regulation of vessel maturation. Nat Med, 2003. 9(6): p. 685-93.

22. Mosadegh, B., et al., Generation of stable complex gradients across two-dimensional surfaces and three-dimensional gels. Langmuir, 2007. 23(22): p. 10910-2.

23. Gillette, B.M., et al., In situ collagen assembly for integrating microfabricated three-dimensional cell-seeded matrices. Nat Mater, 2008. 7(8): p. 636-40.

24. Sudo, R., et al., Transport-mediated angiogenesis in 3D epithelial coculture. FASEB J, 2009. 23(7): p. 2155-64.

25. Ghajar, C.M., et al., Mesenchymal cells stimulate capillary morphogenesis via distinct proteolytic mechanisms. Exp Cell Res, 2010. 316(5): p. 813-25.

26. Saunders, R.L. and D.A. Hammer, Assembly of Human Umbilical Vein Endothelial Cells on Compliant Hydrogels. Cell Mol Bioeng, 2010. 3(1): p. 60-67.

27. Yee, D., et al., Hyaluronic Acid hydrogels support cord-like structures from endothelial colony-forming cells. Tissue Eng Part A, 2011. 17(9-10): p. 1351-61.

CHAPTER 3

THE REQUIREMENT OF THE α6β1 INTEGRIN-LAMININ INTERACTIONS FOR PERICYTE ASSOCIATION OF BMSCS WITH ECS

3.1 INTRODUCTION

In Chapter 2, the perivascular localization of MSCs was effectively recapitulated in our simple MFD. In this chapter, the utility of the microfluidic platform as an artificial perivascular niche will be explored, in order to demonstrate that the interaction between EC-deposited laminin and the α6β1 integrin receptor on the BMSCs is required for the proper perivascular localization of MSCs.

A large body of work suggests that stem cells live in a perivascular niche in almost all adult tissues, where they associate with blood vessels [1]. For instance, hematopoietic stem cells (HSCs) reside along the endosteal surface of trabecular bone in close proximity to both bone forming osteoblasts and the endothelial cells that line blood vessels [2]. HSCs can leave this niche, enter the circulation, and return to the niche. The hypothesis is that this close proximity to endothelial cells may facilitate mobilization of HSCs from the bone marrow into the circulation. Another example would be neural stem cells (NSCs) that are found in two different locations in the brain: within the subventricular zone of the hippocampus and in the olfactory bulb. In both niches, NSCs are located adjacent to endothelial cells similar to HSCs [3]. As mentioned before in Chapter 1, NSCs interact with capillaries in part through their α6β1 integrin and EC-deposited laminin, and this interaction appears to be critical for maintaining NSC quiescence. Given the

fact that MSCs also express α6β1 integrin, the second aim of this thesis utilizes the artificial niche to test the hypothesis that MSCs also require an α6β1 integrin-laminin interaction to occupy a periendothelial location.

This chapter provides two new key contributions. First, it demonstrates that a relatively simple microfluidic platform makes it possible to form pericyte-invested vascular networks in 3D, and effectively recapitulate the perivascular localization of MSCs *ex vivo* to study the molecular interactions between ECs and MSCs via biochemical studies, including integrin blocking assays. Second, the data demonstrate the utility of this platform to mechanistically explore how MSCs interact with the vasculature by showing that the α6β1 integrin receptor is required for the perivascular interactions between MSCs and capillaries.

3.2 METHODS

Fluorescent labeling of HUVECs for both live-cell and fixed-cell imaging: In some experiments, HUVECs were fluorescently tagged using either red fluorescent protein (RFP) or cell tracker dyes in order to facilitate visualization of the capillary networks. RFP labeling was achieved via retroviral transduction using the Phoenix Retrovirus Expression Kit (Orbigen, San Diego, CA) as previously described [4]. For experiments involving the cell tracker dyes, SP-DiIC18 (3) (D7777) and SP-DiIC18 (3) (D7778) (Invitrogen), cells were labeled according to the manufacturer's protocol. In other experiments, cells within 3D fibrin gels in MFDs were fixed and stained for fluorescent imaging at defined end points. The various staining buffers were added and removed via the inlet/outlet reservoirs of the MFDs. The incubation times for different stages of a typical staining procedure were extended to allow for diffusion across the 3D gel

constructs. Fixed and permeabilized cells within the MFDs were incubated with primary antibodies overnight at 48C, while appropriate secondary antibodies for incubated for 3 h at 48C. Cell nuclei were stained with DAPI, 1 mg/mL (Sigma) in PBS for 10 min. The following antibodies were used in this study: GoH3 rat monoclonal anti-a6 integrin, rat IgG (Millipore, Temecula, CA); fluorescein (FITC)-conjugated donkey anti-mouse IgG secondary antibody, 1:100 (Jackson ImmunoResearch, West Grove, PA).

Integrin blocking studies in MFDs: The role of the interaction between α6β1 integrin and laminin in the perivascular association of MSCs and capillaries was assessed using an anti-α6 integrin monoclonal antibody (GoH3; Millipore). First, the optimal concentration of antibody required to block MSC adhesion was identified using standard cell adhesion assays as previously described (Kikkawa et al., 1994). Briefly, 96-well microtiter plates (Nunc, Wiesbaden, Germany) were coated with natural mouse laminin (10 μg/mL) at 37°C for 1 h and then blocked with PBS containing 1% BSA for another hour. Rat monoclonal antibodies against α6 integrin at three different concentrations (24, 30, and 40 μg/mL) were preincubated with MSC suspensions (3×10^5 cells/mL) in serum-free DMEM for 15 min; then 0.1mL of the cell suspension was added to each well of the 96-well plate. Cells were incubated at 37°C for 1 h, at which point non-adherent cells were washed away. The attached cells were fixed and stained with a 0.4% crystal violet in methanol (w/v) for 30 min. After washing with distilled water, the stain was extracted with 0.1M citrate in 50% ethanol. The absorbance of each well of the plates was measured at 590 nm with a microplate reader (Bio-Rad, Philadelphia, PA). Using the results from these adhesion-blocking assays, MFDs with MSC–HUVEC co-cultures (5:1 ratio of MSCs to HUVECs) were used to explore the role of this integrin in their interaction. MSCs were cultured in serum-free DMEM for 2 days prior to seeding within the MFDs. They were then pre-incubated with anti-α6

integrin blocking antibody at 40 µg/mL concentration for 20 min prior to seeding them within 2.5 mg/mL fibrin gels in one of the side channels. HUVECs were seeded within fibrin gels in the other side channel.

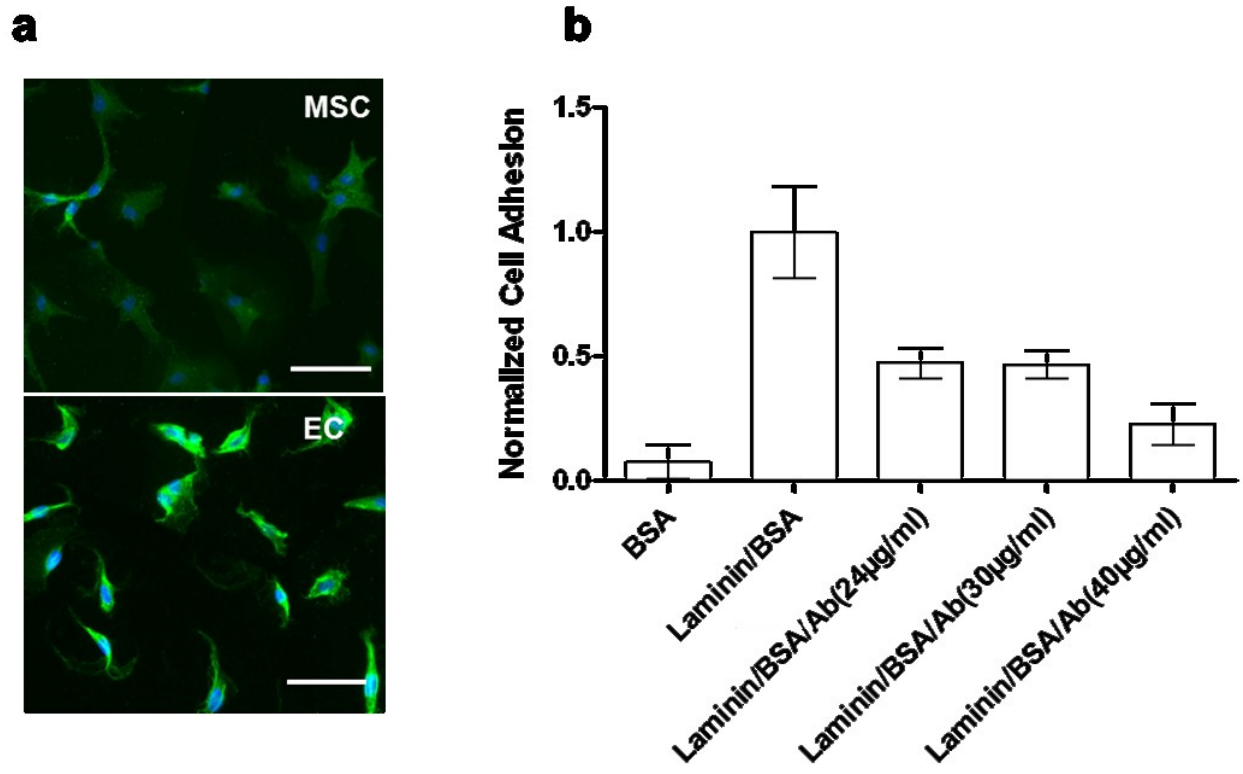

Figure 3-1: Detection of α6 integrin subunit expression in ECs and MSCs as well as disruption of MSC adhesion to laminin coated surfaces via α6 integrin inhibition. (a) Both ECs and MSCs express the α6 integrin subunit (green). Scale bar = 50 µm. (b) Adhesion of MSCs pre-incubated with the anti-α6 integrin blocking antibody to laminin-coated surfaces was quantified using a crystal violet assay. Raw data generated as absorbance values were normalized to control conditions (adhesion to laminin, blocked with BSA) to correspond to the relative numbers of attached cells to various conditions.

A middle channel containing only fibrin physically separated the two populations of cells. Experiments were performed for up to 3 days in MFDs. A complementary experiment where the anti-integrin blocking antibody was added to intact vessels was also performed to determine if

pericytes would dissociate from HUVECs. In these experiments, MSC–HUVEC co-cultures (5:1 ratio) were established in MFDs for 7 days, enabling the formation of HUVEC-lined capillaries surrounded by MSCs as pericytes. Cultures were then incubated with anti-α6 integrin blocking antibody at 40 μg/mL concentration for additional 4 days

Statistical analysis: Statistical analysis was carried out using GraphPad Prism software. Data are reported as means standard deviations. All statistical comparisons were made by performing a one-way analysis of variance (ANOVA), followed by Bonferroni's multiple comparison tests to judge significance between two data sets at a time. P-values <0.05 are considered statistically significant.

3.3 RESULTS

The molecular interactions between MSCs and ECs were probed using the ex vivo perivascular niche. We utilized our microfluidic *ex vivo* model of the perivascular niche to test the hypothesis that MSCs require α6β1 integrin-laminin interactions to occupy a periendothelial location. This hypothesis is based on the fact that NSCs, which also occupy perivascular locations, interact with capillaries in part through their α6β1 integrin and EC-deposited laminin [3], and we reasoned that the common perivascular location of NSCs and MSCs *in vivo* may be due to similar adhesive mechanisms.

To investigate this possibility, it was first confirmed that MSCs express α6β1 integrin (Fig. 3-1a) and that their adhesion to laminin can be blocked in a dose dependent fashion in the presence of a monoclonal antibody targeting the α6 integrin subunit [5] (Fig. 3-1b). Next, this antibody was used to test the requirement for the α6β1 integrin subunit for MSC-EC interactions

in the MFD-based *ex vivo* perivascular niche. EC-MSC co-cultures in 3D fibrin gels were established and matured for 7 days, with the MSCs adopting a pericyte location (Fig. 3-2).

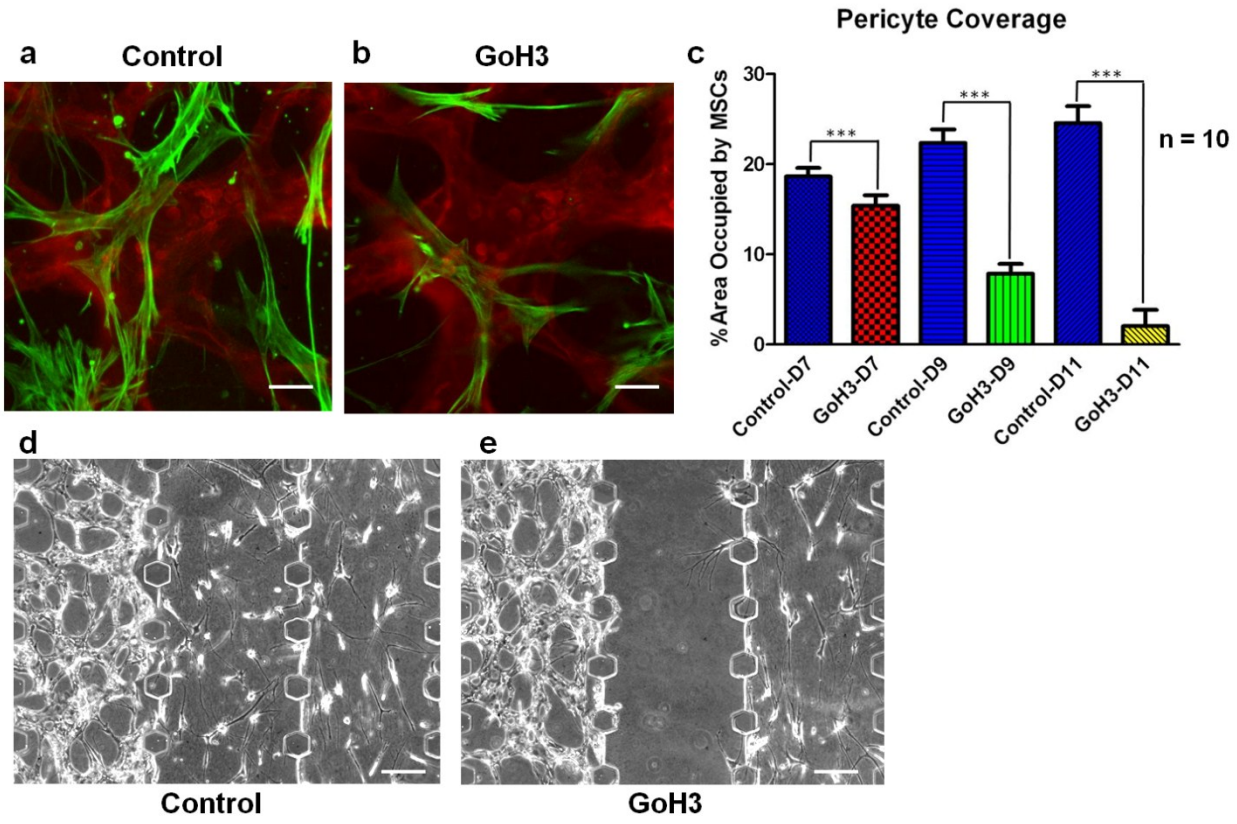

Figure 3-2: EC-MSC interactions require the α6 integrin subunit. (a) Capillary networks were formed by ECs (red) and MSC (green) co-cultures and allowed to mature for 7 days. Cells were fluorescently labeled using cell tracker dyes. (b) Two days after incubating the cultures containing intact capillary networks with an anti-α6 integrin antibody, the association of MSCs with the capillary networks was disrupted. Scale bar = 50 μm**.** (c) The percentage area occupied by MSCs near and around capillaries was quantified in control cultures at days 7, 9, and 11, and compared to cultures incubated with anti-α6 integrin antibody (GoH3) for each time point. A total of 10 fluorescent images were quantified per condition. (d, e) Phase contrast images from day 3 EC-MSC co-cultures within MFDs in the absence (control, left) or presence (right) of the anti-α6 integrin antibody show that blocking α6 integrin also prevents the recruitment of MSCs to the perivascular niche. Capillary networks were formed in the gel channels on the left side, and MSC cultures were initiated on the right. Anti-α6 integrin antibody was added to main channel on the right hand side only, proximal to the MSC. Scale bar = 100 μm.

On day 7, the antibody targeting the α6 integrin subunit was added to the device via one of the media channels proximal to the initial MSC compartment, allowing it to diffuse towards

the capillary networks. After an additional 2 and 4 days of culture, the MSCs moved away from the vascular surface and the extent of pericyte coverage was quantitatively reduced by the presence of the antibody (Fig. 3-2c), presumably due to the competition between the antibody and the laminin-rich basement membrane for the MSC's α6β1 integrin. When the blocking antibody was introduced earlier in the culture period, before the establishment of EC-pericytes interactions, MSCs failed to migrate through the fibrin gels and did not localize adjacent to the EC networks when compared to controls (Fig. 3-2d, e). The blocking antibody was also used to test the requirement for the α6β1 integrin subunit for EC-fibroblast interactions in the MFD-based *ex vivo* perivascular niche. EC-fibroblast co-cultures in 3D fibrin gels were established and matured for 7 days, with the MSCs adopting a pericyte location (Fig. 3-3a) and the blocking antibody targeting α6 integrin was added to cultures in the same fashion as described previously. After an additional 2 and 4 days of culture, the fibroblasts invaded the gels and interact with the vascular surface. Furthermore, addition of the blocking antibody earlier in the culture period did not block EC-fibroblast interactions (Fig. 3-3b).

3.4 DISCUSSION

This chapter describes the application of our well-established microfluidic platform to construct novel 3D models of a perivascular stem cell niche. Utilizing this relatively simple device, we demonstrated that the α6β1 integrin-laminin interactions are required for the pericyte association of BMSCs with ECs. Fibrin matrices were used for the co-culture of ECs and BMSCs within microfluidic channels. These experiments resulted in the formation of a vascular plexus-like morphogenetic structure and a capillary network containing lumens. The morphogenetic process was shown to be dependent on α6β1 integrin-binding.

The development of microfluidic technologies has paved the way for new approaches to manipulate and monitor cells in an environment that more closely mimics the *in vivo* conditions. The major advantage of microfluidic systems is their ability to use small quantities of cells and reagents, precise control of spatial and temporal environment and high resolution visualization of cellular events in real-time [6, 7]. A number of microfluidic devices have been developed to recapture *in vivo* angiogenesis and to study the mechanisms involved in this biological process [6, 8-10]. Some of them are limited to 2D culture. A multi-parameter control microfluidic platform was previously developed to study capillary morphogenesis and demonstrate the role of pro-angiogenic factor gradients, shear stress and interstitial flow in angiogenesis in a defined 3D environment [6]. However, patterning gels in this device with microinjection was cumbersome and required a very complex system including, a manual micromanipulator, microliter syringe, digital microscope and a monitor for visual guidance. These experimental setups are not readily available in most biomedical labs. In this study, we used a simple microfluidic device, which allows precise patterning of 3D gels into microfluidic channel with pipette only, based on modifying and optimizing microfluidic devices developed previously [11].

Many 3D culture systems already exist to study capillary morphogenesis in vitro, including those that serve as models of vasculogenesis [8] as well as those intended to model angiogenesis [12]. However, the key new contribution provided by this study is the recapitulation of the perivascular niche *ex vivo* to mechanistically explore how MSCs interact with the vasculature. It is already widely recognized that MSCs facilitate angiogenesis in part by acting as stabilizing pericytes [13], and that much of their potential therapeutic benefit is based on their capacity to secrete pro-regenerative (including pro-angiogenic) factors [14]. MSCs also facilitate capillary development in part by influencing the expression levels of critical matrix remodeling enzymes

[15]. However, several recent studies suggest that the perivacular location of MSCs and other adult stem cells may act as a critical anatomic cue that maintains their multilineage potential, in part due to their direct and indirect interactions with endothelial cells. NSCs, like MSCs, have also been shown to reside in perivascular niches *in vivo* [3, 16]. NSCs interact with capillaries in part through the binding of their α6β1 integrin to EC-deposited laminin, and this interaction appears to be critical for maintaining their quiescence [3]. In this study, we were able to explore the interaction between MSCs and EC-deposited basement membrane in our artificial perivascular niche.

We report for the first time that the α6β1 integrin receptor is required for the perivascular interactions between MSCs and capillaries, as shown by our data indicating that treating MSCs with an anti-α6 integrin antibody prevented their perivascular association. When the antibody was added to intact vessels with perivascular MSCs, the MSCs moved away from the vascular surface in a manner similar to that observed for neural progenitor cells in mice infused with the same anti-α6 integrin antibody in their lateral ventricle [3]. Interestingly though, the addition of the GoH3 antibody did not inhibit EC-NHLF interactions. NHLFs that were treated with the blocking antibody still invaded the middle channel toward the endothelial forming capillaries (Fig. 3-3b). Nor did the addition of the blocking antibody to NHLFs prevent them from localizing themselves adjacent to EC networks and form perivascular association with the intact capillary networks as shown by our data demonstrating that treating NHLFs with an anti-α6 integrin antibody did not alter the pericytic coverage provided by NHLFs (Fig. 3-3a). These Integrin blocking assays of both EC-MSC and EC-fibroblast co-cultures revealed that the interaction between α6β1 integrin receptor and EC-deposited laminin is a feature unique to MSCs in our model system.

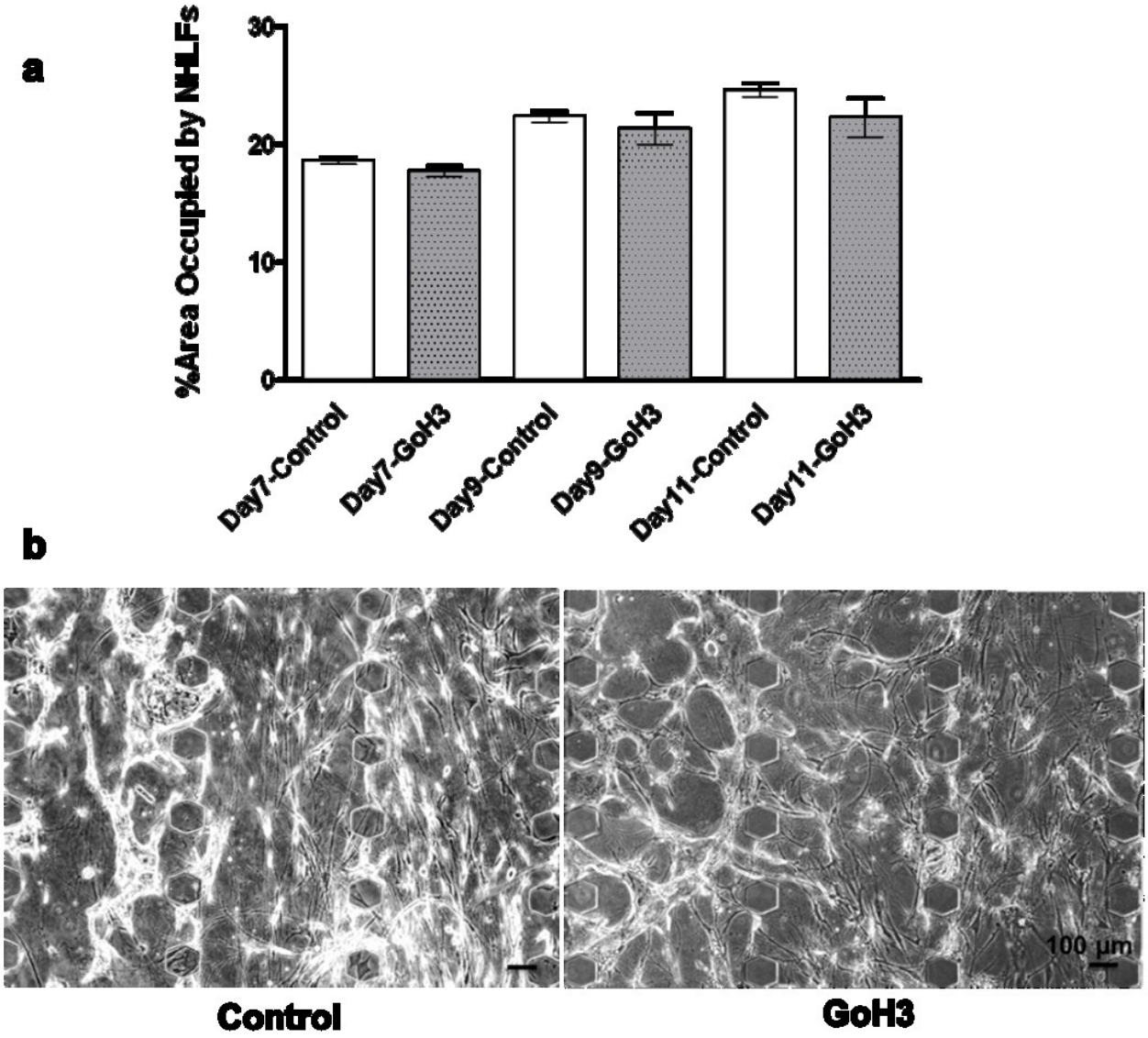

Figure 3-3: EC-NHLF interactions do not require the α6 integrin subunit. (a) The percentage area occupied by MSCs near and around capillaries was quantified in control cultures at days 7, 9, and 11, and compared to cultures incubated with anti-α6 integrin antibody (GoH3) for each time point. A total of 10 fluorescent images were quantified per condition. (b) Phase contrast images from day 3 EC-NHLF co-cultures within MFDs in the absence (control, left) or presence (right) of the anti-α6 integrin antibody show that blocking α6 integrin does not inhibit the interactions between NHLFs and ECs. Capillary networks were formed in the gel channels on the left side, and NHLF cultures were initiated on the right. Anti-α6 integrin antibody was added to main channel on the right hand side only, proximal to the NHLFs. Scale bar = 100 µm.

Collectively, these data confirmed our hypothesis that MSCs' perivascular location requires the interaction between the laminin-rich basement membrane of the capillaries and the α6β1 integrin adhesion receptor on MSCs for their pericytic association. Because other adult stem cells

may also localize to perivascular niches *in vivo* via similar mechanisms, our system may facilitate efforts to dissect the consequences of this association.

3.5 CONCLUSION

Many different approaches to engineer artificial stem cell niches based on biomaterials, drug delivery, and microfluidic approaches are currently being explored [17]. However, a common anatomic feature of many adult stem cell niches, that is, its proximity to the vasculature, may in and of itself be instructive in a way that cannot be recapitulated by the presentation of soluble and insoluble biochemical cues or by endothelial-conditioned media. Furthermore, endothelial cells may also enhance the regenerative potential of progenitor cells independent of their ability to form functional connections to the host vasculature [18]. By leveraging the microfluidic channels within our system to present soluble biochemical cues in gradient fashion and to spatially pattern discrete biomaterials and cell types [19], the method and the supporting data presented here provide a novel way to recapitulate and study perivascular niches *ex vivo*, and suggest a new approach to explore the regulation of adult stem cells. While other groups have demonstrated vasculogenesis within microfluidic systems, we have extended our platform in a novel direction by exploring how MSCs interact with the vessels. This is a possible first step to better understand how MSC multipotency may be regulated by vessel structure.

Summing up the first and second aims of this thesis, I first demonstrated that a relatively simple microfluidic platform supported the formation of a pericyte-invested vascular network in 3D, and effectively recapitulated the perivascular localization of MSCs *ex vivo*. Second, the utility of this platform to mechanistically explore how MSCs interact with the vasculature was

demonstrated by showing that the α6β1 integrin receptor is required for the perivascular interactions between MSCs and capillaries. These two new key contributions were enabled by performing experiments in the microfluidic system, whose small size enabled high resolution imaging more easily than would a thick 3D gel and helped to conserve valuable reagents. Next, I demonstrated the requirement of the interaction between EC-deposited laminin and the α6β1 integrin receptor on the MSCs for the proper perivascular localization of MSCs is demonstrated using our microfluidic platform. Having shown that adult stem cells introduced into this system recapitulate their endogenous perivascular niche, Chapter 5 will focus on further dissecting these molecular interactions using an *in vitro* fibrin-based angiogenesis model that allows for more quantitative analyses.

3.6 REFERENCES

1. Morrison, S.J. and A.C. Spradling, Stem cells and niches: mechanisms that promote stem cell maintenance throughout life. Cell, 2008. 132(4): p. 598-611.

2. Yin, T. and L. Li, The stem cell niches in bone. J Clin Invest, 2006. 116(5): p. 1195-201.

3. Shen, Q., et al., Adult SVZ stem cells lie in a vascular niche: a quantitative analysis of niche cell-cell interactions. Cell Stem Cell, 2008. 3(3): p. 289-300.

4. Ghajar, C.M., et al., The effect of matrix density on the regulation of 3-D capillary morphogenesis. Biophys J, 2008. 94(5): p. 1930-41.

5. Sonnenberg, A., et al., A complex of platelet glycoproteins Ic and IIa identified by a rat monoclonal antibody. J Biol Chem, 1987. 262(21): p. 10376-83.

6. Vickerman, V., et al., Design, fabrication and implementation of a novel multi-parameter control microfluidic platform for three-dimensional cell culture and real-time imaging. Lab Chip, 2008. 8(9): p. 1468-77.

7. Carrion, B., et al., Recreating the perivascular niche ex vivo using a microfluidic approach. Biotechnol Bioeng, 2010. 107(6): p. 1020-8.

8. Chung, S., et al., Cell migration into scaffolds under co-culture conditions in a microfluidic platform. Lab Chip, 2009. 9(2): p. 269-75.

9. Chung, S., et al., Microfluidic platforms for studies of angiogenesis, cell migration, and cell-cell interactions. Sixth International Bio-Fluid Mechanics Symposium and Workshop March 28-30, 2008 Pasadena, California. Ann Biomed Eng, 2010. 38(3): p. 1164-77.

10. Shamloo, A., et al., Endothelial cell polarization and chemotaxis in a microfluidic device. Lab Chip, 2008. 8(8): p. 1292-9.

11. Mosadegh, B., et al., Generation of stable complex gradients across two-dimensional surfaces and three-dimensional gels. Langmuir, 2007. 23(22): p. 10910-2.

12. Koh, W., et al., In vitro three dimensional collagen matrix models of endothelial lumen formation during vasculogenesis and angiogenesis. Methods Enzymol, 2008. 443: p. 83-101.

13. Crisan, M., et al., A perivascular origin for mesenchymal stem cells in multiple human organs. Cell Stem Cell, 2008. 3(3): p. 301-13.

14. Wagner, J., et al., Optimizing mesenchymal stem cell-based therapeutics. Curr Opin Biotechnol, 2009. 20(5): p. 531-6.

15. Ghajar, C.M., et al., Mesenchymal stem cells enhance angiogenesis in mechanically viable prevascularized tissues via early matrix metalloproteinase upregulation. Tissue Eng, 2006. 12(10): p. 2875-88.

16. Tavazoie, M., et al., A specialized vascular niche for adult neural stem cells. Cell Stem Cell, 2008. 3(3): p. 279-88.

17. Lutolf, M.P., P.M. Gilbert, and H.M. Blau, Designing materials to direct stem-cell fate. Nature, 2009. 462(7272): p. 433-41.

18. Kaigler, D., et al., Endothelial cell modulation of bone marrow stromal cell osteogenic potential. FASEB J, 2005. 19(6): p. 665-7.

19. Huang, C.P., et al., Engineering microscale cellular niches for three-dimensional multicellular co-cultures. Lab Chip, 2009. 9(12): p. 1740-8.

CHAPTER 4

BONE MARROW DERIVED MESENCHYMAL STEM CELLS ELICIT AN ANGIOGENIC RESPONSE VIA THEIR α6β1 INTEGRIN RECEPTOR

4.1 INTRODUCTION

BMSCs facilitate the angiogenic behavior of ECs within 3D matrices *in vitro* and in engineered tissues in vivo in part by acting as stabilizing pericytes. However, the molecular interactions between ECs and BMSCs during the process of angiogenesis are poorly understood. In this chapter, a tractable fibrin-based 3D co-culture model of angiogenesis was used to explore the interaction between EC-deposited laminin and the α6β1 integrin adhesion receptor on BMSCs, and to test the hypothesis that this interaction is critical for BMSC-mediated angiogenesis.

Strategies to prevascularize implants are currently at the heart of many ongoing efforts to engineer viable, functional tissues. *In vivo* capillary networks have remarkable functional properties, including the delivery of oxygen and nutrients, which have been difficult to reproduce in tissue engineered constructs. One approach to overcome this challenge has focused on incorporating penetrating vascular networks within tissue constructs prior to implantation, which in turn can successfully integrate with the host vasculature [1-3]. It is widely recognized that cells of a mesenchymal origin contribute to the regulation of microvascular development and function by acting as stabilizing pericytes [4]; therefore, understanding the molecular

mechanisms that govern the perivascular localization of mesenchymal cells with nascent blood vessels will be instrumental in vascularizing functional tissues for clinical implementation.

Angiogenesis, a process crucial to the growth and maintenance of tissues, involves emerging of new capillary blood vessels from pre-existing vasculature [5]. It is well accepted that the investment of nascent capillaries with pericytes during later stages of angiogenesis is essential for endothelial tube stabilization and the production of non-leaky blood vessels [5-7]. Pericytes are thought to be derived from multilineage progenitor cells that exhibit the features of MSCs (3) and form intimate contacts with the ECs in newly developing capillaries through their shared basement membrane (BM) [8, 9]. Our group has previously demonstrated that different stromal cells, including MSCs, support angiogenesis with distinct abilities that impact the functional qualities of *in vitro* and *in vivo* capillaries [10]; therefore, the identity of stromal cells that are co-delivered with ECs is key to promoting vessel maturation in engineered vascular constructs.

Bone marrow mesenchymal stem cells (BMSCs) are non-hematopoietic cells found in the adult bone marrow that have been shown to possess the defining characteristics of multipotency [11-13]. In addition to their potential to differentiate into numerous tissues, BMSCs are also capable of promoting angiogenesis [14-16], thereby making these cells particularly attractive for engineering vascularized tissues. When co-cultured with ECs within the fibrin matrix, BMSCs adopt a pericytic phenotype, occupying perivascular locations within *in vitro* developed capillary networks [17]. Additionally, these cells elicit an angiogenic response from ECs via distinct molecular mechanisms [18, 19]. However, the molecular mechanisms underlying BMSC-mediated angiogenesis have yet to be fully elucidated.

The present study investigates the role of the interaction between α6β1 integrin on BMSCs and EC-derived laminin-rich BM in sprouting angiogenesis in an established 3D fibrin-based *in vitro* model [20]. Using RNA interference, we show that knockdown of the α6 integrin subunit in BMSCs results in a significant decrease in the ability of ECs to form capillary sprouts. We also find that BMSC proliferation is significantly affected by knockdown of the α6 integrin subunit gene, which leads to marked decrease in vessel sprouting. When the deficit in proliferation is compensated for by increasing the initial cell density, deficiency in vessel sprouting persists. This indicates that the α6 integrin subunit expression in BMSCs is, in fact, required for endothelial vessel sprouting. Additionally, fluorescent imaging of co-cultures qualitatively reveals marked decrease in colocalization of α-smooth muscle actin (α-SMA)-laminin expression relative to the control conditions containing either BMSCs expressing the non-targeting shRNA (shNT) or wild type BMSCs. This suggests that the cells with attenuated α6 integrin subunit expression fail to associate with the EC-derived nascent vessels. These data collectively demonstrate that the perivascular asscociation of BMSCs via their α6β1 integrin receptor with the EC-derived laminin-containing BM is required for promoting sprouting angiogenesis.

4.2 METHODS

Cell isolation and culture: Human umbilical vein endothelial cells (HUVECs), were isolated from freshly harvested umbilical cords as previously described [14]. Briefly, the vein was flushed with sterile phosphate buffer saline (PBS) and then incubated with 0.1% collagenase type I (Worthington Biochemical, Lakewood, NJ) for 20 minutes at 37°C. The digestion product and subsequent PBS wash were collected and centrifuged. The cell pellet was resuspended in endothelial growth medium (EGM-2, Lonza, Walkersville, MD), plated onto T-25 flasks, and

allowed to attach overnight. PBS was used to wash away red blood cells the following day. Human BMSCs (Lonza) were cultured in high glucose (4.5 g/L) Dulbecco's Modified Eagle Medium (DMEM, Invitrogen, Carlsbad, CA) supplemented with 10% fetal bovine serum (FBS, Invitrogen). All cultures were incubated at 37°C and 5% CO_2. Media were changed every 2 days and cells were harvested with 0.05% Trypsin-EDTA (Invitrogen). BMSCs were used prior to passage 8 and HUVECs at passage 3.

Construction of the 3D co-culture model: Construction of the 3D co-culture model was performed as described previously [15]. In brief, red fluorescent protein (RFP)-expressing HUVECs (transduced as described below) cultured on 10^4 Cytodex^{TM} microcarrier beads (Sigma-Aldrich Co. St. Louis, MO) were mixed with 5×10^4 BMSCs within a 2.5 mg/mL fibrinogen precursor solution. Five hundred microliters of this solution containing ~100 HUVEC-coated beads was combined with 10 μL of thrombin (50 U/mL) in a single well of a 24-well plate to make one gel construct. This process was repeated until the desired number of gels was constructed. The gel constructs were left undisturbed for 5 min to allow the beads to settle at the bottom of the well before incubating for 25 min at 37°C and 5% CO_2, ample time to induce gelation. Tissues were then cultured in fully supplemented EGM-2 for 7 days. Media were changed every 2 days.

Fluorescent labeling of cells for both live and fixed cell imaging: HUVECs were fluorescently tagged using RFP to facilitate visualization and quantification of vessel networks. RFP-labeling was achieved via retroviral transduction using the Phoenix Ampho Retrovirus Expression system (Orbigen, San Diego, CA), as previously described [18]. Wild type MSCs were fluorescently labeled using a green cell tracker dye, SP-DiOC_{18} (3) (Invitrogen) according to manufacturer's protocol. In other experiments, cells within 3D fibrin gels and 2D cultures

were fixed with 4% paraformaldehyde (Sigma, St. Louis, MO), permeabilized with 0.5% Triton X-100 (Sigma) in TBS-T, and stained for fluorescent imaging at defined end points. In brief, fixed and permeabilized cells were incubated with primary antibodies overnight at 4°C, while appropriate secondary antibodies incubated for 2.5 hours at 4°C. Cell nuclei were stained with DAPI, 1 μg/mL (Sigma) in PBS for 10 minutes. The following antibodies were used for immunofluorescent staining (IF): monoclonal mouse anti-human α-smooth muscle actin (α-SMA), 1:200 (Abcam, Cambridge, MA); Rabbit anti-human laminin, 1:100 (Abcam); monoclonal mouse anti-α6 integrin, 1:50 (Millipore, Billerica, MA); Alexa Flour 488 goat anti-mouse IgG secondary antibody, 1:450 (Invitrogen), and Alexa Flour 594 goat anti-rabbit IgG secondary antibody, 1:450 (Invitrogen).

RNA interference: The expression level of α6 integrin was attenuated by transducing MSCs with the pGIPZ lentiviral shRNA (Open Biosystems, Rockford, IL) specific for the ITGA6 gene. A lentiviral shRNA plasmid against ITGA6 HUVECs were fluorescently tagged using red fluorescent (5'-TGCTGTTGACAGTGAGCGCTTGGTTTTAAGTACAACTGAATAGTGAAGCCACAG ATGTATTCAGTTGTACTTAAAACCAAATGCCTACTGCCTCGGA-3'), and a non-targeting control(5'TGCTGTTGACAGTGAGCGATCTCGCTTGGGCGAGAGTAAGTAGTGAAGCCA CAGATGTACTTACTCTCGCCCAAGCGAGAGTGCCTACTGCCTCGGA-3')wereseparately packaged into the Phoenix Ampho Retrovirus System (Orbigen, San Diego, CA). MSCs were incubated with the lentiviral supernatant for 12 hours. These plasmids were packaged into lentiviral particles using packaging vector (psPAX2, Addgene, Cambridge, MA), and an envelope vector (pCMV-VSVG, Addgene). The lentiviral shRNA plasmids, along with the packaging plasmids, were transfected into 293 HEK cells (Open Biosystems) using

Lipofectamine 2000 (Invitrogen). After a 48 hour incubation period, the lentiviral supernatant was collected. The supernatant was then concentrated by centrifugation at 3000 rpm for 5 minutes, followed by resuspension in PBS. MSCs were incubated in DMEM supplemented with Polybrene (Invitrogen) (5 μg/mL) for 15 minutes at 37°C prior to the addition of the concentrated lentiviral supernatant (27 μL for multiplicity of infection (MOI) =1). The lentiviral medium was removed after 48 hours and replaced by fresh DMEM. Selection of shRNA-expressing MSCs was achieved by culturing MSCs in the presence of 1 μg/mL Puromycin (Sigma-Aldrich) for a period of 4-6 days. Seed 7.0×10^6 HEK293T cells in 10 ml of media (Dulbecco's modified Eagle's medium (DMEM), 10% FBS, GlutaMAX, Sodium Pyruvate). Incubate at 37°C, 5% CO2. When cells are 90% confluent, passage them at 1:3 ratio. Transfection should begin when cells are approximately 70-90% confluent. For each T-75 flask to be transfected, dilute the mixture above into 1.5 mL of serum free Optimum media. Dilute 59 μL of Lipofectamine (L2K) into 1.5 mL of serum free Optimum media. Incubate for 5 min. Add the diluted DNA into diluted L2K, mix and incubate for 20 min. Aspirate the growth medium from the 293T cell flasks. Add 9 ml of 293T cell media to tubes containing the transfection complexes, mix gently, and then add onto the cells. Incubate for 24 hours. Aspirate the transfection mixture and replace it with 12 ml 293T cell media. Incubate for 12 hours. Harvest virus containing supernatant 48 hours post-transfection by removing medium to a 15 mL conical tube. Centrifuge tube containing harvested supernatant at 3000 rpm for 5 minutes.

Reverse transcription and quantitative polymerase chain reaction: Quantitative real time PCR was used to assess the expression levels of ITGA6 in BMSCs following shRNA-mediated silencing. Total RNA was isolated from MSCs using the SV Total RNA Isolation System (Promega, Madison, WI). The RNA concentrations were quantified using a Nanodrop ND-1000

(Thermo Scientific, Wilmington, DE). The RNA concentration and purity of each sample were determined by A260/A280 absorptions using a Nanodrop ND-1000 spectrophotometer. Equal amounts of total RNA from each sample were used to create first strand cDNA using the ImProm-II Reverse Transcription System (Promega). Taqman Gene Expression Assays (Applied Biosystems, Carlsbad, CA) were used to measure the transcript levels of the selected genes. The PCR amplification was performed on a 7500 Fast Real-Time PCR System (Applied Biosystems) in a final volume of 20 µl using cycling parameters (2 min, 50°C; 10 min, 95°C, 15 sec, 95°C, 1 min, 60°C with the latter two steps repeated for 40 times. Each reaction was performed in triplicates and the ΔΔCt method was used for the gene expression analysis [21].

Retrieving cells from 3D fibrin gel constructs: To isolate cells from 3D cultures, fibrin gels needed to be dissolved. trypsin, collagenase, or other proteolytic enzymes did not yield a single cell suspension effectively. Furthermore, longer incubation times with these enzymes required to fully dissolve the gels damaged cells harvested from 3D cultures. Instead, gels were digested with nattokinase (Japan Bio Science Laboratory Co, Ltd), a Bacillus-derived serine protease that is known for its potent fibrinolytic activity, to retrieve the encapsulated cells. More detailed information and validation of this methodology are provided in Chapter 5. Briefly, a fibrinolytic solution was prepared by dissolving 50 FU/mL (fibrin degradation unit) of nattokinase in PBS containing 1mM EDTA (Fisher). Gels were washed with PBS before dislodging them from the well siding using a small spatula. Gels were subsequently dissolved by adding 500 µl of the fibrinolytic solution and incubating at 37°C for 30 min. Upon dissolution, the contents of each well were collected and centrifuged. Cells were then washed with cold PBS for additional procedures.

Fluorescent activated cell sorting (FACS): Cells retrieved from 3D cultures using the fibrinolytic method described in the preceding paragraph were stained through a 40 μm cell strainer (BD Falcon, Franklin Lakes, NJ) to ensure single cellularity and remove the Cytodex microcarrier beads. Cells were then resuspended in ice cold PBS containing 0.1-0.5% bovine serum albumin (BSA, Sigma-Aldrich) and pelleted by centrifugation at 2000 rpm at 4°C for 5 minutes followed by incubation with mouse α-SMA monoclonal antibody, 1:200 (Abcam) in BSA for 1 hour at 4°C. Samples were then washed with cold 0.5% BSA in PBS, and incubated with Alexa Flour 633 goat anti-mouse IgG secondary antibody, 1:450 (Invitrogen) for 30-40 minutes at 4°C. As a negative control, parallel cell suspensions were prepared, and incubated with only the secondary antibody; Samples were then washed twice and resuspended in 0.5% BSA in PBS for flow cytometry analysis.

Quantification of α-SMA protein expression via Western Blot: 3D fibrin constructs were digested in nattokinase solution as described above. 2D cultures were trypsinized using 0.05% trypsin-EDTA (Invitrogen). Cells were collected and lysed in Garner Buffer (50mM Tris, pH 7.5; 150mM NaCl; 1mM phenylmethylsulfonyl fluoride; 1% Triton X-100). The lysate was clarified by centrifugation at 14,000 rpm and 4°C for 10 minutes. The supernatant was collected and total protein concentration was determined using a spectrophotometer (JENWAY, Staffordshire, UK). After boiling, equal amounts of total protein from lysates were loaded into a 10% tris-glycine gel (Invitrogen) and subjected to SDS-PAGE. The separated proteins were then transferred onto a poly (vinylidine fluoride) membrane and probed with a mouse monoclonal anti-human α-SMA antibody (1:200, Abcam, Cambridge, MA). After washing, the membrane was incubated with a horseradish peroxidase-conjugated anti-goat secondary antibody (1:400),

sc-2033, Santa Cruz Biotechnologies). Protein expression was visualized using an enhanced chemiluminescence detection system.

Quantification of total network length: Total network lengths were measured as previously described [18]. Briefly, capillary networks formed by mCherry transduced HUVECs were imaged at three time points post assembly (Day 1, 3, and 7) via fluorescent microscopy (Olympus IX81, Olympus America, Center Valley, PA) using MetaMorph Premier Software (Molecular Devices, Sunnyvale, CA). Tracking the same beads throughout all time points, 10 beads per condition were imaged at low magnification (4x). Total vessel network lengths were measured using the Angiogenesis Tube Formation module of MetaMorph.

Cell proliferation assay: To quantify BMSC proliferation during the culture period, cells were retrieved from 3D cultures following the same protocol used for the FACS assay. The total DNA content of gels was determined and run against a standard curve. DNA analysis was performed on samples at days 1, 3, and 7 of culture using a commercially available DNA assay (PicoGreen, Invitrogen).

Adhesion blocking assay: In addition to qPCR, silencing of the ITGA6 gene in BMSCs was functionally confirmed by testing the adhesion of the silenced cells to laminin, as previously described [17]. To ensure even protein coating and achieve complete coverage, natural mouse laminin (Invitrogen) was covalently attached to tissue culture plastic using the Sulfo-SANPAH hetero-bifunctional linker (Proteochem, Inc., Denver, CO). Briefly, 0.5 mM of Sulfo-SANPAH was dissolved in 0.1M MES (Fisher), 0.5M NaCl (Fisher), pH 6.0 buffer and placed into wells of untreated 96-well tissue culture plates (Nunc, Thermo Scientific). The Sulfo-SANPAH solution was then irradiated with UV light for 15 minutes and removed by rinsing with MES buffer. This

step was repeated with fresh Sulfo-SANPAH and rinsed with MES buffer. 100 µg/mL of laminin was prepared in pH 7.0 PBS and added to the Sulfo-SANPAH activated wells and incubated overnight at 4°C. The wells were rinsed with PBS the next day. The next day, BMSCs (3×10^5 cells/mL) were preincubated in serum-free DMEM for 15 min.

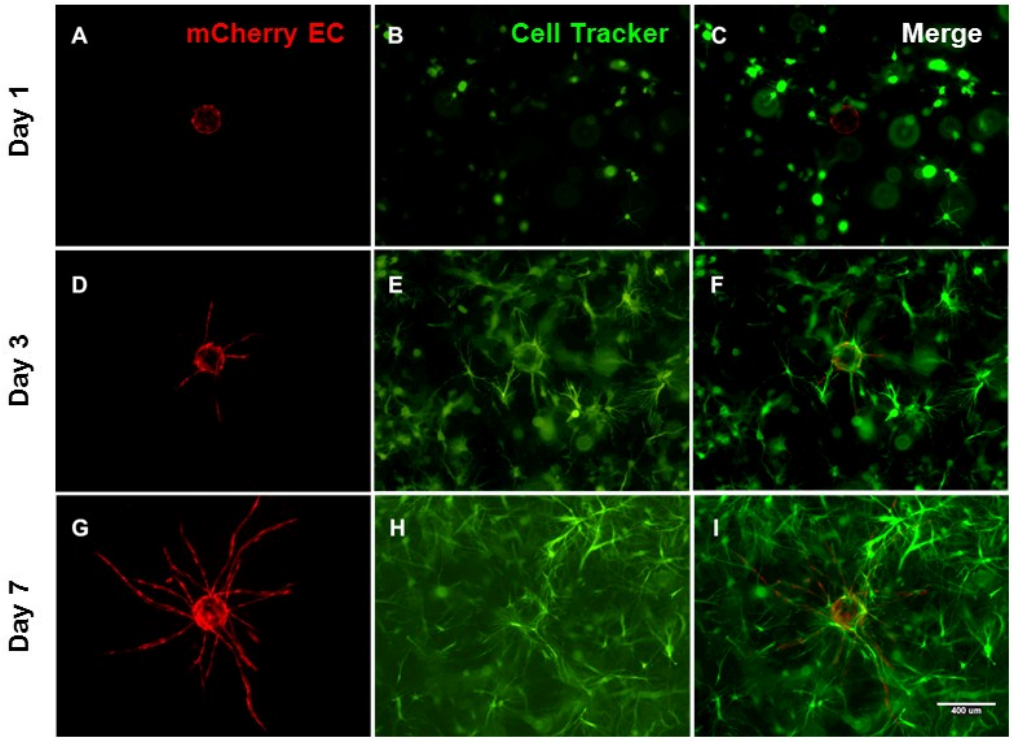

Figure 4-1: ECs recapture their *in vivo* angiogenic capacity in the presence of BMSCs when cultured within three dimensional fibrin gels. mCherry-transduced ECs were cultured within 2.5 mg/mL fibrin hydrogels in the presence of BSMCs fluorescently labeled using a green cell tracker dye and traced from day 1 (top row) through day 3 (middle row), and day 7 (bottom row). Red (A, D, G), green (B, E, H), and merged (C, F, I) channels are shown. Scale bar = 400 µm.

The wells of the 96-well plate were rinsed with PBS; then 0.1 mL of the cell suspension was added to each well. Cells were incubated at 37°C for 1 hour at which point non-adherent cells were washed away. The attached cells were fixed and stained with a 0.4% crystal violet in methanol (w/v) for 30 minutes. After washing with distilled water, the stain was extracted with

0.1M citrate in 50% ethanol. The absorbance of each well of the plates was measured at 590 nm with a Multiskan Spectrum microplate reader (Thermo Fisher Scientific).

Statistical analysis: Statistical analysis was carried out using GraphPad Prism software. Data are reported as means ± standard deviations. All statistical comparisons were made by performing a two-way analysis of variance (ANOVA), followed by Bonferroni's multiple comparison tests to judge significance between two data sets at a time. *P* values less than 0.05 were considered statistically significant.

4.3 RESULTS

BMSCs stimulate ECs to form robust capillary networks when co-cultured within 3D fibrin gels: Prior studies from our laboratory have shown that BMSCs are capable of supporting capillary formation using our well-established angiogenesis model [19]. The vascular networks formed in the presence of BMSCs possessed morphological characteristics similar to capillaries *in vivo*. Figure 4-1 illustrates the progression of vessel sprouting over a 7 day culture period during which ECs coated on microcarrier beads undergo a complex morphogenetic process and elaborated into extensive vascular networks in 3D fibrin gels. To monitor vessel maturation, fluorescent microscopy was used to trace the ECs transduced with mCherry (Fig. 4-1A, D, and G). BMSCs were fluorescently labeled using a green cell tracker dye (Fig. 4-1B, E, and H) in order to qualitatively differentiate capillary networks from the presence of the surrounding stroma. After validating the use of our 3D fibrin-based *in vitro* model for studying BMSC-induced angiogenesis, we went on to utilize this system to address our hypothesis.

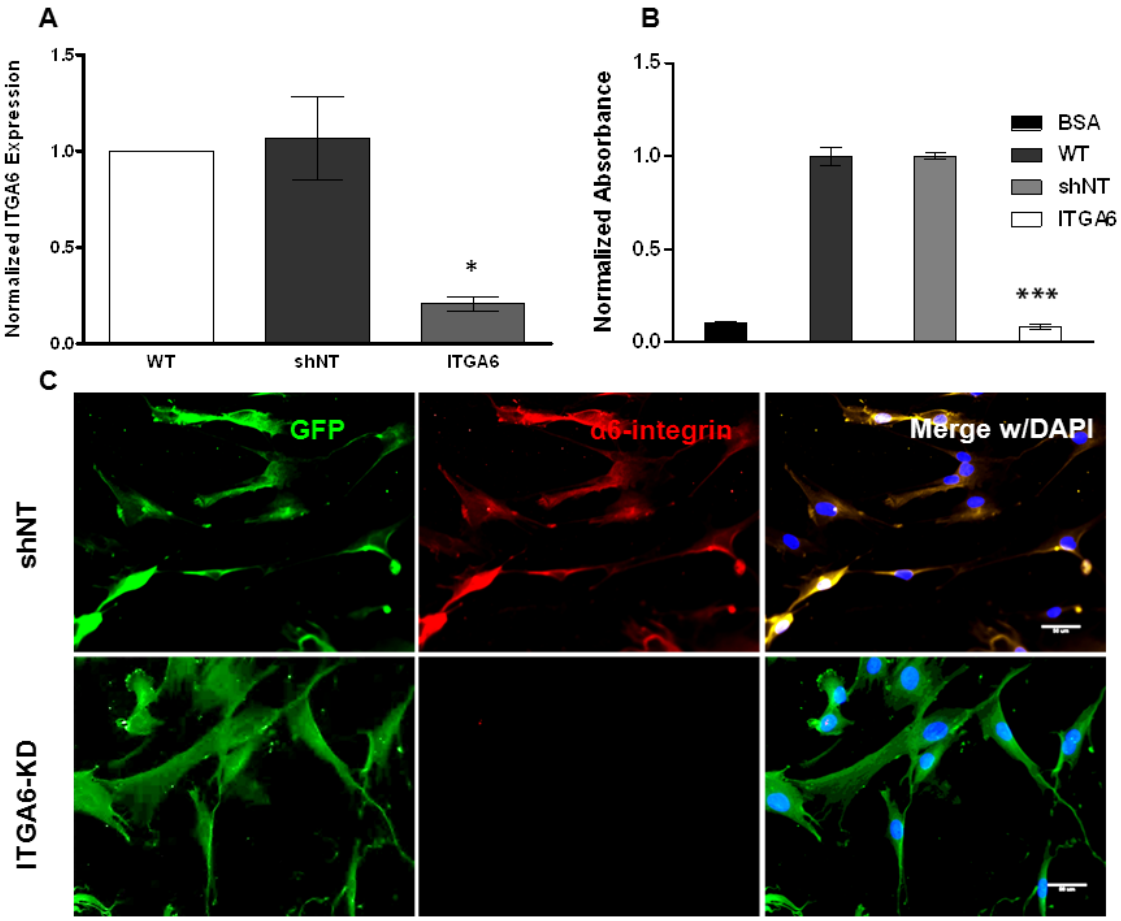

Figure 4-2: α6 integrin subunit expression was successfully attenuated in BMSCs. (A) Expression levels of ITGA6 in BMSCs after knockdown were assessed from three independent experiments via qPCR relative to non-targeting (NT) shRNA control. * refers to $P < 0.05$ with respect to the scrambled control (shNT). 2-way ANOVA followed by post-test analysis using Bonferroni's method was used to compare conditions. (B) Adhesion of BMSCs onto laminin coated surfaces was disrupted via knockdown of α6 integrin. Adhesion of BMSCs with silenced α integrin to laminin-coated surfaces was quantified using a crystal violet assay. Raw data generated as absorbance values were normalized to control conditions (adhesion to laminin, blocked with BSA) to correspond to the relative numbers of attached cells in various conditions. *** refers to $P < 0.0001$ with respect to the scrambled control (shNT). (C) The expression of α6 integrin subunit (red) was confirmed on GFP-expressing BMSCs transduced with non-targeting (NT) shRNA and BMSCs with silenced α6 integrin. Fluorescent images were taken the next day following cell seeding. In overlay images, blue is DAPI stain for nuclei. Scale bar = 50 μm.

.

Knockdown of α6 integrin subunit expression in BMSCs diminishes vessel sprouting: Next, we used our established 3D *in vitro* model to test the hypothesis that α6β1 integrin receptor is required for BMSC-stimulated angiogenesis. This hypothesis is based on the fact that some stem

cells interact with capillaries in part via their α6β1 integrin receptor and EC-deposited laminin in post adult stem cell niches [17, 22]. To investigate this possibility, it was first confirmed that knockdown of ITGA6 resulted in reduced expression of α6 integrin subunit in BMSCs. The expression was reduced by 82% relative to the shNT controls, as measured by qPCR (Fig. 4-2A). Additionally, it was qualitatively confirmed that the BMSCs containing the gene knockdown did not express α6 integrin (Fig. 4-2C). Using adhesion assays [23] confirmed that the adhesion of BMSCs with attenuated α6 integrin to laminin coated surfaces was disrupted (Fig. 4-2B). Next, the established shRNA gene knockdown was used to test the requirement of α6 integrin for EC-BMSC interactions in our angiogenesis model. After 7 days, ECs co-cultured with the BMSCs with attenuated α6 integrin subunit expression demonstrated an 80% reduction in total vessel network length relative to those co-cultured with the BMSCs containing the shNT (Fig. 4-3A, B). Furthermore, ECs co-cultured with BMSCs containing the shNT displayed vessel sprouting to the same extent as those co-cultured with wild type BMSCs as controls. These data collectively suggest that knockdown of α6 integrin subunit expression in BMSCs severely limits EC-derived vessel sprouting.

α6 integrin subunit expression in BMSCs is required for their perivascular association with EC-derived vessel networks: During angiogenesis, BMSCs undergo a phenotypic alteration and differentiate into stabilizing perivascular cells acting as stabilizing pericytes that express α-SMA and NG2 [19]. We hypothesize that BMSCs interact with an EC-derived BM via their α6β1 integrin receptor, and establish pericyte-invested capillary coverage that is a hallmark of a stable capillary network [5, 24]. To address this hypothesis, the requirement of α6 integrin expression for pericytic differentiation of BMSCs and their direct association with the EC-

derived BM was assessed. Co-cultures were fixed and stained for α-SMA (green), a pericyte marker, and laminin (red) at day 7.

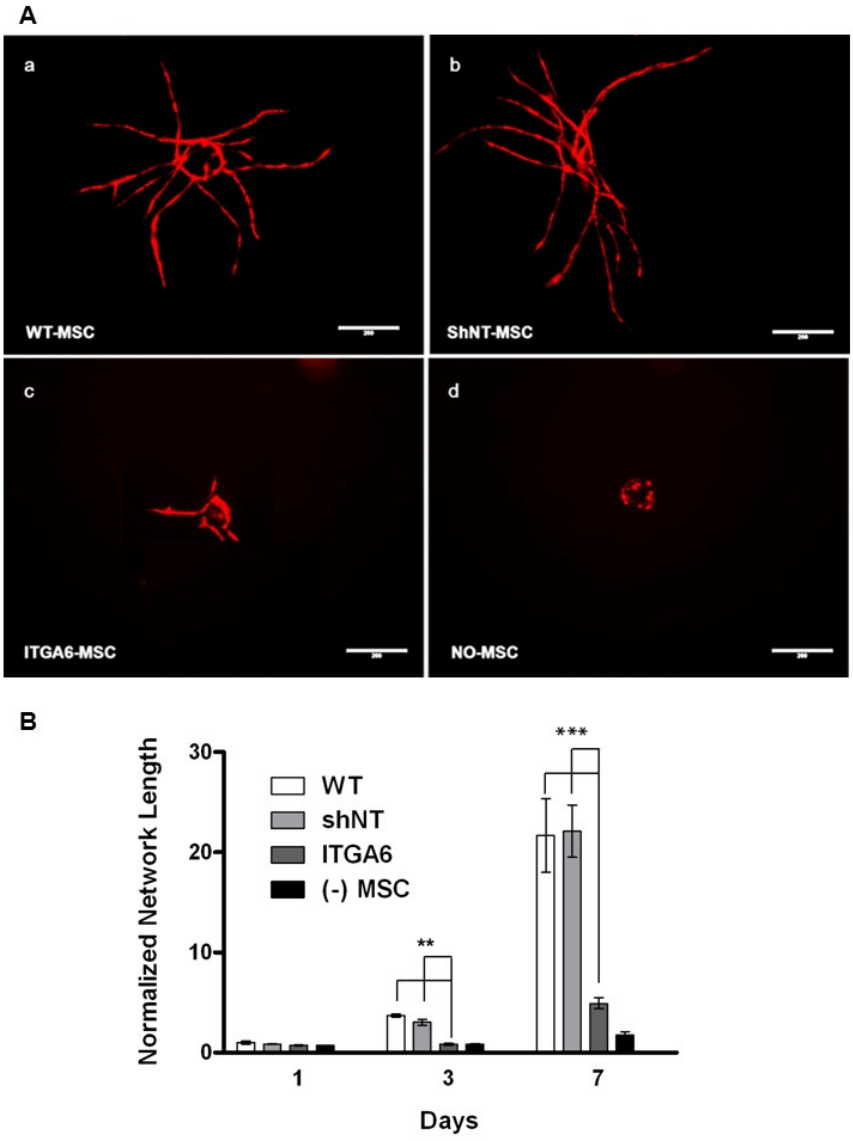

Figure 4-3: Knockdown of α6 integrin subunit expression in BMSCs diminishes vessel sprouting. (A) Day 7 fluorescent images of mCherry-expressing ECs co-cultured with (a) wild type BMSCs, (b) BMSCs transduced with non-targeting (NT) shRNA, (c) BMSCs with shRNA against ITGA6, or (d) no BMSCs. Scale bar = 200 μm. (B) Total vessel network length was quantified from a minimum of 7 fluorescent images over three independent experiments and normalized by day 1 wild type BMSC condition. *** refers to $P \leq 0.001$ with respect to the non-targeting (shNT) and wild type control in the same group. 2-way ANOVA followed by post-test analysis using Bonferroni's method was used to compare group conditions.

Fluorescent imaging of co-cultures qualitatively revealed that knockdown of α6 integrin expression caused BMSCs' failure to associate with the nascent vessels (Fig. 4-4A-c), as gauged by very low expression of α-SMA and poor laminin deposition around the periphery of the vessel structures. Conversely, BMSCs containing the shNT or wild type BMSCs exhibited relatively high expression of α-SMA, and appeared to be associated with the laminin-rich BM, located adjacent around the capillary networks (Fig. 4-4A-a, -b).

To further explore the role of α6 integrin knockdown in the pericytic differentiation of BMSCs, flow cytometry was used to quantitatively assess the percentage of cells expressing α-SMA in distinct culture conditions (Fig. 4-4B). When cultured in 2D, more than 40% of BMSCs expressed α-SMA, whereas the percentage of α-SMA expressing BMSCs that were embedded in 3D fibrin gels was less than 5%. Furthermore, whether cultured on 2D or in 3D fibrin gels, in the absence of ECs, the percentage of α-SMA expressing cells in the knockdown conditions were comparable with those of the control conditions containing the BMSCs expressing the shNT or wild type BMSCs (Fig. 4-4B). When co-cultured with ECs in fibrin gels, however, the number of BMSCs expressing α-SMA increased relative to the BMSCs cultured alone in 3D fibrin gels, and there was a significant increase in the percentage of BMSCs expressing α-SMA in the control conditions as compared to that obtained from 3D-BMSC mono-cultures. More importantly, in EC-MSC-3D co-cultures, the percentages of α-SMA expressing BMSCs significantly decreased in the knockdown conditions relative to the control conditions. Additionally, expression of α-SMA was detected via Western Blotting in the BMSCs with attenuated α6 integrin as compared to that obtained from the BMSCs expressing the shNT and wild type BMSCs in the same culture conditions (Fig. 4-4B). α-SMA expression in BMSCs was detected as a function of culture condition (3D with ECs, in 3D without ECs, and in 2D without ECs). Results were consistent

with our flow cytometry data, revealing increased expression of α-SMA in the BMSCs cultured in 2D and low α-SMA expression in the BMSCs cultured alone in 3D fibrin gels. The same results were also detected via IF staining of the BMSCs cultured either on 2D or in 3D fibrin gels (Fig. 4-5). However, 3D co-cultures containing the BMSCs with attenuated α6 integrin showed significantly lower expression of α-SMA relative to those containing the BMSCs expressing the shNT or wild type BMSCs (Fig. 4-4B-b). Collectively, these results demonstrate that knockdown of α6 integrin significantly limits the ability of BMSCs to differentiate into pericyte-like cells and associate with the EC-derived nascent vessels, presumably through laminin deposited as part of the EC-derived BM.

Knockdown of α6 integrin subunit expression has a significant inhibitory effect on BMSC proliferation: Fluorescent images of co-cultures qualitatively suggested that fewer BMSCs were present around the EC-derived capillary networks in the knockdown conditions (Fig. 4-6A-c), perhaps indicating that the BMSCs with attenuated α6 integrin proliferated at a slower rate relative to the BMSCs containing the shNT or wild type BMSCs (Fig. 4-6A-a, -b). This was confirmed quantitatively by measuring the total DNA extracted from cells at discrete time points as a metric of cell proliferation over the 7 day culture period (Fig. 4-7B) using the PicoGreen dsDNA assay. Cultured in 3D fibrin gels, in the absence of ECs, the BMSCs with attenuated α6 integrin proliferated approximately 40% less than either control cells expressing the shNT or wild type BMSCs, indicating that knockdown of α6 integrin significantly reduces the proliferation ability of BMSCs. To compensate for this deficit in proliferation, the initial seeding density of BMSCs in the fibrin angiogenesis assay was increased in the knockdown conditions in order to compensate for the deficit in proliferation.

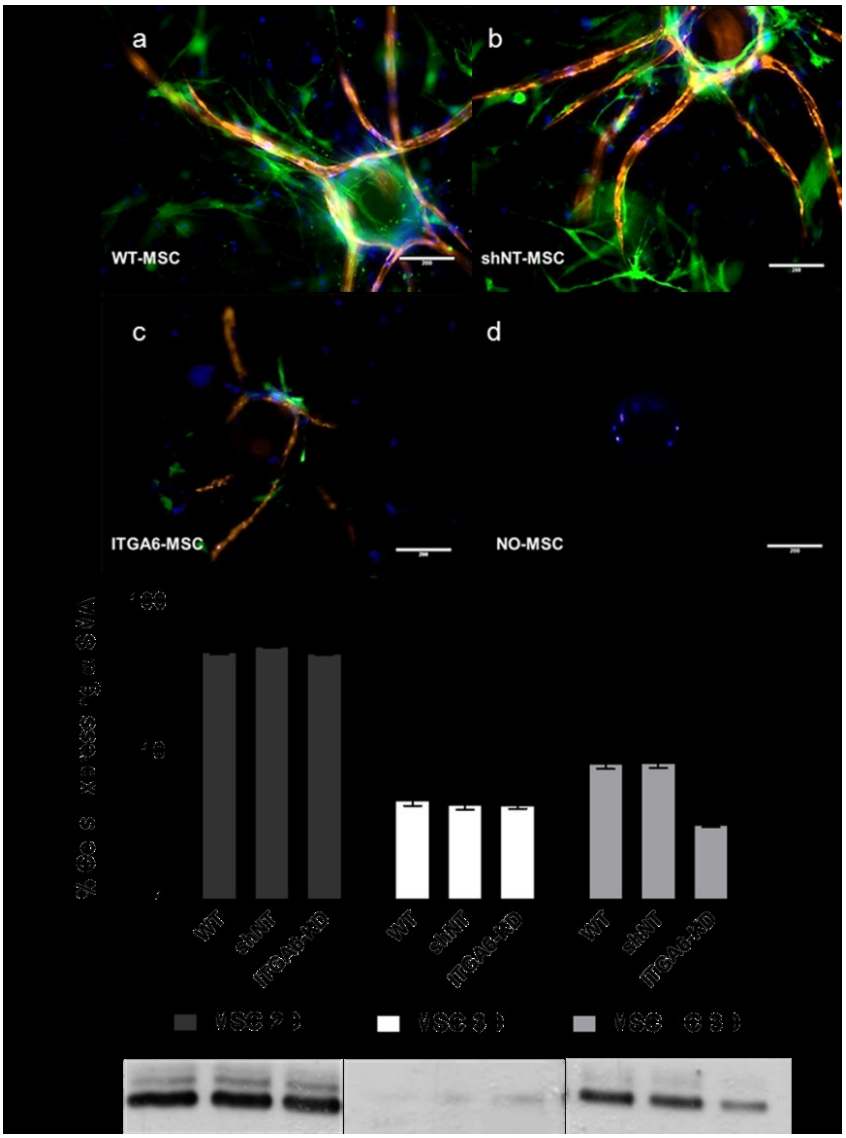

Figure 4-4: BMSCs with attenuated α6 integrin expression fail to associate with the EC-derived vessel networks to the same degree as controls. (A) Representative immunofluorescent images from day 7, 3D co-cultures with ECs cultured on microcarrier beads in the presence of (a) wild type BMSCs (WT), (b) BMSCs transduced with non-targeting (NT) shRNA (shNT) , (c) BMSCs with silenced α6 integrin (ITGA6), or (d) no BMSCs. Cultures were stained for laminin (red), α-SMA (green), and nuclei (DAPI, blue). Scale bar = 200 μm. (B) Flow cytometric analysis of α-SMA expression on WT, shNT, and ITGA6 BMSCs. Graph shows the percentage (%) of BMSCs expressing α-SMA retrieved from day 7 EC-BMSC co-culture conditions in three independent experiments. * refers to $P \leq 0.05$ in comparison to the respective non-targeting and wild type controls in the same group. Also, Western Blot analysis of α-SMA expression in BMSCs as a function of culture condition (3D with ECs, in 3D without ECs, and in 2D without ECs).

Despite the presence of extra BMSCs, sprouting deficiency was still evident (Fig. 4-7A) suggesting that decreased vessel formation is not solely a result of the deficit in BMSC proliferation.

α6 integrin-laminin interactions are not required for vessel sprouting when BMSCs are overlaid as a monolayer on top of the fibrin gels: To further examine the apparent role of α6 integrin knockdown in deficient endothelial vessel sprouting, rather than spread BMSCs throughout EC-containing gels, BMSCs were seeded on top of fibrin gel constructs. This co-culture method allowed the effective isolation of ECs from BSMCs in order to determine whether the physical proximity between these two distinct cell populations mattered for the α6β1 integrin-mediated interactions to regulate vessel sprouting. With this altered configuration, the BMSCs with attenuated α6 integrin stimulated vessel sprouting from the ECs to the same extent as those containing the shNT or wild type BMSCs (Fig. 4-8A). This was also qualitatively observed in fluorescent images of mCherry-expressing ECs at day 7 (Fig. 4-8B), demonstrating that the BSMCs with silenced α6 integrin did not induce any apparent differences in vessel sprouting with respect to either the BMSCs expressing the shNT or wild type BMSCs, when cultured on top of the gels.

4.4 DISCUSSION

This study explored a particular mechanism by which BMSCs stimulate an angiogenic response in ECs within a fibrin matrix. We, along with others, have previously shown that adult stem cells express the laminin receptor α6β1 integrin, which may be involved in their perivascular association [17, 22]. Here, we used RNA interference to demonstrate that EC-derived vessel formation is dependent on the interaction between the α6β1 integrin receptor on

BMSCs and the EC-deposited laminin surrounding the vessel networks. When BMSCs were distributed within 3D fibrin gels, knockdown of α6 integrin subunit expression severely restricted EC-derived vessel formation, BMSC proliferation, and association with the nascent vessels. However, knockdown of α6 integrin expression did not affect vessel sprouting in EC-containing gels with overlaid BMSCs. These findings collectively suggest that the effect of the interactions between the α6β1 integrin receptor on BMSCs and the EC-deposited laminin on capillary formation and sprouting is dependent on the physical proximity between endothelial and stromal populations. Perhaps, this α6β1-mediated proximity induces signals that regulate the ability of ECs to sprout. While these data suggest that knockdown of α6 integrin subunit expression in BMSCs inhibit EC-derived vessel sprouting partly through interference with the α6β1 integrin-laminin interactions, the mechanistic events downstream of this adhesive interaction that regulate network length remain to be fully elucidated.

Vascular pericytes serve as stabilizing constituents in the development of nascent vessels and are distinguished by their intimate association with ECs as well as expression of pericyte markers, including α-SMA [25]. Prior studies have suggested that MSC populations derive from blood vessel walls and that they may be identical to pericytes [4, 26, 27]. Because of their pericytic role in most tissues, MSCs make important contributions to blood vessel stabilization [26, 28] and formation, in part due to their ability to exert paracrine effects on ECs via secreted growth factors and cytokines [29]. Consistent with this idea, our data here have shown that BMSCs are required to induce EC-derived capillary sprouting, as the monocultured ECs embedded within 3D fibrin matrices failed to form nascent vessels (Fig 4-3A-d). Initially, the expression of α6 integrin subunit in BMSCs was attenuated to assess the broad potential role of the α6β1 integrin-laminin interactions in mediating vessel sprouting.

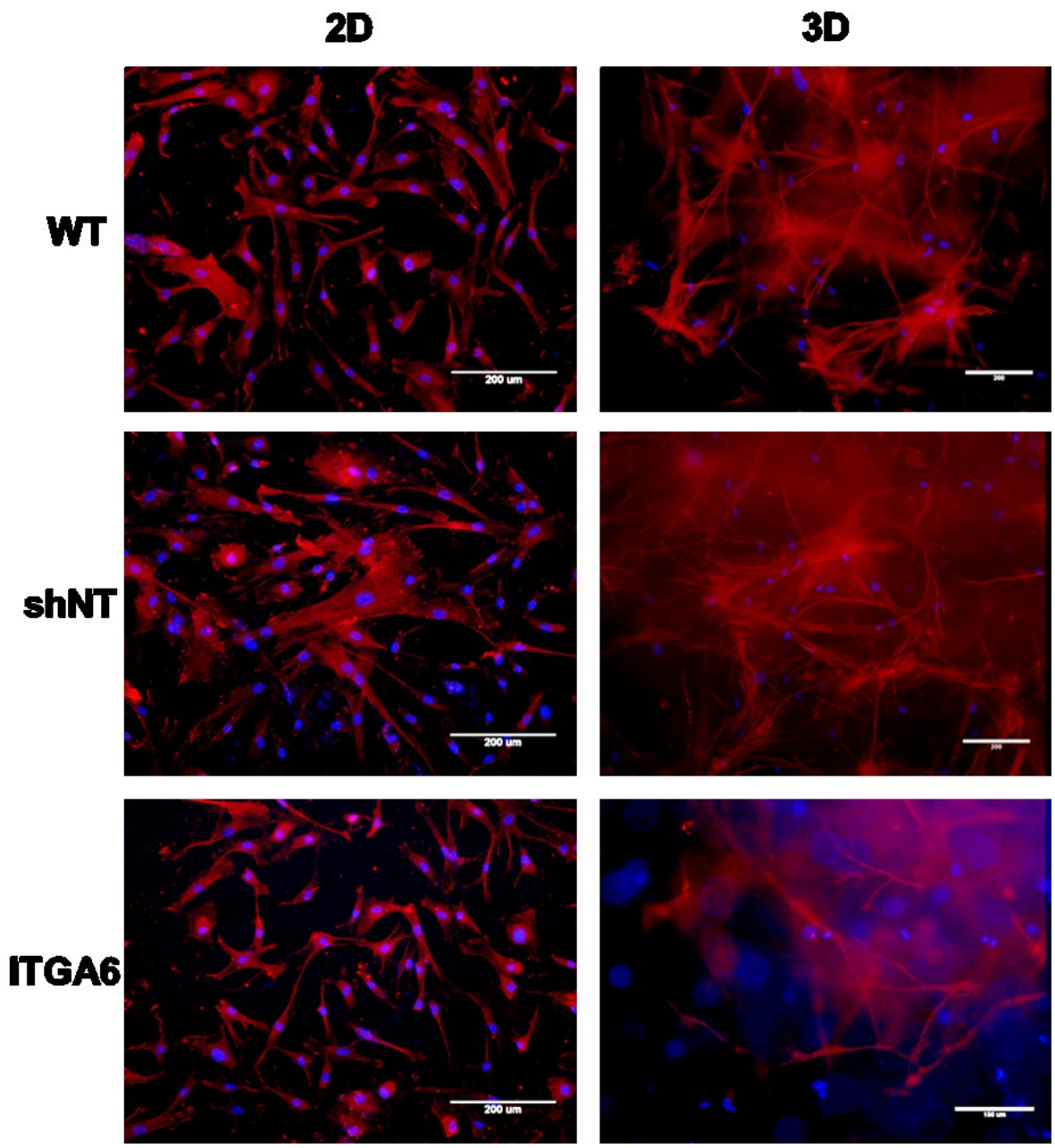

Figure 4-5: Expression of α-SMA was confirmed on wild type BMSCs, BMSCs transduced with shNT, and BMSCs with silenced α6 integrin. Fluorescent images were taken from BMSCs seeded either on 2D or within 3D fibrin gels, 7 days following cell seeding. In all panels, nuclei are stained with DAPI (blue). Scale bar = 200 µm. Expression of α-SMA was confirmed on wild type BMSCs, BMSCs transduced with shNT, and BMSCs with silenced α6 integrin. Fluorescent images were taken from BMSCs seeded either on 2D or within 3D fibrin gels, 7 days following cell seeding. In all panels, nuclei are stained with DAPI (blue). Scale bar = 200 µm.

Down regulation of α6-integrin expression via shRNA-mediated knockdown suppressed vessel sprouting by approximately 80% (Fig. 4-3B). This may be the result of the hampered ability of ECs to form angiogenic sprouts, when BMSCs were distributed throughout EC-containing fibrin gels. Impaired vessel sprouting also led to decreased deposition of laminin in the BM around the periphery of the vessel structures (Fig. 4-4A-c).

Previously, we have shown interactions with ECs [18, 19]. These heterotypic interactions are necessary for vascular BM assembly [30] and are stimulated by pericyte recruitment to EC-derived nascent vessels [31, 32]. As the emergence of the BM matrix is concomitant with the arrival of pericytes around developing microvascular tubes [33], it is reasonable to assume that the disruption of the α6β1 integrin-laminin interactions may influence the process of BMSC differentiation into pericyte-like cells and their association with the EC-derived nascent vessels (Fig. 4-4B). Furthermore, the proximal interactions between ECs and the BMSCS with attenuated α6 integrin expression appeared to have an inhibitory effect on vessel sprouting, as the low levels of α6 integrin in the BMSCs distributed throughout EC-containing fibrin gels significantly restricted vessel (Fig. 4-3A-c, 3-3B). A strikingly different response to α6 integrin inhibition was noted, when BMSCs overlaid on top of fibrin gels. Capillary sprouting occurred with the BMSCs with attenuated α6 integrin that were physically isolated from ECs (Fig. 4-8A). However, knockdown cultures with overlaid BMSCs demonstrated a significant reduction in total vessel network sprouting relative to those containing BMSCs distributed throughout the gels. These results are consistent with our previous reports that distribution of BMSCs in dense fibrin matrices facilitates angiogenesis via paracrine signaling [19], as direct EC-BMSC interactions allow for more effective cross talk and enhanced angiogenesis.

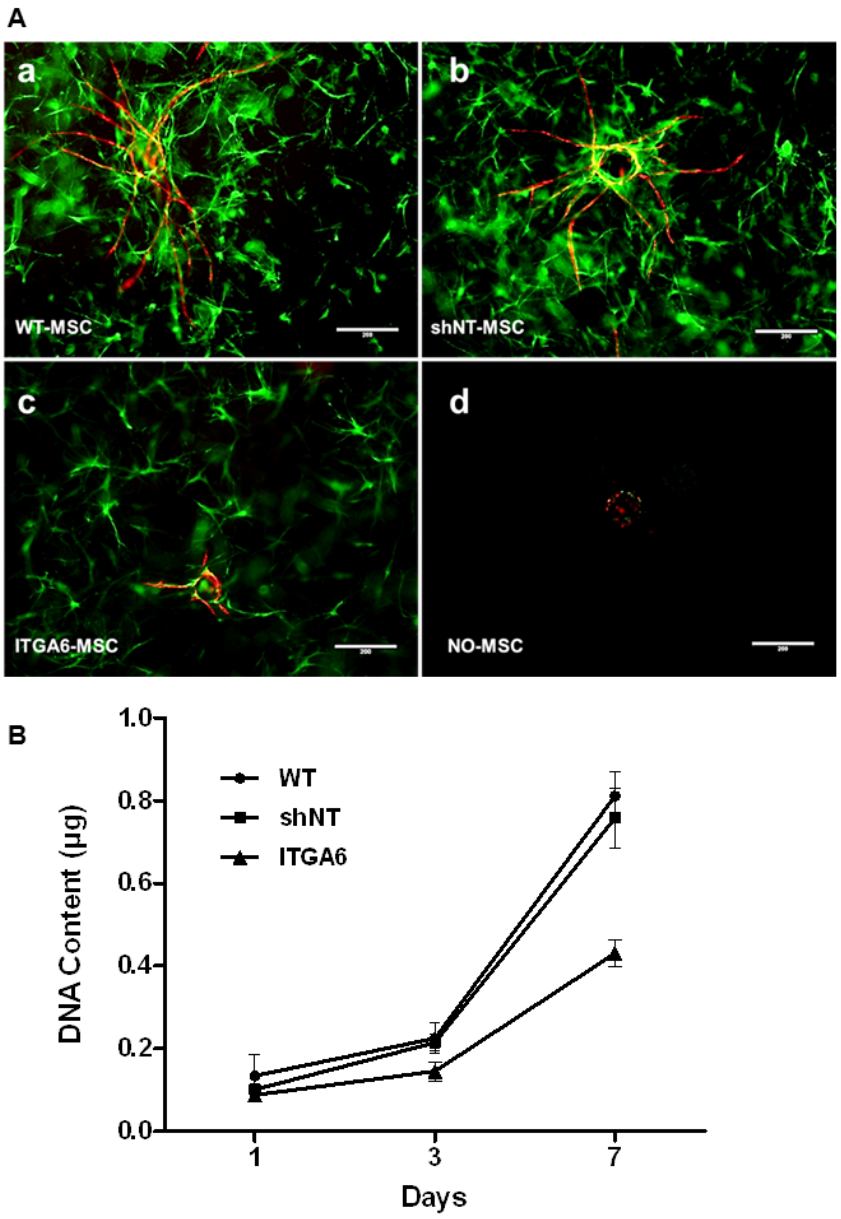

Figure 4-6: BMSCs with attenuated α6 integrin expression proliferate significantly less than control cells expressing the shNT or wild type BMSCs. (A) Representative immunofluorescent images from day 7, 3D co-cultures with mCherry-expressing ECs cultured on microcarrier beads in the presence of (a) wild type BMSCs tagged with a green tracker dye (WT), GFP-expressing (b) BMSCs transduced with non-targeting (NT) shRNA (shNT), (c) BMSCs with silenced α6 integrin (ITGA6), or (d) no BMSCs. (B) The total DNA extracted from cell seeded in 3D fibrin gels was assessed as a measure of cell proliferation over a 7 day culture period. Statistical analysis was obtained by repeating this experiment three times.

Thus, it is likely that α6 integrin inhibition may not alter the ability of BMSCs to release proangiogenic factors that induce ECs to undergo capillary morphogenesis, but, in some manner,

may result in the restricted diffusion of BMSC-secreted proangiogenic cytokines through the matrix despite of the reduced distances that these molecules must travel to arrive at the endothelial sites.

Given the central role of integrins in angiogenic steps that involve changes in endothelial/pericyte adhesion [34], it is difficult to dissect the mechanistic causes for the inhibition of vessel formation in the α6 integrin knockdown conditions. One possible interpretation is that modulation of α6 integrin levels in BMSCs could play a role in EC invasion and subsequent vessel formation, in part by influencing heterotypic interactions via soluble mediators, some of which induce the production of proteolytic enzymes responsible for regulating ECM degradation [35]. We, along with others have previously shown that EC-derived proteases, particularly the family of matrix metalloproteinases (MMPs) [18, 19], initiate the degradation of BM proteins, and finally EC lumenogenesis [36-38]. Conversely, the broad spectrum MMP inhibition in EC-BMSC co-cultures leads to abrogation of vessel formation [19]. A large body of work suggests that MMPs have functions other than promotion of ECM degradation to facilitate EC invasion [39], and that they could also work in tandem with integrins expressed on stromal cells, and angiogenic genes to activate pathways leading to sprouting morphogenesis [40]. Furthermore, numerous studies have demonstrated the *in vitro* association between integrins and MMPs [41-44]. Namely, the role of the collagen-binding α2β1 integrin in the expression of interstitial collagenase matrix metalloproteinase-1 (MMP-1) has been described [45]. Up- or down-regulation of α2 integrin levels in MG-63 cells resulted in induction or reduction of MMP-1 gene expression, respectively. With increasing evidence that MMPs are involved in different processes of angiogenesis, it is possible that α6 integrin inhibition in BMSCs impedes EC-derived vessel sprouting, in part by negatively regulating MMP-dependent

pathways that induce ECM degradation; this might in turn lead to decreased vessel formation and BM deposition, and finally poor pericyte recruitment.

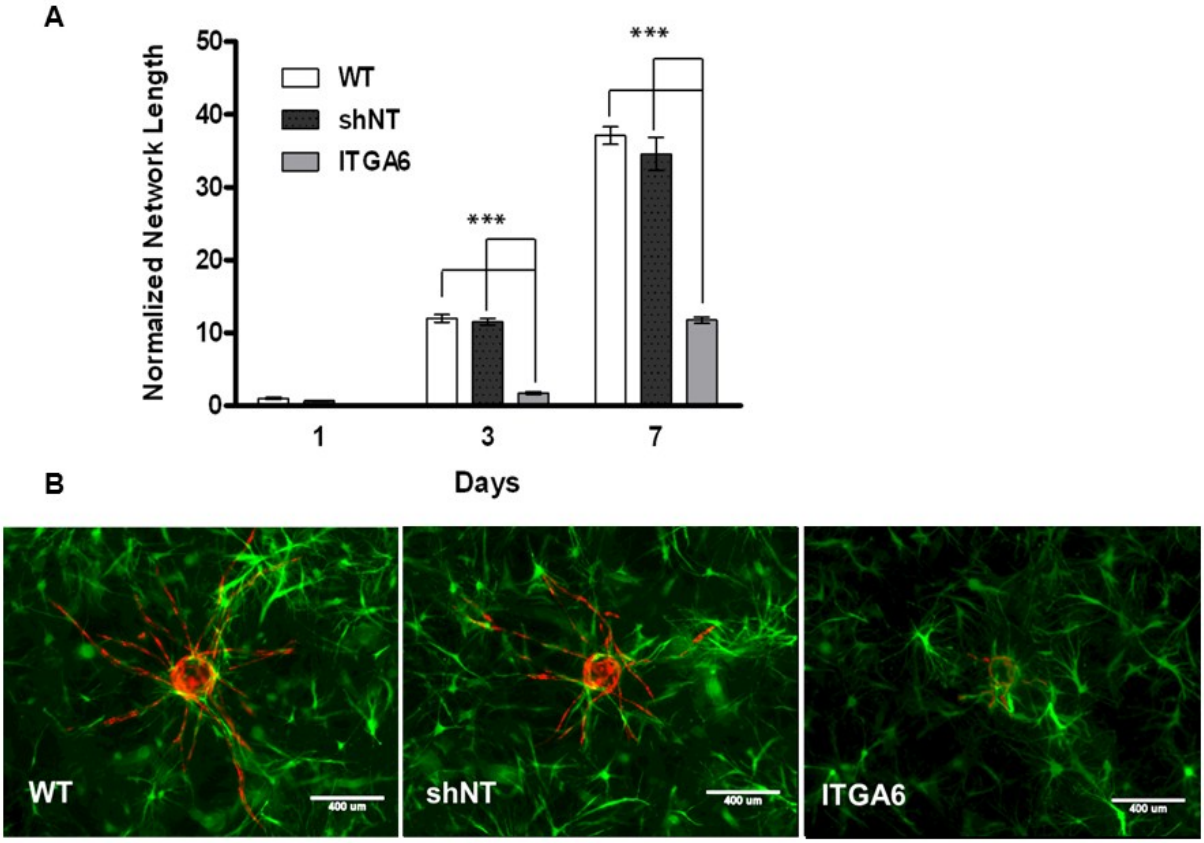

Figure 4-7: Addition of the BMSCs with attenuated α6 integrin does not compensate for sprouting deficiency in the knockdown conditions. (A) Total vessel network length was quantified from a minimum of 7 fluorescent images over three independent experiments and normalized by day 1 wild type BMSC condition. *** refers to $P \leq 0.001$ in comparison to the respective non-targeting control in the same group. 2-way ANOVA followed by post-test analysis using Bonferroni's method was used to compare group conditions. (B) Day 7 fluorescent images of mCherry-expressing ECs co-cultured with GFP-expressing (a) wild type BMSCs, (b) BMSCs transduced with non-targeting shRNA (shNT), (c) BMSCs with shRNA against ITGA6. Scale bar = 400 μm.

Furthermore, suppression of α6 integrin did not fully impair the ability of ECs to form capillary sprouts (Fig. 4-3A, B) suggesting that perhaps α6 integrin inhibition may affect the key

signaling events involved in EC-derived matrix remodeling and degradation, and may not necessarily alter the capacity of ECs to undergo morphogenesis to form angiogenic sprouts.

ShRNA-mediated suppression of α6 integrin had an additional effect on the proliferation of BMSCs. Inhibition of α6 integrin resulted in an unforeseen reduction of BMSCs' proliferative capacity (Fig. 4-6B). This result was initially concluded based on a qualitative reduction in BMSC density surrounding EC-coated beads in the knockdown conditions relative to those containing BMSCs expressing the shNT or wild type BMSCs (Fig. 4-6A). Similarly, knockdown of α6 integrin has previously been shown to have a significant inhibitory effect on 4T1 cell proliferation, but these have not been directly linked [46]. To isolate the knockdown's effect on proliferation from its effect on vessel sprouting, we increased the initial seeding density of ITGA-transduced BMSCs. Our data showed a continued reduction in vessel sprouting despite the addition of BMSCs to compensate for the deficit in proliferation (Fig. 4-7A). This opened the possibility that reduced vessel sprouting is a consequence of α6 integrin inhibition beyond the restricted BMSC proliferation capacity. Thus, the ability of BMSCs to induce EC-derived vessel formation in fibrin may partly be the result of intimate heterotypic contacts via the α6β1 integrin-laminin interactions, which directly or indirectly tune critical matrix remodeling enzymes utilized by ECs to undergo sprouting morphogenesis. The data presented here suggest that this effect is dependent on the physical proximity between EC/BMSC populations as the overlaid BMSCs with attenuated α6 integrin were able to stimulate capillary formation while those distributed throughout EC-containing gels were unable to do so.

4.5 CONCLUSION

The elucidation of the intricate molecular interactions underlying neovascularization remains a challenge. Analysis of the signaling events transduced by cell adhesion molecules to the vascular cells may help unravel the mechanisms that regulate ECM-associated enzymatic activities. The molecular interaction between pericytes and ECs is crucial for the stabilization of newly formed vessels during angiogenesis.

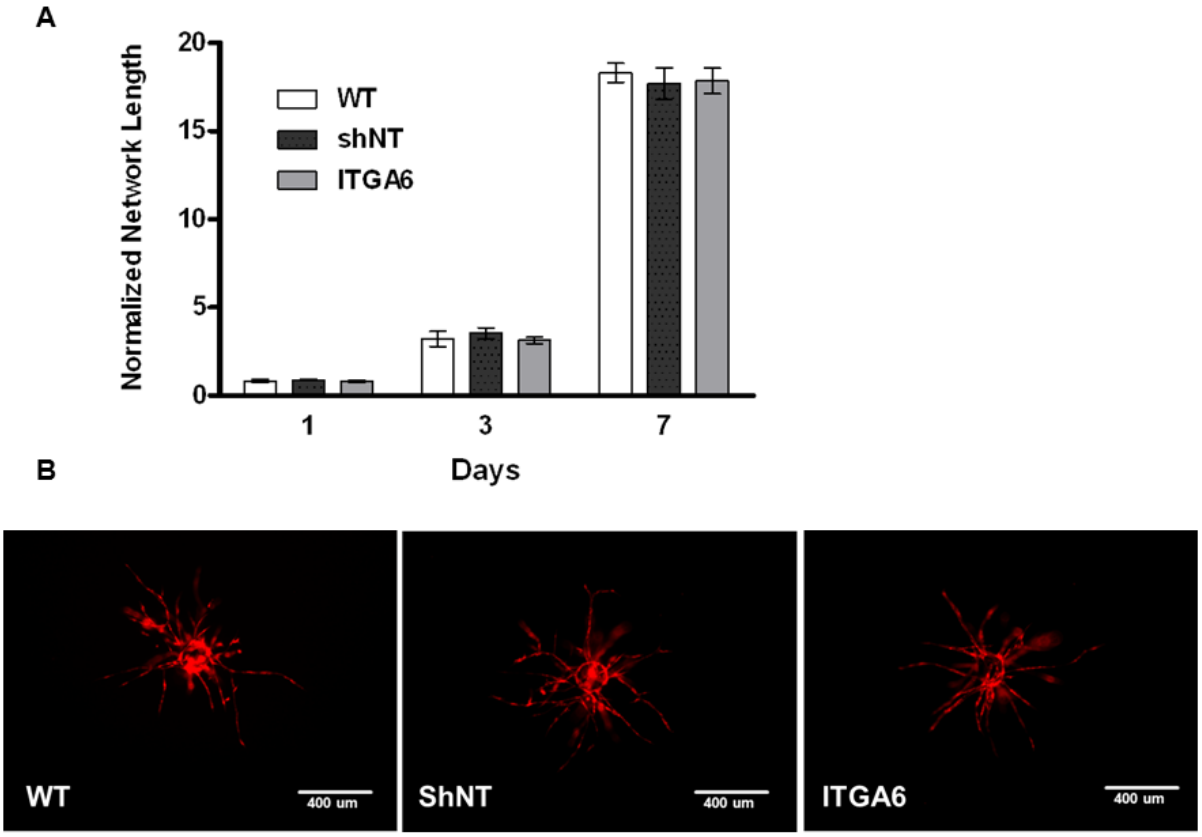

Figure 4-8: α6 integrin-mediated interactions do not regulate vessel sprouting in co-cultures containing overlaid BMSCs. (A) Total vessel network length was quantified from a minimum of 7 fluorescent images over three independent experiments and normalized by day 1 wild type BMSC condition. (B) Day 7 fluorescent images of mCherry-expressing ECs with overlaid (a) wild type BMSCs, (b) BMSCs transduced with the non-targeting shRNA (shNT), (c) BMSCs with shRNA against ITGA6. Scale bar = 400 μm.

The present work demonstrates the role of the interactions between the α6β1 integrin on BMSCs acting as stabilizing pericytes and EC-deposited laminin in sprouting angiogenesis using an established 3D in vitro model. ECs were co-cultured with BMSCs whose α6 integrin subunit was attenuated via RNAi. The expression levels of this integrin subunit expression were reduced by ~80% relative to non-targeting shRNA controls as measured by quantitative polymerase chain reaction (qPCR). After 7 days, ECs co-cultured with BMSCs expressing the α6 integrin shRNA demonstrated a significant reduction in total vessel network length relative to those co-cultured with BMSCs containing the scrambled shRNA. ECs co-cultured with BMSCs transduced with the non-targeting shRNA formed capillary-like networks to the same extent as those co-cultured with wild type BMSCs. Furthermore, fluorescent imaging of co-cultures qualitatively revealed that the BMSCs with knocked-down α6 integrin subunit expression failed to associate with the nascent vessels. Finally, the BMSCs with attenuated α6 integrin expression proliferated approximately 40% less than either control cells expressing non-targeting shRNA or wild type BMSCs. Our data imply that the establishment of heterotypic interactions between ECs and BMSCs in 3D fibrin gels may be an enabling factor for the α6β1 integrin-derived regulation of endothelial vessel formation and stabilization. α6 integrin inhibition in BMSCs distributed throughout EC-containing fibrin gels hampered the ability of ECs to undergo vessel morphogenesis perhaps by downregulating the MMP-dependent signaling pathways that induce ECM degradation; this might in turn lead to reduced BM deposition, and consequent failure of BMSC recruitment to endothelial sites. These findings collectively suggest the requirement of the direct EC-BMSC association through established heterotypic interactions for the BMSCs' ability to promote capillary formation.

This study highlights the importance of the regulation of pericytic association of BMSCs by α6 integrin for angiogenic promoting effects of these cells. In addition to their ability to home to sites of injury [47], resident perivascular MSCs function physiologically to give rise to a regenerative microenvironment via trophic activities [48, 49]. Future studies may have important implications for exploiting the α6 integrin-mediated signaling pathways to manipulate mesenchymal resources that support vessel formation and stabilization under pathological conditions, including diabetes, wound healing, and tumor growth. These implications will be further discussed in Chapter 6.

4.6 REFERENCES

1. Carmeliet, P. and R.K. Jain, Angiogenesis in cancer and other diseases. Nature, 2000. 407(6801): p. 249-57.

2. Zandonella, C., Tissue engineering: The beat goes on. Nature, 2003. 421(6926): p. 884-6.

3. Kaully, T., et al., Vascularization--the conduit to viable engineered tissues. Tissue Eng Part B Rev, 2009. 15(2): p. 159-69.

4. da Silva Meirelles, L., A.I. Caplan, and N.B. Nardi, In search of the in vivo identity of mesenchymal stem cells. Stem Cells, 2008. 26(9): p. 2287-99.

5. Jain, R.K., Molecular regulation of vessel maturation. Nat Med, 2003. 9(6): p. 685-93.

6. Gerhardt, H. and C. Betsholtz, Endothelial-pericyte interactions in angiogenesis. Cell Tissue Res, 2003. 314(1): p. 15-23.

7. McDonald, D.M. and P.L. Choyke, Imaging of angiogenesis: from microscope to clinic. Nat Med, 2003. 9(6): p. 713-25.

8. Cuevas, P., et al., Pericyte endothelial gap junctions in human cerebral capillaries. Anat Embryol (Berl), 1984. 170(2): p. 155-9.

9. Hall, A.P., Review of the pericyte during angiogenesis and its role in cancer and diabetic retinopathy. Toxicol Pathol, 2006. 34(6): p. 763-75.

10. Grainger, S.J. and A.J. Putnam, Assessing the permeability of engineered capillary networks in a 3D culture. PLoS One, 2011. 6(7): p. e22086.

11. Hauner, H., P. Schmid, and E.F. Pfeiffer, Glucocorticoids and insulin promote the differentiation of human adipocyte precursor cells into fat cells. J Clin Endocrinol Metab, 1987. 64(4): p. 832-5.

12. Grigoriadis, A.E., J.N. Heersche, and J.E. Aubin, Differentiation of muscle, fat, cartilage, and bone from progenitor cells present in a bone-derived clonal cell population: effect of dexamethasone. J Cell Biol, 1988. 106(6): p. 2139-51.

13. Ferrari, G., et al., Muscle regeneration by bone marrow-derived myogenic progenitors. Science, 1998. 279(5356): p. 1528-30.

14. Ghajar, C.M., et al., Mesenchymal stem cells enhance angiogenesis in mechanically viable prevascularized tissues via early matrix metalloproteinase upregulation. Tissue Eng, 2006. 12(10): p. 2875-88.

15. Ghajar, C.M., et al., The effect of matrix density on the regulation of 3-D capillary morphogenesis. Biophys J, 2008. 94(5): p. 1930-41.

16. Au, P., et al., Bone marrow-derived mesenchymal stem cells facilitate engineering of long-lasting functional vasculature. Blood, 2008. 111(9): p. 4551-8.

17. Carrion, B., et al., Recreating the perivascular niche ex vivo using a microfluidic approach. Biotechnol Bioeng, 2010. 107(6): p. 1020-8.

18. Kachgal, S., et al., Bone marrow stromal cells stimulate an angiogenic program that requires endothelial MT1-MMP. J Cell Physiol, 2012. 227(11): p. 3546-55.

19. Ghajar, C.M., et al., Mesenchymal cells stimulate capillary morphogenesis via distinct proteolytic mechanisms. Exp Cell Res, 2010. 316(5): p. 813-25.

20. Nakatsu, M.N. and C.C. Hughes, An optimized three-dimensional in vitro model for the analysis of angiogenesis. Methods Enzymol, 2008. 443: p. 65-82.

21. Schmittgen, T.D., et al., Real-time PCR quantification of precursor and mature microRNA. Methods, 2008. 44(1): p. 31-8.

22. Shen, Q., et al., Adult SVZ stem cells lie in a vascular niche: a quantitative analysis of niche cell-cell interactions. Cell Stem Cell, 2008. 3(3): p. 289-300.

23. Sonnenberg, A., et al., A complex of platelet glycoproteins Ic and IIa identified by a rat monoclonal antibody. J Biol Chem, 1987. 262(21): p. 10376-83.

24. Kalluri, R., Basement membranes: structure, assembly and role in tumour angiogenesis. Nat Rev Cancer, 2003. 3(6): p. 422-33.

25. Armulik, A., A. Abramsson, and C. Betsholtz, Endothelial/pericyte interactions. Circ Res, 2005. 97(6): p. 512-23.

26. Crisan, M., et al., A perivascular origin for mesenchymal stem cells in multiple human organs. Cell Stem Cell, 2008. 3(3): p. 301-13.

27. Covas, D.T., et al., Multipotent mesenchymal stromal cells obtained from diverse human tissues share functional properties and gene-expression profile with CD146+ perivascular cells and fibroblasts. Exp Hematol, 2008. 36(5): p. 642-54.

28. Traktuev, D.O., et al., A population of multipotent CD34-positive adipose stromal cells share pericyte and mesenchymal surface markers, reside in a periendothelial location, and stabilize endothelial networks. Circ Res, 2008. 102(1): p. 77-85.

29. Gnecchi, M., et al., Paracrine mechanisms in adult stem cell signaling and therapy. Circ Res, 2008. 103(11): p. 1204-19.

30. Davis, G.E. and D.R. Senger, Endothelial extracellular matrix: biosynthesis, remodeling, and functions during vascular morphogenesis and neovessel stabilization. Circ Res, 2005. 97(11): p. 1093-107.

31. Stratman, A.N., et al., Pericyte recruitment during vasculogenic tube assembly stimulates endothelial basement membrane matrix formation. Blood, 2009. 114(24): p. 5091-101.

32. Senger, D.R. and G.E. Davis, Angiogenesis. Cold Spring Harb Perspect Biol, 2011. 3(8): p. a005090.

33. Stratman, A.N., et al., Endothelial-derived PDGF-BB and HB-EGF coordinately regulate pericyte recruitment during vasculogenic tube assembly and stabilization. Blood, 2010. 116(22): p. 4720-30.

34. Silva, R., et al., Integrins: the keys to unlocking angiogenesis. Arterioscler Thromb Vasc Biol, 2008. 28(10): p. 1703-13.

35. Basbaum, C.B. and Z. Werb, Focalized proteolysis: spatial and temporal regulation of extracellular matrix degradation at the cell surface. Curr Opin Cell Biol, 1996. 8(5): p. 731-8.

36. Saunders, W.B., K.J. Bayless, and G.E. Davis, MMP-1 activation by serine proteases and MMP-10 induces human capillary tubular network collapse and regression in 3D collagen matrices. J Cell Sci, 2005. 118(Pt 10): p. 2325-40.

37. Stratman, A.N., et al., Endothelial cell lumen and vascular guidance tunnel formation requires MT1-MMP-dependent proteolysis in 3-dimensional collagen matrices. Blood, 2009. 114(2): p. 237-47.

38. Sacharidou, A., et al., Endothelial lumen signaling complexes control 3D matrix-specific tubulogenesis through interdependent Cdc42- and MT1-MMP-mediated events. Blood, 2010. 115(25): p. 5259-69.

39. Egeblad, M. and Z. Werb, New functions for the matrix metalloproteinases in cancer progression. Nat Rev Cancer, 2002. 2(3): p. 161-74.

40. Davidson, B., et al., Coordinated expression of integrin subunits, matrix metalloproteinases (MMP), angiogenic genes and Ets transcription factors in advanced-stage ovarian carcinoma: a possible activation pathway? Cancer Metastasis Rev, 2003. 22(1): p. 103-15.

41. Seftor, R.E., et al., Role of the alpha v beta 3 integrin in human melanoma cell invasion. Proc Natl Acad Sci U S A, 1992. 89(5): p. 1557-61.

42. Segain, J.P., et al., Induction of fibroblast gelatinase B expression by direct contact with cell lines derived from primary tumor but not from metastases. Cancer Res, 1996. 56(23): p. 5506-12.

43. Deryugina, E.I., et al., Functional activation of integrin alpha V beta 3 in tumor cells expressing membrane-type 1 matrix metalloproteinase. Int J Cancer, 2000. 86(1): p. 15-23.

44. Morini, M., et al., The alpha 3 beta 1 integrin is associated with mammary carcinoma cell metastasis, invasion, and gelatinase B (MMP-9) activity. Int J Cancer, 2000. 87(3): p. 336-42.

45. Riikonen, T., et al., Integrin alpha 2 beta 1 is a positive regulator of collagenase (MMP-1) and collagen alpha 1(I) gene expression. J Biol Chem, 1995. 270(22): p. 13548-52.

46. Wang, Y., et al., Integrin subunits alpha5 and alpha6 regulate cell cycle by modulating the chk1 and Rb/E2F pathways to affect breast cancer metastasis. Mol Cancer, 2011. 10: p. 84.

47. Hall, B., M. Andreeff, and F. Marini, The participation of mesenchymal stem cells in tumor stroma formation and their application as targeted-gene delivery vehicles. Handb Exp Pharmacol, 2007(180): p. 263-83.

48. Dennis, J.E. and A.I. Caplan, Analysis of the developmental potential of conditionally immortal marrow-derived mesenchymal progenitor cells isolated from the H-2Kb-tsA58 transgenic mouse. Connect Tissue Res, 1996. 35(1-4): p. 93-9.

49. Caplan, A.I., All MSCs are pericytes? Cell Stem Cell, 2008. 3(3): p. 229-30.

CHAPTER 5

A SAFE AND EFFICIENT METHOD TO RETRIEVE CELLS FROM THREE-DIMENSIONAL FIBRIN GELS

5.1 INTRODUCTION

Chapter 4 described how BMSCs promote angiogenesis in ECs, partly via the interactions between their α6β1 integrin adhesion receptor with EC-deposited laminin. In order to do more rigorous analyses of the BMSCs distributed throughout fibrin gels required retrieving these cells from 3D matrices. Proteolytic enzymes, including trypsin and collagenase, have been used for primary cell isolation from a variety of tissue types. However, longer incubation times with these enzymes required for dissolving fibrin gels results in damaged cells. In this chapter, some of these enzymes will be used to demonstrate their inability to yield a single cell suspension effectively. To this end, the goal is to develop and apply an efficient and safe method to recover cells encapsulated within 3D fibrin hydrogels, starting with brief introduction to the importance of developing protocols for retrieving BMSCs, in particular, from 3D matrices.

Bone marrow stromal cells, commonly referred to as mesenchymal stem cells (MSCs), are non-hematopoietic cells found in the adult bone marrow that possess multipotent characteristics. MSCs have the ability to differentiate into multiple lineages, including osteogenic, adipogenic, and chondrogenic phenotypes. Due to their high degree of plasticity and relative ease of isolation from many tissues [1-5], MSCs have been explored in numerous clinical trials for tissue engineering and regenerative medicine applications. Despite the apparent therapeutic potential of

MSCs, most likely through trophic factor secretion [6], current understanding of the intrinsic and extrinsic components of the microenvironment that regulate their activity *in vivo* remains incomplete. Fundamental knowledge regarding these components is desirable, not only to better understand MSC biology, but also to improve the translational potential of these cells.

The current dogma is that developing physiologically relevant artificial models capable of instructing stem cells will require a more accurate recapitulation of their native niche [7, 8]. In an attempt to reconstruct the stem cell microenvironment that more closely mimicks *in vivo* conditions, many investigators are exploring the use of three- dimensional culture systems. Recent studies suggest that MSCs maintained in two-dimensional culture systems gradually lose their proliferative potential, colony forming efficiency, and differentiation capacity with time [9-11]. While the evidence that 3D culture method provide a cellular environment more consistent with that *in vivo* is persuasive [12-17], there is still a clinical need for an optimized culture model for large scale, long term expansion of stem cells with uniform properties that are capable of differentiating into selected mature cell types of high purity [18]. Furthermore, the development of efficient methods to safely extract these cells from 3D tissue culture is important, both to meet the high cell volumes required for therapeutic applications and to characterize how cells grown in 3D models are regulated by various components of an artificial niche.

In this particular study, we focused on MSC encapsulation within fibrin, in part because fibrin is a widely-used material [19], that has been shown to promote cell survival and proliferation both *in vitro* and *in vivo* [20-23]. There is compelling evidence that fibrin supports delivery of stem cells, such as bone marrow mononuclear cells (BMMNC) [24, 25], human MSCs [20, 26, 27], and stimulate MSC differentiation toward osteogenic and chondrogenic differentiation [27-29]. In our own work, we have used fibrin extensively as an ECM analog

capable of supporting capillary morphogenesis *in vitro* [30], and neovascularization *in vivo* [31]. We have also shown that co-cultures of MSCs and endothelial cells in 3D fibrin hydrogels readily form pericyte-invested capillary networks [30, 32], which has prompted our efforts to better understand how the perivascular location of MSCs may influence their phenotype [32]. However, our efforts were hampered in part because we needed a simple yet effective method to safely recover and characterize MSCs residing in the fibrin hydrogels.

Recovery of cells from collagen hydrogels and collagen-based tissues can be readily achieved using collagenase, but no comparably simple method to retrieve viable cells from 3D fibrin culture models exists, to the best of our knowledge. In most cases, commonly used proteolytic enzymes, including Trypsin and Collagenase, have been used for primary cell isolation from a variety of tissue types [33-36]. However, when used to dissolve fibrin for *in vitro* models, these enzymes do not yield a single cell suspension effectively. Furthermore, longer incubation times with these enzymes required for dissolving the gels may damage the cells harvested for subcultivation or other studies. Previous studies have used 3D fibrin gels as biomimetic substrates for isolation of stem cells residing in various tissues [37, 38]. Using urokinase, cells outgrown from these tissues were isolated by selective degradation of the 3D fibrin gels. In this paper, we used nattokinase, a Bacillus-derived serine protease that is known for its potent fibrinolytic activity [39, 40], to recover encapsulated MSCs from 3D fibrin gels. Compared with other fibrinolytic enzymes like urokinase and plasmin, nattokinase is more efficient in degrading fibrin gels [40]. We demonstrated that nattokinase yields significantly higher MSC recovery as compared with other proteolytic enzymes, including Trypsin and TrypLE. Additionally, we found that this enzyme mediated recovery is not harmful, as assessed by cellular proliferation and viability in 3D culture. Finally, using our extraction protocol, we

showed that cells recovered from 3D hydrogels were capable of differentiating into osteogenic and adipogenic lineages.

3D cultures allow researchers to more closely recapitulate actual *in vivo* conditions for cell-based studies. In particular, stem cell research has already benefited from this new perspective. Fibrin gels provide a natural provisional matrix for cell survival and proliferation, and thus can be used to better understand how various components of an artificial niche may impact stem cells maintained in a 3D microenvironment. However, despite the potential of 3D fibrin gels for studying the phenotypic behavior of stem cells in response to the interactions with their niche elements, there is still a need for a simple yet effective method for cell recovery from these 3D hydrogels. The extraction method, presented in this study, is not only an effective system for safe recovery of MSCs residing in the fibrin gels, but could also potentially be used to safely and efficiently harvest a variety of cell types from 3D fibrin cultures for subsequent use in numerous applications, including expansion, bioassays, and *in vivo* implantation.

5.2 METHODS

Cell culture: Human bone marrow-derived MSCs were obtained from a commercial source (Lonza, Walkersville, MD) at passage 2. As part of the manufacturer's quality control, these MSCs were tested for purity by flow cytometry and for their ability to differentiate into osteogenic, chondrogenic and adipogenic lineages. Cells are positive for the cell surface markers CD105, CD166, CD29 (integrin β1), and CD44, and negative for CD14, CD34 and CD45. MSCs were maintained in high glucose (4.5 g/L) Dulbecco's modified Eagle medium (DMEM, Invitrogen, Carlsbad, CA) supplemented with 10% fetal bovine serum (FBS, Invitrogen). All

cultures were incubated at 37°C and 5% CO2. Media were changed every 2 days. MSCs grown in 2D cultures were harvested with 0.05% Trypsin-EDTA (Invitrogen). MSCs were used prior to passage 8.

Construction of the 3D culture model: MSCs were encapsulated within 3D fibrin gels similar to those to create a 3D co-culture model of capillary morphogenesis described previously [41]. In brief, 5×10^4 MSCs were mixed within a 2.5 mg/mL fibrinogen solution (Sigma-Aldrich, St. Louis, MO; Lot#069K7636v, 65-85% protein). Five hundred microliters of this solution containing MSCs was combined with 10 μL of thrombin (50 U/mL; Sigma) in a single well of a 12-well plate to make one gel construct. This process was repeated until the desired number of gels was constructed. Constructs were left undisturbed for 5 min to allow partial gelation before incubating for an additional 25 min at 37°C and 5% CO_2. Gels were then cultured in DMEM supplemented with 10% FBS. Media were changed every 2 days. Cells were retrieved from 3D fibrin gels at three time points post assembly: days 1, 7, and 14.

Retrieving viable cells from 3D fibrin gel constructs: MSCs embedded in 3D fibrin gels were recovered using one of three methods: our novel recovery technique (Fig. 4-1) involving the fibrinolytic enzyme nattokinase, or methods involving 0.05% Trypsin-EDTA (Gibco, Grand Island, NY) or TrypLE (Invitrogen). In our new method, a fibrinolytic solution was prepared by dissolving 50 FU/mL (fibrin degradation unit) of nattokinase (NSK-SD, Japan Bio Science Laboratory Co., Ltd, Osaka, Japan), in PBS containing 1 mM EDTA (Fisher Scientific). Gels were washed with PBS before dislodging them from the well siding using a small spatula. Gels were subsequently dissolved by adding 500 μl of the fibrinolytic solution and incubating at 37°C for 30 min. Upon dissolution, the contents of each well were collected and centrifuged. Cells were then washed with cold PBS before subsequent procedures.

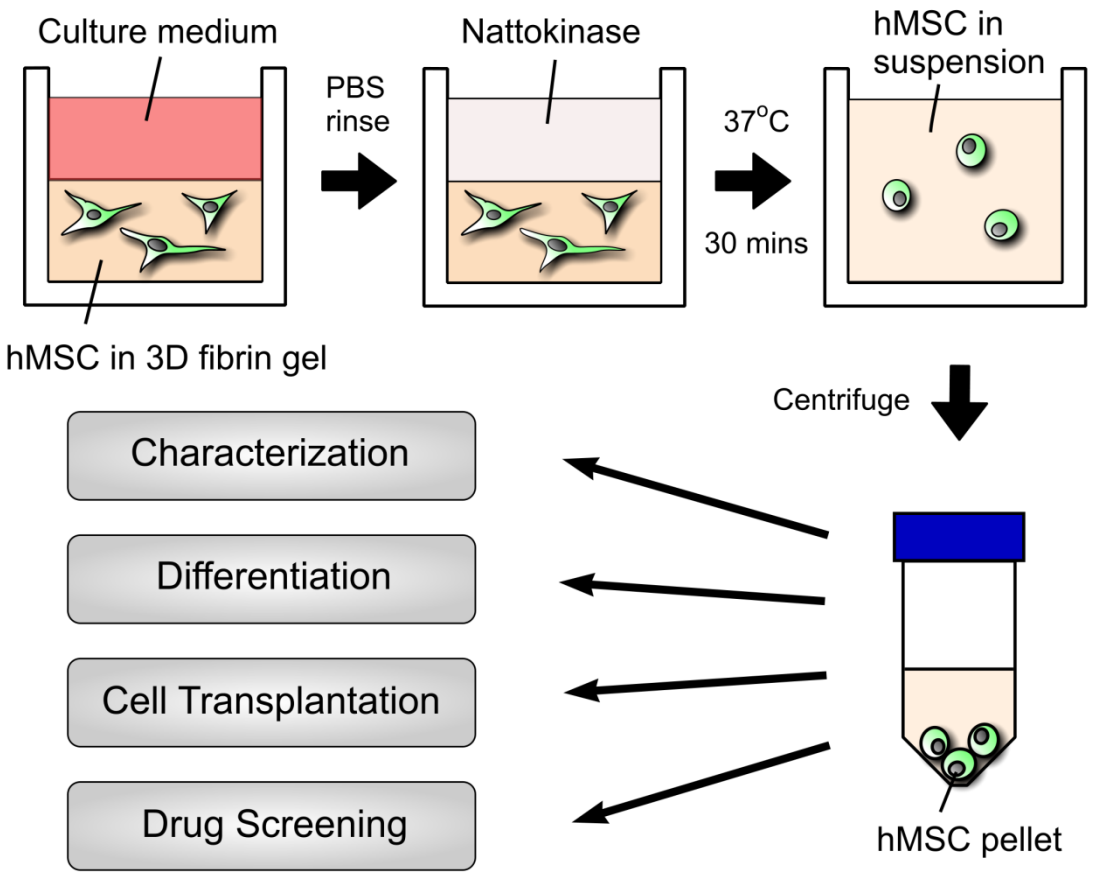

Figure 5-1: Illustration depicting how MSCs were grown and extracted from 3D fibrin gels. The key ingredient of our successful extraction method is nattokinase, a serine protease of the subtilisin family that has strong fibrinolytic activity. Demonstrated for MSCs, this method can be readily adapted to retrieve any other cell type from 3D fibrin gel constructs for various applications, including characterization, differentiation, cell transplantation, and drug screening**.**

Quantitative polymerase chain reaction (qPCR): The multilineage potential of MSCs recovered following fibrinolysis was determined in part via qPCR to assess the expression of genes associated with osteogenic and adipogenic differentiation. In brief, MSCs cultured for up to 14 days were retrieved from either 3D fibrin gels using our novel nattokinase-base recovery method or collected from 2D cultures via standard trypsinization. Harvested cells were then subjected to standard adipogenic or osteogenic induction protocols (described below) in 2D culture for 7 and 21 days, respectively [42-45]. Total RNA was isolated from cells using the SV

Total RNA Isolation System (Promega, Madison, WI). The RNA concentration and purity of each sample were determined by A260/A280 absorptions using a Nanodrop ND-1000 (Thermo Scientific, Rochester, NY) spectrometer. Equal amounts of total RNA from each sample were used to create first strand cDNA using the ImProm-II Reverse Transcription System (Promega). The PCR amplification was performed with the DAPA SYBR® Fast Universal Master Mix (Kapa Biosystems, Woburn, MA) on a 7500 Fast Real-Time PCR System (Applied Biosystems) in a final volume of 20 µl using cycling parameters (3 min 95°C; 3 sec, 95°C; 20 sec, 60°C with the latter two steps repeated for 40 times). Each reaction was performed in triplicate and the ΔΔCt method was used for the gene expression analysis. PPIA was used as the housekeeping gene as it has been shown to have the most stable expression levels under different conditions [46]. The primer sequences of the genes for q-PCR are provided in Table 4-1.

Gene	Sense primer	Anti-sense primer
BGLAP	5'-AGGCACCCTTCTTTCCTCTTC-3'	5'-TTCCTCTTCTGGAGTTTATTTGGGA-3'
CEBPA	5'-ATGCAAACTCACCGCTCCAAT-3'	5'-GAGGCAGGAAACCTCCAAATAAA-3'
PPARG	5'-ATTACGAAGACATTCCATTCACAAG-3'	5'-CTCAGAATAATAAGGTGGAGATGC-3'
PPIA	5'-GTCTTGTGTGTTGTCTGGTTA-3'	5'-ATGTTTGATGTTTATTTCCACCTTG-3'
RUNX2	5'-CAGAAGGGAGGAGATGTGTGTA-3'	5'-TTGCTAATGCTTCGTGTTTCCA-3'

Table 5-1: Depicts primer sequences designed via Primer-Blast and used for qPCR.

Quantification of cell viability via fluorescent activated cell sorting (FACS): To assess viability, cells were retrieved from 3D cultures 6 hours after initial cell seeding using the nattokinase fibrinolytic solution described above. Cells were then resuspended in ice cold PBS containing 0.1-0.5% bovine serum albumin (BSA, Sigma Aldrich), pelleted by centrifugation at

2000 rpm at 4°C for 5 minutes, and then incubated with a 3 μM solution of propidium iodide (PI, Invitrogen) in staining buffer (100 mM Tris, pH 7.4, 150 mM NaCl, 1 mM CaCl2, 0.5 mM MgCl2, 0.1% Nonidet P-40) for 15 minutes at room temperature. Samples were then washed twice and resuspended in 0.5% BSA in PBS for flow cytometry analysis. Unstained cell suspensions were prepared in parallel as control samples.

Multilineage differentiation protocols: For adipogenic differentiation, MSCs retrieved from 2D cultures or extracted from a 3D fibrin gel were reseeded at the density of 20,000 (cells/cm^2). 24-well plates were used for functional assays. 6-well plates were used for gene expression assays via qPCR. Cells were maintained in either adipogenic growth media (AGM, a control), consisting of αMEM (Gibco), 10% FBS, 1% penicillin/streptomycin (CellGro, Manassas, VA), and 5 mg/mL gentamicin (Gibco), or adipogenic induction media (AIM), consisting of AGM, 1 μM dexamethasone (Sigma-Aldrich, St. Louis, MO), 0.5 mM 3-isobutyl-1-methylxanthine (IBMX) (Acros Organics, Geel, Belgium), 10 μg/mL insulin (Gibco), 0.2 mM indomethacin (Sigma-Aldrich) [47]. For osteogenic differentiation, MSCs retrieved from 2D cultures or extracted from a 3D fibrin gel were reseeded at 5,000 cells/cm^2, in a 24-well plate for functional assays, or in a 6-well plate for qPCR. Cells were maintained in osteogenic growth media (OGM), consisting of αMEM (Gibco), 20% FBS, 2mM L-glutamine (CellGro), 1% penicillin/streptomycin, and 5mg/mL gentamicin, or osteogenic base media (OBM), consisting of OGM, 10mM β-glycerol phosphate (Sigma-Aldrich), and 50 μg/mL L-ascorbic acid (Fisher Scientific). After 14 days in OBM, cells were cultured in osteogenic mineralization media (OMM, containing OBM + 100nM dexamethasone (Sigma-Aldrich)) as previously reported [47]. For simplicity OBM and OMM will be referred to as osteogenic induction media (OIM).

Oil red O staining, imaging, and quantification: Adipogenic differentiation was assessed in part by staining cultures with Oil Red O and quantifying as previously described [48]. Briefly, a 12.2 mM stock solution of Oil Red O dye (Sigma) was dissolved in isopropanol. Cells were fixed in 4% paraformaldehyde at 4°C for 30 minutes after 7 and 14 days of culture in AIM. Cells were then rinsed in PBS at least twice. Stock Oil Red O solution was added to PBS at a ration of 3:2 to create the working solution. The working solution was filtered with a 0.22 micron filter (Millipore, Billerica, MA) prior to use. Each well was immersed in the Oil Red O working solution for 20 minutes. After staining, each well was quickly rinsed 3 times in a 60/40 isopropanol/PBS solution to remove excess Oil Red O. The wells were then rinsed twice in PBS and imaged on an Olympus microscope IX51 equipped with a DP25 color camera. After imaging, 4% IGEPAL-CA630 (Sigma) in isopropanol was added to each well and protected from light for 15 minutes. Each well was then analyzed with a Thermo Scientific Multiskan Spectrum spectrophotometer at 520 nm to determine the absorbance of each well. The absorbance of Oil Red O was normalized to the total cell number in each well as determined by nuclei counting using DAPI staining [49]. Three images per condition were analyzed to determine the number of cells per well. Four wells per condition were used to quantify the levels of Oil Red O.

Von kossa staining: Cells were rinsed in PBS twice and then fixed with 4% paraformaldehyde at 4°C for 30 minutes after 14 and 21 days in OIM. After fixation, cells were rinsed in double distilled (DD) water three times and then immersed in 5% $AgNO_3$ (Sigma) and subjected to UV light (~365 nm) for 40 minutes. After UV exposure cells were rinsed three times in DD water. The cells were then rinsed in sodium thiosulfate (Sigma) for 3 minutes and rinsed in DD water three times. Images were taken on an Olympus IX51 with a DP25 color camera.

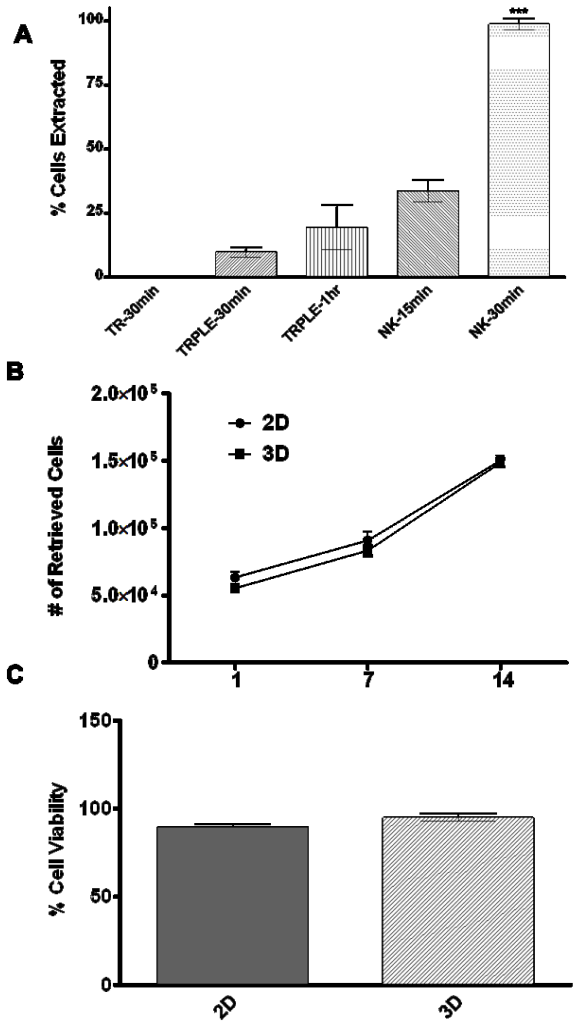

Figure 5-2: Enzyme-assisted extraction of MSCs from 2D and 3D cultures. (a) Nattokinase yielded significantly higher percent of MSCs extracted from 3D fibrin gels relative to the other proteolytic enzymes (Trypsin and TrypLE). Gels were dissolved 6 hours after initial cell seeding (50K cells/gels). Retrieved cells were pooled together from a total of 3 gels for each technical sample. *** refers to $p \leq 0.001$ with respect to the other conditions. (b) The number of cells retrieved from 3D using nattokinase was comparable to that harvested from 2D (using Trypsin) after up to 2 weeks in culture. MSCs were retrieved from cultures at day 1, 7, and 14. (c) Flow cytometry data showed nearly 100% cell viability after extraction with nattokinase. 14 day MSCs were stained with PI for viability analysis. The percentage of live cells was assessed based on the number of unstained cells. (b, c) Trypsin and nattokinase were used to recover cells from 2D and 3D cultures, respectively**.**

Calcium quantification: Calcium content in osteogenic cultures was quantified using the ortho-cresolphthalein complexone (OCPC) method, as previously described [42, 43]. Cells were

washed in PBS twice before incubation in 1 mL of 1 N acetic acid overnight. The OCPC solution was prepared by adding OCPC to DD water with 1 N KOH and 1 N acetic acid.

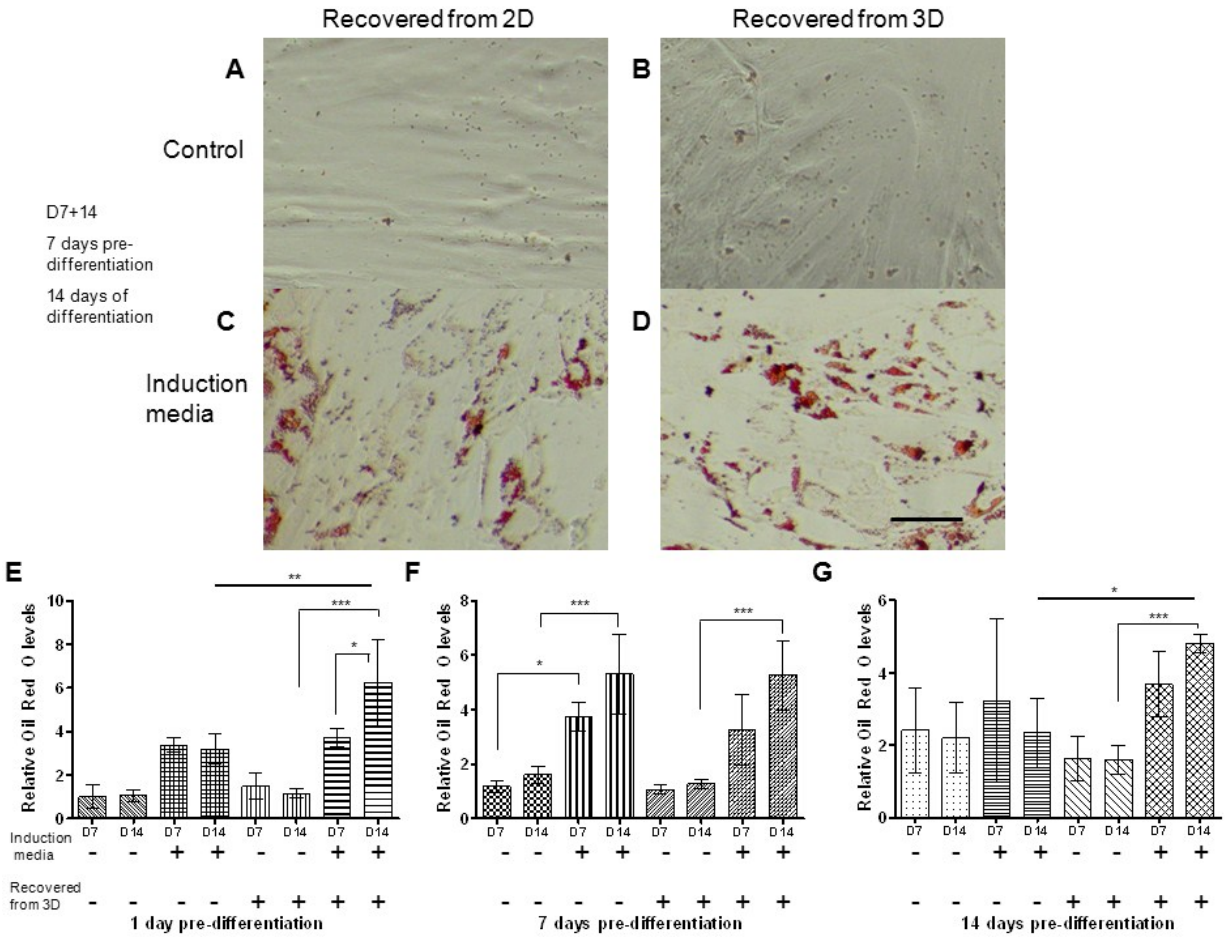

Figure 5-3: MSCs maintain their potential to become adipogenic after extraction from 3D fibrin gels. Micrographs from MSCs grown on 2D TCPS (A, C) or in 3D fibrin gels (B, D) for 7 days and then extracted and maintained in growth media (A, B) or differentiated in adipogenic media (C, D) for 14 additional days. Cells in C and D were stained using the Oil Red O method. Scales bar = 200 μm. Results in E show differences in cells grown for 1 day in 2D or 3D environments; recovered and then subjected to growth media or adipogenic induction media for 7 (A) or 14 (B) days. Results in F show differences in cells grown for 7 days in 2D or 3D environments; recovered and then subjected to growth media or adipogenic media for 7 (A) or 14 (B) days. All conditions were normalized by cell number per well and then again relative to levels expressed by 2D control A (after 1 day of pre-differentiation). * refers to $P \leq 0.05$, ** refers to $p \leq 0.01$, and *** refers to $p \leq 0.001$ for statistical significance.

The dissolved solutions (10 µL per replicate) were then mixed with a working solution (300 µL per replicate) of OCPC solution and ethanolamine/boric acid/8-hydroxyquinoline buffer (all from Sigma, except KOH (Acros)). Absorbance values were recorded using a Thermo Scientific Multiskan Spectrum spectrophotometer at 570 nm. Calcium values were quantified via a standard curve from 0-150 µg/mL. Samples and standards were assayed in triplicate.

Statistical analysis: Statistical analyses were carried out using GraphPad Prism software. Data are reported as means ± standard deviations. All statistical comparisons were made by performing a one-way analysis of variance (ANOVA), followed by Tukey's multiple comparison tests to judge significance between two data sets at a time. *P* values less than 0.05 were considered statistically significant.

5.3 RESULTS

Nattokinase efficiently degrades 3D fibrin gels without damaging cells. In this study, we developed and applied a new method (Fig. 5-1) to recover cells encapsulated within 3D fibrin hydrogels based on nattokinase, a powerful fibrinolytic enzyme that is mostly known for its blood thinning effects. To validate the method, we first quantified the percentage of cells extracted from 3D fibrin gels (Fig. 5-2A). Six hours after initial cell encapsulation, fibrin gels were degraded using either Trypsin TrypLE or our nattokinase solution. A 30-minute incubation in the nattokinase solution enabled nearly 100% of the entrapped cells to be recovered. By comparison, a significantly lower percentage of the encapsulated MSCs were retrieved from the gels using either Trypsin or TrypLE. Quantification of propidium iodide staining via flow cytometry revealed similar levels of cell viability in 3D gels digested using nattokinase to those

obtained for recovered cells from 2D cultures (Fig. 5-2B). In addition, we also cultured the MSCs within 3D fibrin gels for up to 14 days, and quantified the number of cells retrieved via nattokinase to assess their proliferation rates. Data showed that MSCs proliferated at comparable rates in both 2D and 3D (Fig. 5-2C).

MSCs retrieved from 3D fibrin gels maintain their adipogenic potential. To assess the adipogenic differentiation potential of MSCs retrieved from 3D fibrin gels, harvested cells were grown in media with various factors known to induce adipogenic differentiation followed by staining for the presence of lipid deposits with Oil Red O [44]. Lipid deposits were detected at 7 and 14 days after induction (Fig. 5-3C, D). Quantitative assessment of Oil Red O levels (Fig. 5-3E, F, G) shows that MSCs retrieved from 3D fibrin gels via nattokinase can be readily induced to form lipid droplets and with the levels of Oil Red O comparable to those from cells cultured exclusively in 2D. These data suggest that nattokinase extraction of MSCs from fibrin does not diminish their ability to differentiate into adipocytes.

MSCs retrieved from 3D fibrin gels maintain their osteogenic potential. To assess MSCs' osteogenic differentiation potential, cells were cultured in OIM after extraction from 3D fibrin gels using nattokinase, and compared to those grown exclusively on tissue culture polystyrene (TCPS) as a control. Mineral deposition was visualized via the common Von Kossa phosphate staining protocol. MSCs differentiated in OIM after growth on 2D TCPS or recovered from 3D fibrin gels stained positive for phosphates after 14 and 21 days (Fig. 5-4C, D). In parallel, the amounts of calcium deposited by the MSCs were quantified via the OCPC method. Cells cultured in OIM showed elevated calcium levels (compared to non-induced controls), regardless of whether or not they were grown exclusively in 2D or had first been extracted from 3D fibrin gels via nattokinase (Fig. 5-4E, F, G).

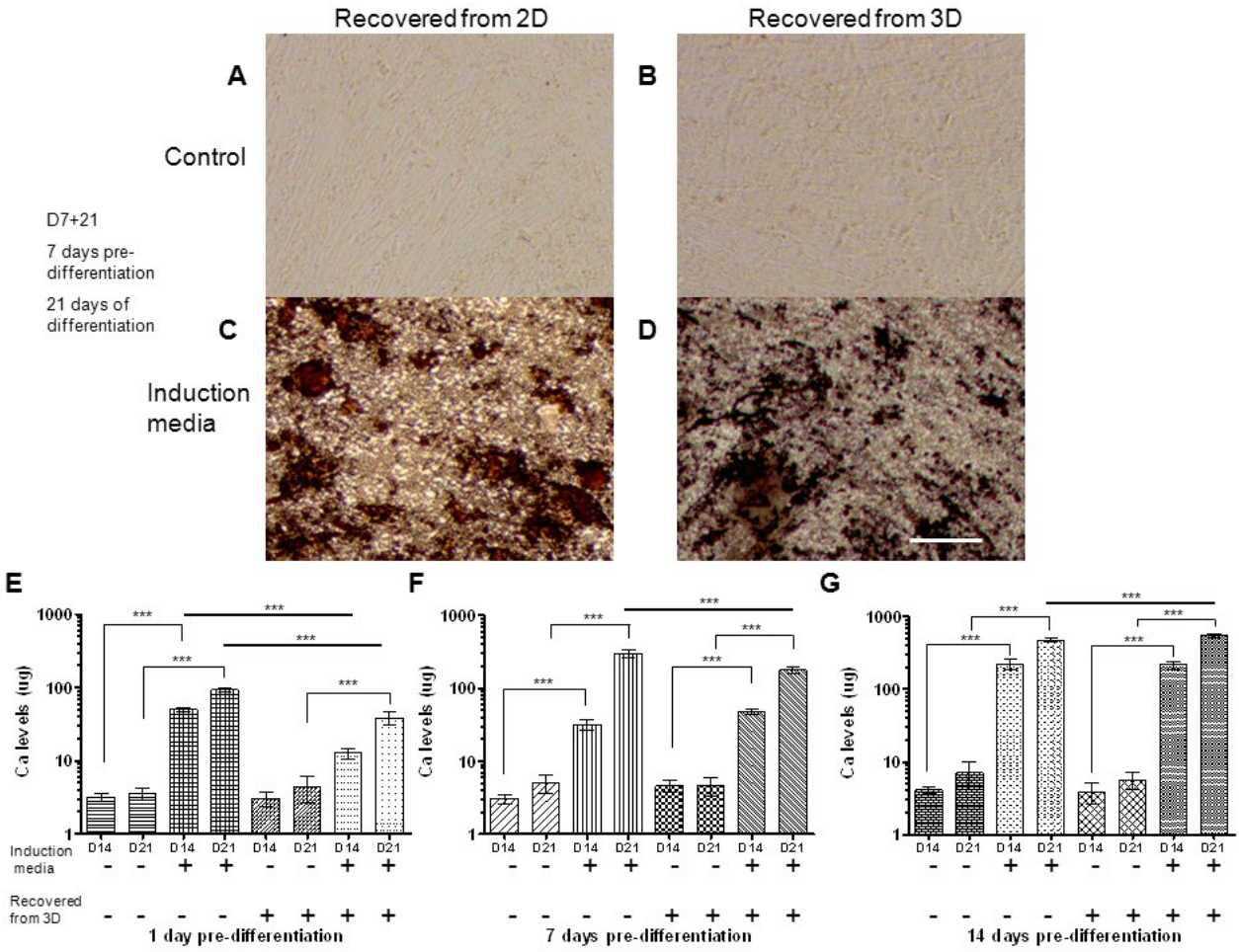

Figure 5-4: MSCs maintain the potential to become osteogenic after extraction from 3D fibrin gels. Micrographs from MSCs grown on 2D TCPS (A, C) or in 3D fibrin gels (B, D) for 7 days and then extracted and maintained in growth media (A, B) or differentiated in osteogenic media (C, D) for 21 additional days cells in C and D were stained using Von Kossa method. Scale bar = 200 μm. Results in E show differences in cells grown for 1 day in 2D or 3D environments; recovered and then subjected to growth media or osteogenic induction media for 14 (A) or 21 (B) days. Results in F show differences in cells grown for 7 days in 2D or 3D environments; recovered and then subjected to growth media or osteogenic media for 14 (A) or 21 (B) days. Results in G show differences in cells grown for 14 days in 2D or 3D environments; recovered and then subjected to growth media or osteogenic media for 14 (A) or 21 (B) days. Calcium levels between 14 and 21 day differentiation time points did increase significantly (*** refers to $p \leq 0.001$) for both 2D and 3D conditions.

Specifically, cells grown for 14 days in 3D gels and recovered with nattokinase and then differentiated for 14 additional days showed equivalent calcium levels compared to cells grown

on a 2D surface. Collectively, these data qualitatively and quantitatively suggest that nattokinase extraction of MSCs from fibrin does not reduce their osteogenic differentiation potential.

MSCs retrieved from 3D fibrin gels express genes associated with osteogenic and adipogenic lineages. Finally, we quantified the expression of several genes associated with adipogenic and osteogenic differentiation to further assess how well MSCs extracted from 3D fibrin gels via nattokinase sustain their multipotency. As for the Oil Red O, Von Kossa, and calcium assays described above, MSCs were first grown on 2D TCPS or within 3D fibrin gels for 14 days, recovered, subjected to the appropriate induction media favorable for differentiation. Gene expression analysis was performed on cells after 7 and 21 days in adipogenic and osteogenic-specific culture conditions, respectively. Similar levels of *PPARγ* and *CEBPα* were detected in cells cultured in adipogenic media for 7 days (Fig. 5-5A, B), regardless of whether they had first been cultured in 3D fibrin gels and recovered with nattokinase or cultured exclusively on 2D TCPS. However, control cultures grown in baseline medium did not show adipogenic differentiation. Likewise, qPCR analysis confirmed that MSCs retrieved from 3D fibrin gels via nattokinase were also able to upregulate the gene expression levels of *Runx2* and *BGLAP* in response to osteogenic inductive media (Fig. 5-5C, D). These finding collectively suggest that nattokinase extraction of MSCs from 3D fibrin gels does not negatively impact their ability to express key genes associated with adipogenic and osteogenic differentiation.

5.4 DISSCUSSION

In much of our lab work, fibrin, a natural protein-based material that serves as the provisional ECM during wound healing, has been utilized. Fibrin has proven to be useful in numerous tissue

engineering applications, and is FDA approved as a hemostatic material.

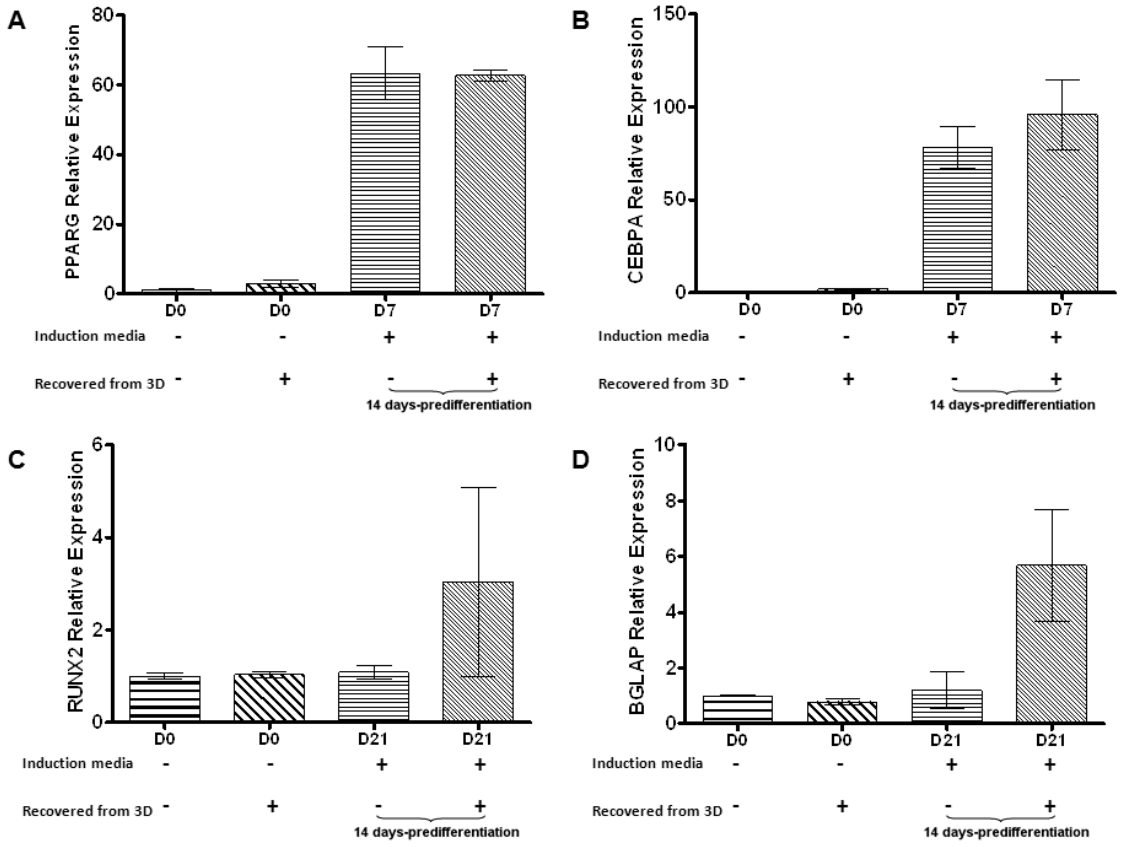

Figure 5-5: qPCR analysis of adipogenic and osteogenic marker gene expression levels in MSCs retrieved from culture conditions. Gene expression analysis showed that nattokinase extraction did not negatively affect the osteogenic and adipogenic potential of MSCs. MSCs were recovered from 2D and 3D cultures at day 14 and subjected to adipogenic and osteogenic induction media for 7 and 21 days, respectively. Total RNA were extracted and subjected to qPCR analysis to assess for (A) *PPARG*, (B) *CEBPA*, (C) *RUNX2*, and (D) *BGLAP* expression.

Its rapid sell-assembly driven by thrombin-mediated alteration of fibrinogen makes fibrin an attractive 3D substrate in which cells can adhere, spread, proliferate, and undergo complex morphogenetic programs. However, there is significant need for simple, cost-effective methods to safely retrieve cells encapsulated within fibrin hydrogels in order to perform additional analyses or use the cells for therapy. In this chapter, we present a safe and efficient protocol for the isolation of cells from 3D fibrin gels. The key ingredient of our successful extraction method

is nattokinase, a serine protease of the subtilisin family that has strong fibrinolytic activity. Our data show that MSCs recovered from 3D fibrin gels using nattokinase are not only viable, but also retain their proliferative and multilineage potential. Demonstrated for MSCs, this method can be readily adapted to retrieve any other cell type from 3D fibrin gel constructs for various applications, including expansion, bioassays, and in vivo implantation.

Removing MSCs from 3D fibrin cells with nattokinase was both efficient and had no deleterious effect on MSC cell proliferation (Fig. 5-2B). This result suggests that MSC proliferation is similar in 3D fibrin gels as it is on 2D tissue culture plastic. In addition, nattokinase extraction did not influence their potential to become osteogenic or adipogenic. Specifically, analysis of Oil Red O levels, an indicator of lipid formation, showed that nattokinase extraction from 3D gels had no negative effects when compared to control cells (Fig. 5-3). Furthermore, q-PCR analysis of gene expression levels known to signify adipogenic differentiation, PPARG-a key regulator of adipogenesis and CEBPA-a positive feedback loop regulator of PPARG expression [45], suggested that nattokinase extraction after 14 days in 3D culture followed by 7 days of exposure to differentiation media did not affect the adipogenic potential of MSCs (Fig. 5-5A, B). We also assessed the potential of extracted MSCs to become osteogenic to confirm multipotentiality. Von Kossa staining and calcium levels suggested qualitatively and quantitatively that nattokinase did not functionally alter the ability of MSCs to synthesis a matrix capable of mineralization (Fig. 5-4). qPCR gene expression analysis also confirmed that cells were osteogenic after nattokinase extraction. The expression of BGLAP (osteocalcin) in cells extracted from 3D was elevated with respect to cells grown on 2D surfaces (Fig. 5-5D). Osteocalcin has been shown to be expressed in cells with a mature osteogenic phenotype [50]. RUNX2 expression (Fig 5-5C) was not significantly upregulated after 21 days of

induction preceded by 21 days in 3D fibrin gels. This can be expected as RUNX2 is an early marker of osteogenic expression [51]. Collectively, these data suggest that extraction of MSCs from 3D fibrin gels using nattokinase does not negatively modify their multipotency.

Ensuring that nattokinase extraction did not influence multipotency was important to address because MSCs have been touted and used for many different applications including: infracted myocardium repair, bone synthesis, soft tissue regeneration, cancer treatments, and other therapies [52]. While the therapeutic mechanisms of MSCs are yet to be fully elucidated it is clear that a large number of cells (~107) are needed for various therapy applications as the number of cells that differentiate and engraft to the implantation site is quite low [52]. Because of their low frequency in bone marrow and the large number needed for in vivo treatments, in vitro expansion of MSCs is necessary to obtain the required number to meet the demands of therapeutic methods [53]. Therefore, 3D expansion of MSCs and subsequent extraction with nattokinase is one viable option to obtain the requisite quantity of cells needed for in vivo therapies.

The reason for greater efficiency of nattokinase is likely due to the high affinity and fibrinolytic nature of nattokinase to cross-linked fibrin [54]. A previous report suggested that nattokinase has higher affinity to cross-linked fibrin than plasmin [55]. We are unaware of direct comparisons of the affinity of nattokinase to fibrin in comparison to trypsin; however, plasmin and trypsin are known to share similar specificity, though trypsin has markedly lower affinity to fibrin compared to plasmin [56]. Thus, trypsin's lower affinity to fibrin is likely the reason that trypsin is less efficient (at attacking the serine peptide in fibrin) compared to nattokinase for cell extraction. Proteases that act to degrade the fibrin gel network can be either specific or non-specific. Specific proteases act on exclusive peptide sites (depending on the protease).

Specifically, the 'catalytic triad' located in the carboxyl-terminal region of the serine protease (i.e. nattokinase) attacks the target serine peptide bond [57]. Trypsin is a specific protease for matrix digestion and is commonly used to passage cells during 2D cell culture. One downside to trypsin treatment is that it is known to cause an upregulation in proteins that regulate apoptosis as cell surface proteins are often cleaved causing changes or disruptions in cell function [58]. Interestingly, trypsin is a known activator of the major fibrinolytic protease plasmin. Plasmin is a broad spectrum protease capable of degrading multiple ECM targets including fibrin [59]. Alternatives to trypsin and plasmin that have been cited in literature include Proteinase K (a non-specific protease), collagenase, and Accutase. Previously, urokinase has been utilized for isolation of cells by degradation of 3D fibrin gel constructs [60]. Urokinase (urokinase-type plasminogen activator) is a serine protease that cannot bind directly to fibrin as it lacks a lysine binding site, thus is not an ideal selection for cell extraction. With evidence presented in this chapter, it is convincing that the method using nattokinase is by far has greater efficiency with respect to cell recovery from fibrin gels.

5.5 CONCLUSION

In this chapter, the importance of developing protocols for retrieving BMSCs from 3D matrices is described. MSCs display multipotent characteristics that make them ideal for potential therapeutic applications. MSCs are typically cultured as monolayers on tissue culture plastic, but there is increasing evidence suggesting that they may lose their multipotency over time *in vitro*, and eventually cease to retain any resemblance to *in vivo* resident MSCs. 3D culture systems that more closely recapitulate the physiological environment of MSCs and other cell types are increasingly being explored for their capacity to support and maintain cell

phenotypes. The therapeutic utility of MSCs relies upon the ability to culture and expand these cells in 3D matrices, and consequently retrieve them. In this chapter, a safe and efficient method is introduced is not limited to retrieving MSCs from fibrin gels and can be used for recovery of a variety of cell types. The particular need for such method arose when more quantitative analyses of the BMSCs distributed throughout fibrin gels required retrieving these cells from 3D matrices.

5.6 REFERENCES

1. Rao, M.S. and M.P. Mattson, Stem cells and aging: expanding the possibilities. Mech Ageing Dev, 2001. 122(7): p. 713-34.

2. Sarugaser, R., et al., Isolation, propagation, and characterization of human umbilical cord perivascular cells (HUCPVCs). Methods Mol Biol, 2009. 482: p. 269-79.

3. De Coppi, P., et al., Isolation of amniotic stem cell lines with potential for therapy. Nat Biotechnol, 2007. 25(1): p. 100-6.

4. Yen, B.L., et al., Brief report--human embryonic stem cell-derived mesenchymal progenitors possess strong immunosuppressive effects toward natural killer cells as well as T lymphocytes. Stem Cells, 2009. 27(2): p. 451-6.

5. Yen, M.L., et al., Efficient Derivation and Concise Gene Expression Profiling of Human Embryonic Stem Cell-Derived Mesenchymal Progenitors (EMPs). Cell Transplant, 2011. 20(10): p. 1529-45.

6. Caplan, A.I. and J.E. Dennis, Mesenchymal stem cells as trophic mediators. J Cell Biochem, 2006. 98(5): p. 1076-84.

7. Lutolf, M.P. and H.M. Blau, Artificial stem cell niches. Adv Mater, 2009. 21(32-33): p. 3255-68.

8. Gilbert, P.M. and H.M. Blau, Engineering a stem cell house into a home. Stem Cell Res Ther, 2011. 2(1): p. 3.

9. Banfi, A., et al., Proliferation kinetics and differentiation potential of ex vivo expanded human bone marrow stromal cells: Implications for their use in cell therapy. Exp Hematol, 2000. 28(6): p. 707-15.

10. Baxter, M.A., et al., Study of telomere length reveals rapid aging of human marrow stromal cells following in vitro expansion. Stem Cells, 2004. 22(5): p. 675-82.

11. Reiser, J., et al., Potential of mesenchymal stem cells in gene therapy approaches for inherited and acquired diseases. Expert Opin Biol Ther, 2005. 5(12): p. 1571-84.

12. Mendez-Ferrer, S., et al., Mesenchymal and haematopoietic stem cells form a unique bone marrow niche. Nature, 2010. 466(7308): p. 829-34.

13. Markway, B.D., et al., Enhanced chondrogenic differentiation of human bone marrow-derived mesenchymal stem cells in low oxygen environment micropellet cultures. Cell Transplant, 2010. 19(1): p. 29-42.

14. Wang, W., et al., 3D spheroid culture system on micropatterned substrates for improved differentiation efficiency of multipotent mesenchymal stem cells. Biomaterials, 2009. 30(14): p. 2705-15.

15. Jahn, K., et al., Pellet culture model for human primary osteoblasts. Eur Cell Mater, 2010. 20: p. 149-61.

16. Ungrin, M.D., et al., Reproducible, ultra high-throughput formation of multicellular organization from single cell suspension-derived human embryonic stem cell aggregates. PLoS One, 2008. 3(2): p. e1565.

17. Cook, M.M., et al., Micromarrows--three-dimensional coculture of hematopoietic stem cells and mesenchymal stromal cells. Tissue Eng Part C Methods, 2012. 18(5): p. 319-28.

18. King, J.A. and W.M. Miller, Bioreactor development for stem cell expansion and controlled differentiation. Curr Opin Chem Biol, 2007. 11(4): p. 394-8.

19. Breen, A., T. O'Brien, and A. Pandit, Fibrin as a delivery system for therapeutic drugs and biomolecules. Tissue Eng Part B Rev, 2009. 15(2): p. 201-14.

20. Ho, W., et al., The behavior of human mesenchymal stem cells in 3D fibrin clots: dependence on fibrinogen concentration and clot structure. Tissue Eng, 2006. 12(6): p. 1587-95.

21. Christman, K.L., et al., Injectable fibrin scaffold improves cell transplant survival, reduces infarct expansion, and induces neovasculature formation in ischemic myocardium. J Am Coll Cardiol, 2004. 44(3): p. 654-60.

22. Syedain, Z.H., et al., Controlled compaction with ruthenium-catalyzed photochemical cross-linking of fibrin-based engineered connective tissue. Biomaterials, 2009. 30(35): p. 6695-701.

23. Huang, N.F., et al., Bone marrow-derived mesenchymal stem cells in fibrin augment angiogenesis in the chronically infarcted myocardium. Regen Med, 2009. 4(4): p. 527-38.

24. Ryu, J.H., et al., Implantation of bone marrow mononuclear cells using injectable fibrin matrix enhances neovascularization in infarcted myocardium. Biomaterials, 2005. 26(3): p. 319-26.

25. Ruger, B.M., et al., Vascular morphogenesis by adult bone marrow progenitor cells in three-dimensional fibrin matrices. Differentiation, 2008. 76(7): p. 772-83.

26. Bensaid, W., et al., A biodegradable fibrin scaffold for mesenchymal stem cell transplantation. Biomaterials, 2003. 24(14): p. 2497-502.

27. Catelas, I., et al., Human mesenchymal stem cell proliferation and osteogenic differentiation in fibrin gels in vitro. Tissue Eng, 2006. 12(8): p. 2385-96.

28. Dickhut, A., et al., Chondrogenesis of mesenchymal stem cells in gel-like biomaterials in vitro and in vivo. Front Biosci, 2008. 13: p. 4517-28.

29. Baumgartner, L., et al., Human mesenchymal stem cells: Influence of oxygen pressure on proliferation and chondrogenic differentiation in fibrin glue in vitro. J Biomed Mater Res A, 2010. 93(3): p. 930-40.

30. Ghajar, C.M., et al., Mesenchymal cells stimulate capillary morphogenesis via distinct proteolytic mechanisms. Exp Cell Res, 2010. 316(5): p. 813-25.

31. Grainger, S.J. and A.J. Putnam, Assessing the permeability of engineered capillary networks in a 3D culture. PLoS One, 2011. 6(7): p. e22086.

32. Carrion, B., et al., Recreating the perivascular niche ex vivo using a microfluidic approach. Biotechnol Bioeng, 2010. 107(6): p. 1020-8.

33. Kossack, N., et al., Isolation and characterization of pluripotent human spermatogonial stem cell-derived cells. Stem Cells, 2009. 27(1): p. 138-49.

34. Sun, N., et al., Feeder-free derivation of induced pluripotent stem cells from adult human adipose stem cells. Proc Natl Acad Sci U S A, 2009. 106(37): p. 15720-5.

35. Alongi, D.J., et al., Stem/progenitor cells from inflamed human dental pulp retain tissue regeneration potential. Regen Med, 2010. 5(4): p. 617-31.

36. Farias, V.A., et al., Human umbilical cord stromal stem cell express CD10 and exert contractile properties. Placenta, 2011. 32(1): p. 86-95.

37. Yang, Y.I., et al., Fibrin matrix-supported three-dimensional organ culture of adipose tissue for selective outgrowth, expansion, and isolation of adipose-derived stem cells. Acta Biomater, 2011. 7(12): p. 4109-19.

38. Choi, M.Y., et al., The isolation and in situ identification of MSCs residing in loose connective tissues using a niche-preserving organ culture system. Biomaterials, 2012. 33(18): p. 4469-79.

39. Urano, T., et al., The profibrinolytic enzyme subtilisin NAT purified from Bacillus subtilis Cleaves and inactivates plasminogen activator inhibitor type 1. J Biol Chem, 2001. 276(27): p. 24690-6.

40. Sumi, H., et al., A novel fibrinolytic enzyme (nattokinase) in the vegetable cheese Natto; a typical and popular soybean food in the Japanese diet. Experientia, 1987. 43(10): p. 1110-1.

41. Ghajar, C.M., et al., The effect of matrix density on the regulation of 3-D capillary morphogenesis. Biophys J, 2008. 94(5): p. 1930-41.

42. Ter Brugge, P.J. and J.A. Jansen, In vitro osteogenic differentiation of rat bone marrow cells subcultured with and without dexamethasone. Tissue Eng, 2002. 8(2): p. 321-31.

43. Rao, R.R., et al., Exogenous mineralization of cell-seeded and unseeded collagen-chitosan hydrogels using modified culture medium. Acta Biomater, 2012. 8(4): p. 1560-5.

44. Pittenger, M.F., et al., Multilineage potential of adult human mesenchymal stem cells. Science, 1999. 284(5411): p. 143-7.

45. McBeath, R., et al., Cell shape, cytoskeletal tension, and RhoA regulate stem cell lineage commitment. Dev Cell, 2004. 6(4): p. 483-95.

46. Fink, T., et al., Instability of standard PCR reference genes in adipose-derived stem cells during propagation, differentiation and hypoxic exposure. BMC Mol Biol, 2008. 9: p. 98.

47. Prockop, D.J., D.G. Phinney, and B.A. Bunnell, Methods and protocols. Preface. Methods Mol Biol, 2008. 449: p. v-vii.

48. Stacey, D.H., et al., In vitro adipogenic differentiation of preadipocytes varies with differentiation stimulus, culture dimensionality, and scaffold composition. Tissue Eng Part A, 2009. 15(11): p. 3389-99.

49. Tarnowski, B.I., et al., Automatic quantitation of cell growth and determination of mitotic index using DAPI nuclear staining. Pediatr Pathol, 1993. 13(2): p. 249-65.

50. Shur, I., et al., Differential gene expression of cultured human osteoblasts. J Cell Biochem, 2001. 83(4): p. 547-53.

51. Psaltis, P.J., et al., Enrichment for STRO-1 expression enhances the cardiovascular paracrine activity of human bone marrow-derived mesenchymal cell populations. J Cell Physiol, 2010. 223(2): p. 530-40.

52. Parekkadan, B. and J.M. Milwid, Mesenchymal stem cells as therapeutics. Annu Rev Biomed Eng, 2010. 12: p. 87-117.

53. Banfi, A., et al., Replicative aging and gene expression in long-term cultures of human bone marrow stromal cells. Tissue Eng, 2002. 8(6): p. 901-10.

54. Fujita, M., et al., Purification and characterization of a strong fibrinolytic enzyme (nattokinase) in the vegetable cheese natto, a popular soybean fermented food in Japan. Biochem Biophys Res Commun, 1993. 197(3): p. 1340-7.

55. Fujita, M., et al., Thrombolytic effect of nattokinase on a chemically induced thrombosis model in rat. Biol Pharm Bull, 1995. 18(10): p. 1387-91.

56. Kolev, K., et al., Functional evaluation of the structural features of proteases and their substrate in fibrin surface degradation. J Biol Chem, 1997. 272(21): p. 13666-75.

57. Collen, D., The plasminogen (fibrinolytic) system. Thromb Haemost, 1999. 82(2): p. 259-70.

58. Huang, H.L., et al., Trypsin-induced proteome alteration during cell subculture in mammalian cells. J Biomed Sci, 2010. 17: p. 36.

59. Morgan, H. and P.A. Hill, Human breast cancer cell-mediated bone collagen degradation requires plasminogen activation and matrix metalloproteinase activity. Cancer Cell Int, 2005. 5(1): p. 1.

60. Chao, S.C., et al., Overexpression of urokinase-type plasminogen activator in pterygia and pterygium fibroblasts. Mol Vis, 2011. 17: p. 23-31.

CHAPTER 6

CONCLUDING REMARKS

6.1 CONCLUSIONS

The overall goal of this dissertation was to better understand the molecular players involved in the perivascular association of stem cells that contribute to capillary morphogenesis. Two *in vitro* models were employed to explore one specific molecular interaction between α6β1 integrin receptor on BMSCs and EC-deposited laminin: one exploiting a 3D microfluidic platform of vasculogenesis model, one using a 3D fibrin-based angiogenesis model. Three aims (see Chapter 1) were designed to address the roles played by BMSCs within fibrin matrices in mediating and supporting EC-derived vessel formation and maturation.

Specific Aim 1 was to adapt a 3D established microfluidic device [1] to study capillary morphogenesis. The motivation behind this aim stemmed in part from our previous work exploring capillary formation in 3D [2]. One of the shortcomings of our model system was the inability to compartmentalize distinct cell types, and lack of optical clarity. Therefore, this first aim sought to transfer our existing model system into a microfluidic platform, creating a 3D environment to recapitulate a perivascular niche. This versatile multichannel device was explicitly designed to allow multiple discrete constructs of 3D cell-laden hydrogels to be easily patterned. In addition, the optical clarity and relatively thin profile of the device allowed for higher resolution imaging, while the small volumes allowed valuable reagents to be conserved. In this microfluidic device, ECs and stromal cells (either fibroblasts or BMSCs) were

micropatterend in distinct 3D culture compartments. Results (presented in Chapter 2) demonstrated that ECs formed a primitive vascular plexus, and matured into robust capillary networks with hollow well-defined lumens. Both BMSCs and fibroblasts localized to a perivascular niche within the capillary networks and formed pericytic associations with the ECs. However, the two stromal cell types promoted capillary morphogenesis with distinct kinetics.

The goal of specific Aim 2 was to utilize our microfluidic platform to explore the role of the α6 integrin subunit in BMSCs in perivascular association with EC-deposited laminin. This hypothesis was based on published *in vivo* studies suggesting that this integrin is required for the perivascular association of other stem cells in the body (Fig. 6-1) [3]. Prior studies reported that this integrin receptor plays a critical role in neural stem cell adhesion to vascular cells. Given the presence of blood vessels in other stem cell niches, we hypothesize that the molecular interaction between α6β1 integrin on BMSCs and EC-deposited laminin might prove to be generally significant. A comparison of integrin blocking assays of both EC-BMSC and EC-fibroblast co-cultures revealed that the interaction between α6β1 integrin receptor on BMSCs and EC-deposited laminin is a feature unique to BMSCs in our model system (presented in Chapter 3). Furthermore, blocking this integrin inhibited BMSC adhesion to endothelial tubes, altering their close proximity to the intact capillary networks, indicating that it plays a functional role in BMSC direct association within the perivascular niches in our microfluidic devices.

The key contributions provided by the first two aims are two-fold. First, it was demonstrated that a relatively simple microfluidic platform could support the formation of a pericyte-invested vascular network in 3D, and effectively recapitulate the perivascular localization of MSCs *ex vivo*. Second, the utility of this platform to mechanistically explore how MSCs interact with the

vasculature was demonstrated by showing that the α6β1 integrin receptor is required for the perivascular interactions between MSCs and capillaries.

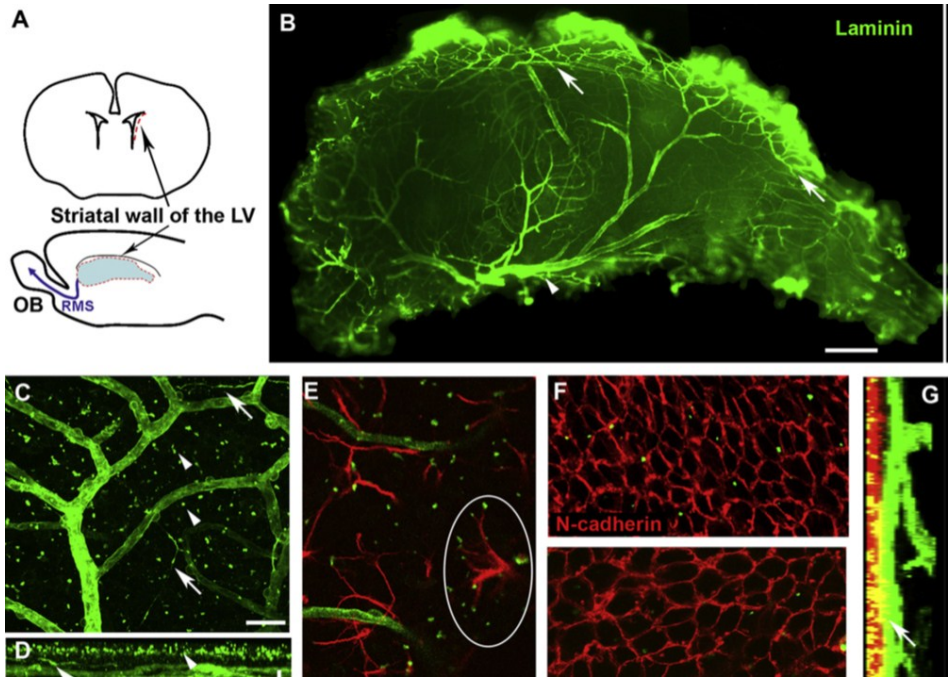

Figure 6-1: A dense plexus of blood vessels and associated laminin-positive structure in the subventricular zone (SVZ) of the brain. (A) SVZ whole mounts were dissected from the striatal wall of the lateral ventricle (red outline). (B) Laminin staining shows the dense network of blood vessels in the SVZ. Scale bar = 300 µm. (C-D) Laminin staining reveals blood vessels, laminin specks (arrowheads), and fractones (arrows). (E) Laminin specks were frequently contracted by $GFAP^+$ processes, as circled. (F) N-cadherin (upper red), or β-catenin (lower red) show the pavemented ependymal cell layer. Some laminin specks (green) are seen in the ependymal layer. Scale bar = 20 µm. (G) Z stacks of confocal images of an SVZ whole mount stained for N-cadherin (red) and laminin (green) viewed from the z axis. Scale bar = 10 µm. Images reproduced from: Shen, Q. Cell Stem Cell, 2008; 3(3): p. 289-300.

Specific Aim 3 sought to translate these findings to a tractable 3D fibrin-based co-culture of angiogenesis model to explore the functional role of these integrin-mediated interactions in sprouting angiogenesis. We used this model to be able to more quantitatively assess changes in capillary sprouting and BMSC association as a consequence of α6 integrin inhibition (presented in Chapter 4). Using RNA interference, we found that knockdown of the α6 integrin subunit in

BMSCs significantly reduced capillary sprouting, and caused their failure to associate with nascent blood vessels. Furthermore, we demonstrated that the BMSCs with attenuated α6 integrin had significantly lower proliferation rate, relative to either control cells expressing non-targeting shRNA or wild type BMSCs. In experiments designed to compensate for this deficit in proliferation, deficient sprouting persisted. Thus, we concluded that deficient sprouting is the result of α6 integrin inhibition, and not solely dependent on the deficit in proliferation. In addition, the proximity between EC-BMSC populations mattered in that knockdown of the integrin influenced vessel sprouting ability of ECs only when the BMSCs with attenuated α6 integrin were distributed throughout EC-containing fibrin gels. When the BMSCs with silenced α6 integrin were cultured as a monolayer on top of fibrin gels, vessel sprouting occurred. These findings eliminated the possibility of the knockdown treatment having an off target effect on the ability of BMSCs to release proangiogenic growth factors. Our data collectively led us to assume that perhaps α6 integrin inhibition partly results in restricted diffusion of BMSC-secreted factors through the matrix despite of the reduced distances that these molecules must travel to arrive at the endothelial sites. Furthermore, the α6β1 integrin-laminin interactions appeared to influence the process of BMSC differentiation into pericyte-like cells and their association with the EC-derived nascent vessels.

Finally, in order to further quantitatively characterize the expression of pericyte markers in BMSCs to investigate the influence of their contact with capillary networks in our fibrin-based model of angiogenesis, we developed a safe and efficient protocol (detailed in Chapter 5) to retrieve BMSCs from EC-containing gels. To isolate cells from 3D cultures, fibrin gels needed to be dissolved. Trypsin, collagenase, or other proteolytic enzymes would not yield a single cell suspension effectively. Furthermore, longer incubation times with these enzymes required for

dissolving the gels damaged cells harvested from 3D cultures. A solution was to instead digest the gels with a nattokinase enzyme to retrieve the encapsulated cells. Nattokinase is a Bacillus-derived serine protease that is known for its potent fibrinolytic activity [4, 5]. Nattokinase is also gentle and will not harm cells harvested for sub-cultivation or other studies. Results (see Chapter 5) demonstrated that BMSCs recovered from 3D fibrin gels using nattokinase are not only viable, but also retain their proliferative and multilineage potential. Demonstrated for MSCs, this method can be readily adapted to retrieve any other cell type from 3D fibrin gel constructs for various applications, including expansion, bioassays, and in vivo implantation.

Results from completing Aims 1-3 give rise to two overarching conclusions that can be considered for future studies: 1) mesenchymal stem cells recapitulate a complex microenvironment in 3D fibrin gels that can mediate capillary formation and maturation, and 2) the proximity established between EC-BMSC populations may have regulatory effects on the potential of integrin-mediated machineries for partly influencing neovascularization. This was demonstrated (see Chapter 4) by quantifying the extent of vessel sprouting, as in the knockdown conditions, the ability of ECs to undergo capillary morphogenesis was hampered, when the BMSCs were distributed throughout fibrin gels. Whether this effect of EC-BMSC proximity is strictly a cell culture phenomenon, or if it has broader implications, remains to be fully elucidated.

6.2 LIMITATIONS

As mentioned previously, given the pivotal role of integrins in molecular changes involved in endothelia/pericyte adhesion during neovascularization, it is not an easy task to unravel the

mechanistic consequences of α6 integrin inhibition that ultimately leads to reduced vessel formation. Additionally, there are further considerations that need to be explored.

Firstly, BMSCs used in our experiments were commercially available cells from Lonza. Using a commercial source of MSCs may introduce some heterogeneity in our cell populations with respect to proliferation and differentiation potential, due in part to inherent manufacturing variability. Profiling surface antigen expression of MSCs has been an ongoing challenge. Unlike the specific markers that characterize embryonic [6] and hematopoietic stem cells [7], there is no general consensus in the stem cell community regarding the identities of prospective MSC surface markers. Presently, MSCs are characterized by their adherence to plastic surface, a panel of cell-surface markers, and their *in vitro* and *in vivo* differentiation capacity [8-13]. These cells have raised high hopes for their applications in regenerative medicine. However, the lack of common standards and of a precise definition of cell preparations remains a major obstacle for research and application of MSCs. STRO-1 has been suggested to be the most definite MSC marker. STRO-1 positive MSCs can become smooth muscle cells, adipocytes, osteoblasts, and chondrocytes [14], which is consistent with the functional role of MSCs. In addition, the International Society for Cellular Therapy (ISCT) has established criteria for defining MSCs based on a combination of multiple surface markers. The ISCT report on MSC criteria specifies CD73, CD90, and CD105 as positive markers, and CD14, CD45, as negative markers of MSC population. Therefore, in our experiments, we attempted to recognize the MSCs by the monoclonal antibody STRO-1 and sort them out form ECs via fluorescent activated cell sorting (FACS).

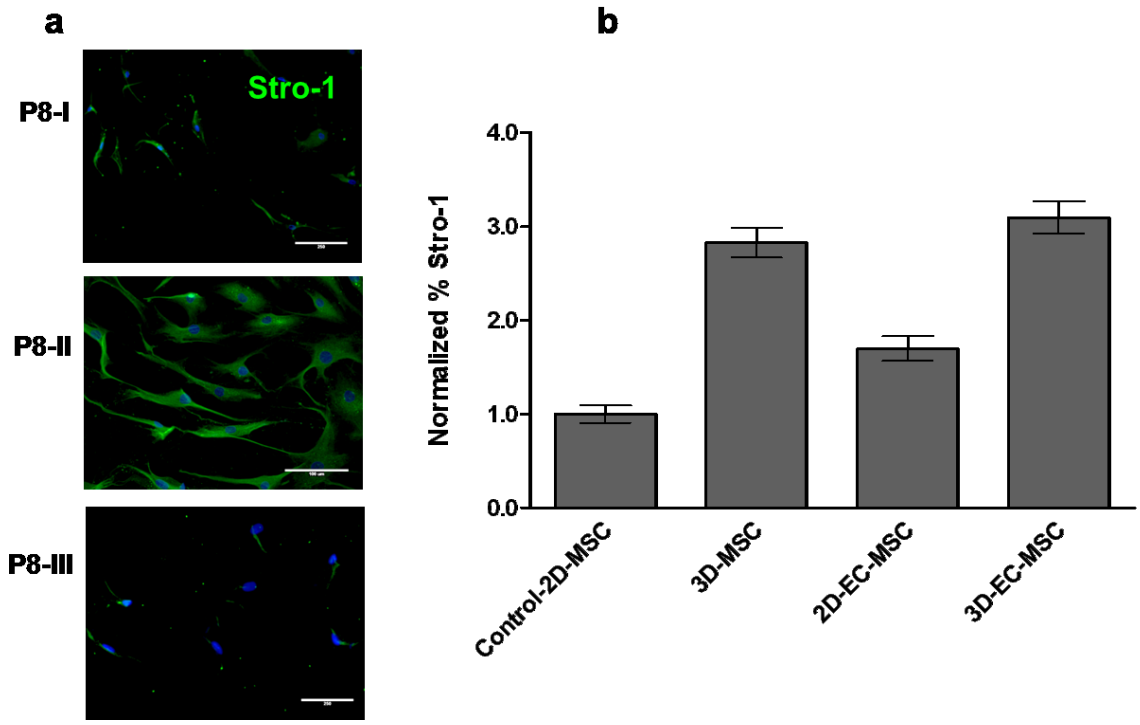

Figure 6-2: Analysis of STRO-1 surface antigen expression in BMSCs. (a) fluorescent microscopy using an antibody against STRO-1 (green). Cells from three distinct lots were cultured on polystyrene and immunofluorescently stained STRO-1 and DAPI (blue). (b) Cells cultured for 48 hours expressing low levels of STRO-1 as analyzed by FACS. The degree of STRO-1 expression levels varies among different conditions.

Our results have provided evidence that the degree of STRO-1 expression significantly differs among different MSC lots, suggesting that there is heterogeneity with respect to the degree with which they express STRO-1 (Fig. 6-2b). Furthermore, STRO-1 expression levels among different conditions were significantly but consistently low. Additionally, staining pattern of STRO-1 was heterogeneous as revealed by immunofluorescent images of three distinct populations (Fig. 6-2a). The heterogeneity of starting populations renders comparison of results between different groups difficult, and may also in part account for the lack of reproducibility. Future studies may require the use of harvested and isolated MSCs from human patients undergoing bone marrow aspiration procedures.

Secondly, it is noteworthy that microfluidics have not yet been widely adapted by the cell biology community. Our microfluidic platform is no exception. A very important limitation is that there is no efficient way of safely retrieving cells out of the gel chambers for the purpose of subsequent analysis. Another challenge to overcome when working with these devices is their high failure rate. These pitfalls made our assessments mostly qualitative. Therefore, we used our larger scale model of angiogenesis to explore the EC-MSC integrin-mediated interactions in a more rigorous and quantitative manner. An accurate and reproducible metric to measure the total vessel network length is used in this model of angiogenesis, in which ECs sprout from microcarrier beads that serve as a zero reference to facilitate quantification. This model provides a reference point for comparisons over time. Using this model enabled us to address our hypothesis in a more quantitative manner.

6.3 IMPLICATIONS AND FUTURE DIRECTIONS

The results derived from the aims fulfilled for this study provide a better understanding of the role of α6 integrin receptor on MSCs in their perivascular association with EC-deposited BM, and in capillary morphogenesis in fibrin. This study has implications on two important issues that need to be further explored.

Need for stem cell niche models that recapitulate in vivo conditions. Stem cells in a multicellular organism have their own unique microenvironment, composed of several factors that influence their self-renewal and differentiation status. In general, these factors fall into one of two categories: soluble cues (i.e., growth factors) and insoluble cues (i.e., the ECM and cell-cell interactions) [15, 16]. Since controlling the proliferation and differentiation of stem cells in

culture is important for basic research [17], and for eventual tissue engineering/regenerative medicine applications [18], consideration of these cues for *in vitro* cultivation of cells is crucial for recapitulating stem cells' natural niche. There are both intrinsic and extrinsic factors from the MSC microenvironment that can influence MSC fates. One of the key features of the MSC microenvironment is the element of the vasculature. Recent studies suggest that the physical proximity of MSCs to the vasculature *in vivo* is instructive in the regulation of MSC fate [19]. It is important that the 3D physiologic environment of perivascular niches be more closely recapitulated in order to explore important cell-cell heterotypic interactions, as monolayer cultures often provoke cellular expression profiles and behaviors distinct from those which occur *in vivo* [20]. A promising route toward dissecting these molecular interactions between MSC and the vasculature involves generation of novel cell culture platforms that mimic crucial biochemical or structural aspects of the niche. Such platforms can be particularly useful in the context of MSC function with respect to elements of the niche, including the vasculature. We anticipate that our microfluidic device provides a novel platform to create an artificial niche and assess the integrated effects of multiple cues on MSC interactions with nascent capillaries. The most significant advantage of using this microfluidic platform is the ability to spatially segregate the ECs and the MSCs in discrete microchannels. Although not fully exploited here, the initial spatial control theoretically allows for any multicellular morphogenetic process to be monitored as a function of both space and time. This feature allows for assessing the effects of the physical proximity between EC-BMSC populations on the ability of their crosstalk to regulate vascularization. Doing so would result in a culture system in which the ability of the α6β1 integrin-laminin interactions to induce capillary formation could be assessed as a function of the physical distance between EC-BMSC populations and time. Because the volumes of the cellular

gel constructs embedded within microchannels are very small, usually several microliters, the amounts of biological reagents used would be quite small. This is an important factor in achieving conservation of expensive reagents. The experiments with the integrin blocking antibody (presented in Chapter 4) are a perfect example of this added feature, as the amount of antibody utilized is far less in this system than in a more "conventional" 3D gel system in a multiwell plate. Furthermore, the relatively thin and optically clear microfluidic cell culture chamber minimizes background fluorescence, which in turn allows for obtaining significantly higher image quality as compared to larger 3D cellular gel constructs that may be several millimeters in thickness. This advantage is quite evident in our confocal image of 3D sprouting of capillary networks within the devices. These two key features were useful for performing experiments in the microfluidic system, whose small size enabled high resolution imaging more easily than would a thick 3D gel and helped to conserve valuable reagents. Furthermore, the additional capabilities offered by a microfluidic system will conceivably facilitate our future efforts to explore how additional features of the microenvironment influence the perivascular association of MSCs.

As previously mentioned in Chapter 4, it is possible that the physical proximity between EC-BMSC populations enables the α6β1-mediated adhesion signaling to influence cell-cell heterotypic interactions that regulate the ability of ECs to sprout. Investigation of stem cell niches in various tissues has revealed that stem cell behavior is critically regulated by interactions with surrounding cells and more importantly, by direct physical contact through membrane proteins and insoluble ECM proteins [21]. While BMSCs have been shown to be beneficial in capillary formation and maturation, in our assays, reciprocal signaling between ECs and MSCs via the α6 integrin may also influence MSC fate and their potential to become

stabilizing pericytes. Again, to be able to assess the influence of this particular integrin receptor expressed in MSCs on their fate, we must consider MSCs not solely in monotypic culture, but as a part of a greater 3D microenvironment comprised of the molecules stimulated as a result of heterotypic interactions. The data in this thesis really represent the key contribution regarding the role of the α6β1 integrin in the perivascular association of the MSCs, and provide the important foundation for future mechanistic studies aimed at addressing how this molecular interaction between MSCs and capillary networks may regulate the multipotency of MSCs.

EC-pericyte interactions: therapeutic opportunities. Targeting tumour vessels for anti-tumour therapy has evolved from vision to clinical reality over the last four decades. Given the major contribution of integrins to angiogenesis and that the expansion of solid tumors is dependent on neovascularization; these molecules provide an appealing target for antiangiogenic therapy. However, the majority of integrin-derived angiogenesis inhibitors target ECs. EC-derived integrin targeting has proved to be somewhat beneficial in preventing neovascularization of tumors. However, successful eradication of established tumors may require not only prevention of neovascularization, but also destruction of existing tumor blood vessels to reduce a tumor mass. Therefore, it is important that cancer and other angiogenesis-dependent diseases be diagnosed after blood vessels are established. Long term therapeutic benefits could be achieved by targeting not only the overt tumor cells but also other constituent cell types (Fig. 6-3).

Mural cells/pericytes are also being targeted for antiangiogenic therapy, targeting both their recruitment and interaction with ECs. As previously mentioned (Chapter 1), depletion of pericytes causes hyperdilation of tumor vessels and increased apoptosis of tumor cell endothelium [22]. Several studies have shown that targeting ECs by vascular endothelial growth factor receptor-2 (VEGFR-2) inhibition is not beneficial in regressing established tumor blood

vessels, because of resistance of treatment conferred by the overlying pericytes [23]. However, combining VEGFR-2 inhibitors with PDGFR-β inhibitors (expressed by pericytes) resulted in regression of late-stage tumors [24], EC apoptosis, blood vessel destabilization and regression, and finally tissue hypoxia. Additionally, targeting both ECs and pericytes reduced the hydrostatic pressure of the tumor vessels, allowing for efficient drug delivery [25] and enhancing the effect of chemotherapy.

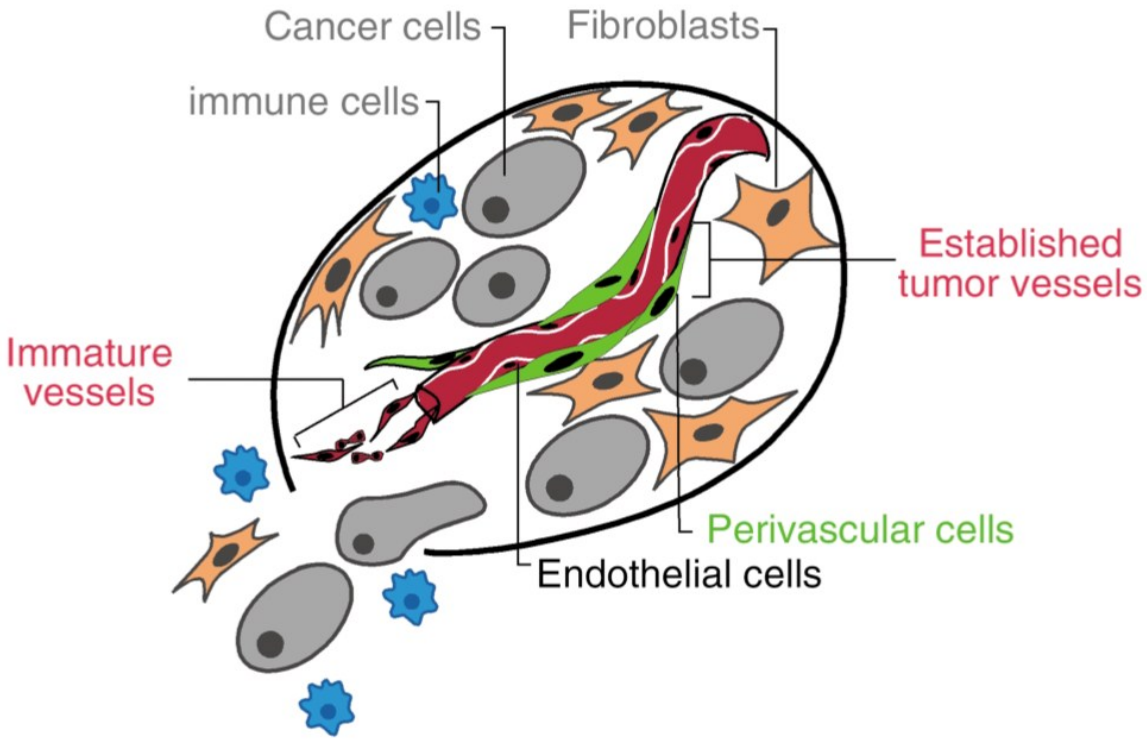

Figure 6-3: A schematic representation of tumor microenvironment and constituent cell types. Image reproduced from: *Bergers*, G, *JCI,* 2003; 111(9):1287–1295.

Targeting of other specific markers expressed by pericytes, which have shown to reduce angiogenesis, include NG2 [26] and MMPs that are secreted by pericytes.[27]. These findings suggest that combined targeting of ECs and pericytes to more efficiently decrease both blood vessel number and tumor growth and hopefully may provide a more effective mode of treatment

for established tumors. There is evidence that the level of vessel maturation strongly influences the response of tumor vessels to antivascular therapy [28]. This has implications for human cancers in which some of the most common types (i.e., breast, colon, prostate) have vessels with moderate to extensive pericyte coverage [29]. It has been demonstrated that tumors from mice treated with integrin α4β1 inhibitors significantly inhibited the association of mural cells with endothelia in vivo [30]. Furthermore, tumors that had been treated with anti–integrin α4β1 antagonists exhibited far fewer intact vessels with lumens than control-treated tumors.

Because of their tumor-trophic migratory capacity, MSCs have emerged as promising delivery vehicles of antitumor substances in therapy of malignant tumors, including glioblastoma [31]. Recent results from both animal models and human tumors have suggested that MSCs also migrate to tumor tissues, where they incorporate into the tumor stroma [32, 33]. There is compelling evidence that MSCs can differentiate into fibroblasts, myofibrobalsts, or pericyte-like cells and induce neovascularization, resulting in the promotion of tumor growth *in vivo* [34, 35]. These findings collectively suggest that MSCs play an important role in tumor progression, making them an attractive anti-cancer target. To this end, selective inhibition of α6β1integrin-mediated adhesion to laminin could be a potential therapeutic target to possibly inhibit blood vessel maturation via mesenchymal support. To date this, the role of integrin α6β1 in tumor progression has not been fully elucidated. Thus, studies assessing the influence of the interaction between α6β1integrin and EC-deposited laminin on mesenchymal perivascular coverage during pathological angiogenesis may advance anti-vascular therapy in human cancer.

6.4 REFERENCES

1. Huang, C.P., et al., Engineering microscale cellular niches for three-dimensional multicellular co-cultures. Lab Chip, 2009. 9(12): p. 1740-8.

2. Ghajar, C.M., et al., Mesenchymal cells stimulate capillary morphogenesis via distinct proteolytic mechanisms. Exp Cell Res, 2010. 316(5): p. 813-25.

3. Shen, Q., et al., Adult SVZ stem cells lie in a vascular niche: a quantitative analysis of niche cell-cell interactions. Cell Stem Cell, 2008. 3(3): p. 289-300.

4. Urano, T., et al., The profibrinolytic enzyme subtilisin NAT purified from Bacillus subtilis Cleaves and inactivates plasminogen activator inhibitor type 1. J Biol Chem, 2001. 276(27): p. 24690-6.

5. Sumi, H., et al., A novel fibrinolytic enzyme (nattokinase) in the vegetable cheese Natto; a typical and popular soybean food in the Japanese diet. Experientia, 1987. 43(10): p. 1110-1.

6. Brivanlou, A.H., et al., Stem cells. Setting standards for human embryonic stem cells. Science, 2003. 300(5621): p. 913-6.

7. Baum, C.M., et al., Isolation of a candidate human hematopoietic stem-cell population. Proc Natl Acad Sci U S A, 1992. 89(7): p. 2804-8.

8. Kogler, G., et al., A new human somatic stem cell from placental cord blood with intrinsic pluripotent differentiation potential. J Exp Med, 2004. 200(2): p. 123-35.

9. Haynesworth, S.E., M.A. Baber, and A.I. Caplan, Cell surface antigens on human marrow-derived mesenchymal cells are detected by monoclonal antibodies. Bone, 1992. 13(1): p. 69-80.

10. Gronthos, S., et al., Surface protein characterization of human adipose tissue-derived stromal cells. J Cell Physiol, 2001. 189(1): p. 54-63.

11. Tocci, A. and L. Forte, Mesenchymal stem cell: use and perspectives. Hematol J, 2003. 4(2): p. 92-6.

12. Zuk, P.A., et al., Human adipose tissue is a source of multipotent stem cells. Mol Biol Cell, 2002. 13(12): p. 4279-95.

13. Javazon, E.H., K.J. Beggs, and A.W. Flake, Mesenchymal stem cells: paradoxes of passaging. Exp Hematol, 2004. 32(5): p. 414-25.

14. Dennis, J.E., et al., The STRO-1+ marrow cell population is multipotential. Cells Tissues Organs, 2002. 170(2-3): p. 73-82.

15. Flaim, C.J., S. Chien, and S.N. Bhatia, An extracellular matrix microarray for probing cellular differentiation. Nat Methods, 2005. 2(2): p. 119-25.

16. Scadden, D.T., The stem-cell niche as an entity of action. Nature, 2006. 441(7097): p. 1075-9.

17. Hansen, R.K. and M.J. Bissell, Tissue architecture and breast cancer: the role of extracellular matrix and steroid hormones. Endocr Relat Cancer, 2000. 7(2): p. 95-113.

18. Guillot, P.V., et al., Stem cell differentiation and expansion for clinical applications of tissue engineering. J Cell Mol Med, 2007. 11(5): p. 935-44.

19. Lo Celso, C., et al., Live-animal tracking of individual haematopoietic stem/progenitor cells in their niche. Nature, 2009. 457(7225): p. 92-6.

20. Griffith, L.G. and M.A. Swartz, Capturing complex 3D tissue physiology in vitro. Nat Rev Mol Cell Biol, 2006. 7(3): p. 211-24.

21. Jones, D.L. and A.J. Wagers, No place like home: anatomy and function of the stem cell niche. Nat Rev Mol Cell Biol, 2008. 9(1): p. 11-21.

22. Song, S., et al., PDGFRbeta+ perivascular progenitor cells in tumours regulate pericyte differentiation and vascular survival. Nat Cell Biol, 2005. 7(9): p. 870-9.

23. Erber, R., et al., Combined inhibition of VEGF and PDGF signaling enforces tumor vessel regression by interfering with pericyte-mediated endothelial cell survival mechanisms. FASEB J, 2004. 18(2): p. 338-40.

24. Bergers, G., et al., Benefits of targeting both pericytes and endothelial cells in the tumor vasculature with kinase inhibitors. J Clin Invest, 2003. 111(9): p. 1287-95.

25. Tong, R.T., et al., Vascular normalization by vascular endothelial growth factor receptor 2 blockade induces a pressure gradient across the vasculature and improves drug penetration in tumors. Cancer Res, 2004. 64(11): p. 3731-6.

26. Ozerdem, U. and W.B. Stallcup, Pathological angiogenesis is reduced by targeting pericytes via the NG2 proteoglycan. Angiogenesis, 2004. 7(3): p. 269-76.

27. Chantrain, C.F., et al., Mechanisms of pericyte recruitment in tumour angiogenesis: a new role for metalloproteinases. Eur J Cancer, 2006. 42(3): p. 310-8.

28. Gee, M.S., et al., Tumor vessel development and maturation impose limits on the effectiveness of anti-vascular therapy. Am J Pathol, 2003. 162(1): p. 183-93.

29. Eberhard, A., et al., Heterogeneity of angiogenesis and blood vessel maturation in human tumors: implications for antiangiogenic tumor therapies. Cancer Res, 2000. 60(5): p. 1388-93.

30. Garmy-Susini, B., et al., Integrin alpha4beta1-VCAM-1-mediated adhesion between endothelial and mural cells is required for blood vessel maturation. J Clin Invest, 2005. 115(6): p. 1542-51.

31. Aboody, K.S., et al., Neural stem cells display extensive tropism for pathology in adult brain: evidence from intracranial gliomas. Proc Natl Acad Sci U S A, 2000. 97(23): p. 12846-51.

32. Studeny, M., et al., Mesenchymal stem cells: potential precursors for tumor stroma and targeted-delivery vehicles for anticancer agents. J Natl Cancer Inst, 2004. 96(21): p. 1593-603.

33. Kidd, S., et al., Direct evidence of mesenchymal stem cell tropism for tumor and wounding microenvironments using in vivo bioluminescent imaging. Stem Cells, 2009. 27(10): p. 2614-23.

34. Spaeth, E.L., et al., Mesenchymal stem cell transition to tumor-associated fibroblasts contributes to fibrovascular network expansion and tumor progression. PLoS One, 2009. 4(4): p. e4992.

35. Bexell, D., et al., Bone marrow multipotent mesenchymal stroma cells act as pericyte-like migratory vehicles in experimental gliomas. Mol Ther, 2009. 17(1): p. 183-90.